BORROW PITS ON ESTUARINE SEDIMENT DYNAMICS, BARATARIA BAY, LOUISIANA

MARTIJN BREGMAN[1], IOANNIS Y. GEORGIOU[1], MIKE MINER[1], JOHN SWARTZ[1], SYED KHALIL[2], RICK RAYNIE[2]

[1]The Water Institute [2]Louisiana Coastal Protection and Restoration Authority

Produced for and funded by: Louisiana Coastal Protection and Restoration Authority under Task Order 72 Louisiana Sediment Management Plan (LASMP), Subtask 1: Central Coast Regional Sediment Inventory and Sediment Budget Program, Activity 1.3 Borrow Area Monitoring and Management 2 (BAMM2): Barataria Bay

THE WATER INSTITUTE

COASTAL PROTECTION AND RESTORATION AUTHORITY CPRA

August 2023

Report #P-00392-2

ACKNOWLEDGEMENTS

This project was supported by the Coastal Protection and Restoration Authority under Task Order 72 Louisiana Sediment Management Plan (LASMP), Subtask 1: Central Coast Regional Sediment Inventory and Sediment Budget Program, Activity 1.3 Borrow Area Monitoring and Management 2: Barataria Bay.

The authors thank Matthew Hiatt and Jay Merrill from Louisiana State University for sharing their Barataria Bay wave deployment data, which was used to calibrate the wave model.

Geologists, geomorphologists, and engineers from the Institute and CPRA contributed to this work and the development of this report.

This report was reviewed, edited, and formatted by Charley Cameron of the Institute.

ABOUT THE WATER INSTITUTE

The Water Institute is an independent, non-profit, applied research institution advancing science and developing integrated methods to solve complex environmental and societal challenges. We believe in and strive for more resilient and equitable communities, sustainable environments, and thriving economies. For more information, visit www.thewaterinstitute.org.

CITATION

Martijn Bregman, Ioannis Y. Georgiou, Mike Miner, Syed Khalil, John Swartz, and Rick Raynie (2023). Assessing the Impact of In-Bay Borrow Pits on Estuarine Sediment Dynamics, Barataria Bay, Louisiana. Prepared by The Water Institute for the Coastal Protection and Restoration Authority. Baton Rouge, LA.

Cover Photo: Photo from NASA Earth Observatory by Lauren Dauphin | NASA Landsat imagery of Barataria Bay captured during high tide in October 2020

PREFACE

This report was developed by The Water Institute (the Institute) for the Coastal Protection and Restoration Authority under Task Order 72 Louisiana Sediment Management Plan (LASMP), Subtask 1: Central Coast Regional Sediment Inventory and Sediment Budget Program, Activity 1.3 Borrow Area Monitoring and Management 2 (BAMM2): Barataria Bay.

The report summarizes the analysis to evaluate the consequences of borrowing sediment from inter-distributary bays in the Mississippi River Delta Plain (MRDP), specifically in Barataria Bay. The report details the model development methods, scenarios examined, and results of the numerical model experiment. It discusses the implications for siting and monitoring hypothetical borrow pits at selected locations within Barataria Bay. Further, the study provides additional insight into the impact of borrow pits on local hydrodynamics and quantifies the effects of borrow pits on the tidal prism and evaluates the impact of borrow pits on local and regional sediment budgets, including the potential effects on marsh shorelines along the bay perimeter, and borrow pit influence on sediment exchange at tidal inlets fronting Barataria Bay.

EXECUTIVE SUMMARY

The 2023 Louisiana Coastal Master Plan (CMP) requires 700–800 million m^3 of sediment for marsh creation and land bridge restoration (CPRA, 2023) and an estimated 5–11 billion m^3 is needed to offset future land losses (Blum & Roberts, 2009; Khalil et al., 2018). Suitable sediment resources are scarce in the Mississippi River Delta Plain (MRDP). The Louisiana Sediment Management Plan (LASMP; Khalil et al., 2010, 2018; Underwood, 2012), and its component Borrow Area Management and Monitoring (BAMM) program, aim to identify and characterize sediment resources and optimize borrow area use while minimizing negative environmental impacts. For barrier island restoration, the preferred borrow areas of high-quality sand to supplement the regional sediment budget are located offshore or within sand bars in the Lower Mississippi River. However, transportation distances can be cost-prohibitive and recent works demonstrate that in-bay borrow areas could also provide restoration-compatible sediment for selected restoration projects (CB&I, 2015; Robichaux et al., 2020; Hollis et al., 2023). Previous work by CB&I (2015) evaluated conceptual borrow areas and found limited effects of borrow pits locally and no impacts to marsh-adjacent shorelines, but also emphasized the need to collect more monitoring data around borrow areas.

This study extends the previous research by CB&I (2015) and investigates the influence of borrow pit location and orientation, the impact of tropical cyclones on borrow pits, and the effects of borrow pits on local and regional hydrodynamics and sediment dynamics. Additionally, this study quantifies the extent to which borrow pits intercept sediment that would have been transported to other more beneficial or less beneficial parts of the system. The study focuses on the Barataria Basin, a microtidal basin in the MRDP connected to the Gulf of Mexico via multiple tidal inlets. Several paleochannel deposits with restoration-compatible sediment were identified in the basin (Hollis et al., 2023), which has experienced wetland loss due to sea level rise and subsidence (Couvillion et al., 2017; Penland et al., 2001).

The numerical model utilized in this study is based on the Delft3D Flexible Mesh (FM) modeling suite (Kernkamp et al., 2011) and includes coupled hydrodynamics, sediment transport, and morphology, and employs a mobile bed approach. The model was calibrated to achieve reasonable skill in reproducing water levels, tidal phasing, tidal prism, wind waves, suspended sediment concentrations, and morphology. The modeling framework was established to simulate morphological changes over 20 years, considering mixed meteorological forcing consisting of quiescent conditions, cold fronts, and tropical cyclones. The influence of the location, geometry, and orientation of hypothetical borrow pits was evaluated through five scenarios with various configurations of two borrow pits in Barataria Bay, which were situated at locations where restoration-compatible sediment was located at depth (Hollis et al., 2023).

The model results indicate that the impact of borrow pits on the tidal prism of Barataria Basin is negligible (<<1%) and within the model's margin of error. However, regardless of size, depth, and orientation, borrow pits do influence local hydrodynamics, particularly during higher energy events like cold fronts and tropical cyclones, increasing wave heights and circulation patterns locally when wind or tidal currents align with the pit's length. This effect is less likely to occur when the borrow pit width is aligned with winds or currents. Despite the less favorable conditions resulting from these currents, borrow pits remain depositional during high-energy events because they significantly reduce wave-driven bed shear stress.

Infilling rates of the evaluated borrow pits are approximately 120,000 m^3/year, with minor differences of less than 7% among the configurations. Borrow Pit 1, evaluated in two orientations, displayed slightly higher infilling (2%) when oriented NE-SW instead of NW-SE. Borrow Pit 2, tested only in NE-SW orientation, exhibited the highest infilling rate, but the range of infilling rate differences does not exceed 7%. Other factors influencing Borrow Pit 2's higher infilling rate could be its lower length-to-width aspect ratio (closer to a square) and proximity to tidal inlets. This highlights the importance of borrow pit location and orientation when planning and designing borrow pits. Simulated vertical infilling rates for the evaluated pits are approximately 0.075 m/year (0.25 ft/year), a result that is consistent with measured infilling rates in comparable in-bay borrow areas that are not influenced by fluvial sediment sources (0.06–0.21 m/year or 0.2–0.7 ft/year; CB&I, 2015). Model results also demonstrate that the majority (>80%) of infilling takes place during cold fronts, with a significantly lower infilling (<20%) occurring during tropical storms, and much lower (~2%) infilling during quiescent conditions.

The sediment captured by the borrow pits is mainly sourced (>90%) from the Barataria Bay floor, specifically near the excavation footprint, resulting in localized decimeter-scale erosion. Additionally, most evaluated borrow pits act as sediment sinks, reducing overall sediment export from the bay to the Gulf of Mexico. Of the hypothetical pits evaluated in this study, Borrow Pit 2 was the most effective, reducing sediment export at tidal inlets by approximately 250,000 m^3 over the 20-year simulation period, representing 0.3% of the absolute sediment export volume from the Barataria Basin (around 91 million m^3), or 10% of the sediment captured by the borrow pit. The remaining borrow pit locations and orientations showed similar trends, with a change in sediment export being only a small fraction (<1%) of the total sediment volumes exported via tidal inlets.

The marshes at the perimeter of Barataria Bay are not negatively affected by the sediment trapped by borrow pits evaluated in this study. The presence of the borrow pits in the alternatives evaluated does not significantly influence sediment exchange at the marsh-bay interface or other distal environments such as tidal inlets. The study did not evaluate an exhaustive set of scenarios or locations of borrow pits to discern whether a more direct impact could occur on proximal marshes or tidal inlets. The excavation of pits closer to the marsh shoreline or tidal inlets may lead to different outcomes. Additionally, each of the investigated pits covers approximately 0.5% of the total surface area of Barataria Bay. Following CB&I's (2015) recommendations, additional field investigations and monitoring is recommended to improve understanding of complex hydrodynamics around borrow pits, as complex flow patterns around the pit continue to challenge regional-scale numerical modeling. Moreover, in interior bays like Barataria Bay, it would be helpful to obtain measurements of suspended sediment concentrations throughout the water column at multiple locations during high-energy events, and the subsequent bed elevation response so as to elucidate sediment dynamics and the bay response during stormier conditions, as these events are the primary drivers of bay erosion and borrow pit infilling. Conducting regular repeat bathymetry collections in Barataria Bay or similar bays with borrow pits would provide valuable insights into long-term morphological changes and support future impact predictions as well as provide additional datasets for model calibration. Understanding of the governing processes of borrow pit infilling and sediment origin remains limited, but repeat hydrographic surveys, seismic surveys, coring, and radioisotope dating could support improved understanding.

TABLE OF CONTENTS

LIST OF FIGURES

LIST OF TABLES

LIST OF ACRONYMS

Acronym	Term
ADCIRC	Advanced Circulation Model
BAMM	Borrow Area Management and Monitoring Program
BP	Borrow Pit
CMP	Coastal Master Plan
CPRA	Coastal Protection and Restoration Authority
DEM	Digital Elevation Model
ESLR	Eustatic Sea Level Rise
FM	Flexible Mesh
GIWW	Gulf Intracoastal Waterway
ICM	Integrated Compartment Model
LASMP	Louisiana Sediment Management Plan
LMRMP	Lowermost Mississippi River Management Program
LSU	Louisiana State University
MRDP	Mississippi River Delta Plain
NOAA	National Oceanic and Atmospheric Administration
RMSE	Root Mean Square Error
SWAMP	System-Wide Assessment and Monitoring Program
USACE	U.S. Army Corps of Engineers
USGS	United States Geological Survey

UNIT TABLE

Abbreviation	Term
cm	Centimeter
ft.	Feet
ft^2	Square Feet
ft^3	Cubic Feet
mg	Milligram
km	Kilometer
km^2	Square Kilometer
L	Liter
m	Meter
m^2	Square meter
m^3	Cubic meter
mm	Millimeter
s	Second
yd^3	Cubic Yard
µm	Micrometer or micron

1.0 STUDY BACKGROUND AND OBJECTIVES

To implement the state's 2023 Coastal Master Plan (CMP), Louisiana needs approximately 700–800 million m^3 of sediment to build marsh creation and land bridge restoration projects (CPRA, 2023), whereas 5–11 billion m^3 of sediment is needed to offset future land losses (Blum & Roberts, 2009; Khalil et al., 2018). However, suitable sediment resources for marsh and barrier island restoration projects are scarce in the Mississippi River Delta Plain (MRDP). The Louisiana Sediment Management Plan (LASMP) was developed to inform long-term restoration planning and management of sediment resources (Khalil et al., 2010, 2018; Underwood, 2012). An essential component of LASMP is the Borrow Area Management and Monitoring (BAMM) program, which aims to increase understanding of the physical characteristics and environmental impacts of borrow areas. The goal of the program is to optimize the use of borrow areas while minimizing negative environmental impacts (CB&I, 2015).

According to the 2023 CMP (Louisiana Coastal Protection and Restoration Authority [CPRA], 2023), the preferred borrow areas for coastal restoration projects, when transportation distances are not a factor, are those located offshore on the inner continental shelf or within sand bars in the Lower Mississippi River, rather than within the system that is being restored. This is to supplement the deficit in the regional sediment budget. However, modern interdistributary bays in the MRDP, such as Barataria Bay, feature several buried paleochannels that form potential in-bay borrow areas for restoration-compatible sediment (Hollis et al., 2023). This sediment, known as "mixed sediment" and defined by Khalil et al. (2022), contains the adequate amounts of sand and silt fractions necessary for marsh creation projects. Other potential in-system sediment resources, not considered in this study, could include sediment dredged for the maintenance or deepening of navigation channels. Such projects include the Calcasieu Ship Channel maintenance dredging and the Port Fourchon deep draft improvements. These in-bay borrow areas are particularly relevant for restoration projects located at a significant distance from out-of-system sediment resources, as using out-of-system sources for such projects can become cost-prohibitive. Projects that could benefit from in-system borrow areas include the restoration of historic ridges and bay rims found within basins. These features have the potential to influence surge propagation during tropical storms and the propagation of the tidal wave, and thus mitigate an expanding tidal prism. In these cases, out-of-system borrow areas may be too far away to be practical, making ridge and bay rim restoration of this type a potential use case for sourcing of in-system sediment. However, such a use case would require sufficient project-specific testing of the potential impacts of within-bay sediment extraction on the regional sediment budget. It would be additionally beneficial to study the cumulative effects of multiple in-system borrow projects over time. Therefore, it is critical to have a comprehensive understanding and assessment of sediment dynamics, regional sediment budgets, and available sediment resources within the system to assess the impacts of using in-system borrow sediment.

Recent works (CB&I, 2015; Robichaux et al., 2020; Hollis et al., 2023) demonstrate that excavations in the MRDP are efficient sediment traps that could retain suspended sediment that would otherwise be exported from the estuarine system. This study builds on previous work by CB&I (2015); during their evaluation of conceptual in-bay borrow areas, CB&I demonstrated limited effects on the local wave climate. The study also found that infilling was primarily caused by the settlement of suspended sediment rather than bedload (CB&I, 2015) and suggested that marsh-adjacent shorelines would not be affected by

the borrow pits, although they did suggest situating pits at least ~450 m (1500 ft) away from adjacent shorelines and recommended monitoring these pits through collection of bathymetric surveys and aerial photography. Regarding monitoring, CB&I (2015) recommended several measures. First, they suggested monitoring hypoxic conditions. Second, they recommended the installation of permanent survey monuments to ensure consistent surveys. Third, they advised collecting dual-frequency bathymetry to achieve a better definition of the water-seafloor interface. Lastly, they stressed the importance of monitoring future proposed borrow areas. CB&I (2015) emphasized that site-specific conditions should be considered, making it necessary to independently monitor and evaluate each borrow area. They pointed out the limited availability of model calibration and validation data, which leads to uncertainty in the models. To reduce this uncertainty, CB&I recommended implementing better monitoring practices.

CB&I (2015) did not consider the influence of the location and orientation of the borrow pits or evaluate the potential impact of tropical cyclones. Furthermore, none of the studies mentioned here (CB&I, 2015; Robichaux et al., 2020; Hollis et al., 2023) evaluated the potential impact of borrow pits on the tidal prism, determined the origin of sediment that is captured by the borrow pits, or analyzed how borrow pits could influence regional sediment budgets.

The objective of this study is to quantify the extent to which borrow areas influence local and regional hydrodynamics and sediment dynamics, and to what degree they intercept sediment that could be beneficial or disruptive to the system. To meet this objective, the following research questions were asked:

- How significant is the effect of in-bay sediment mining of one to two large dredge pits on the tidal prism?
- What is the potential of in-bay borrow pits to capture sediment that would otherwise (a) be deposited elsewhere within the system or (b) exported to the Gulf of Mexico? Part (a) of this question is relevant for understanding whether borrow pits intercept sediment that would otherwise have been transported to a more beneficial part within the system (e.g., marshes). Part (b) aims to understand whether pits worsen or mitigate the deficit in the regional sediment budget.
- What is the influence of pit orientation on local to regional sediment dynamics?

It should be noted that this study only investigated the effects of one to two large dredge pits, and not the cumulative effects of multiple dredge pits over a longer time period. Further study is required to estimate the effects of multiple dredge pits including potential threshold excavation volumes that might have significant impacts to the system.

1.1 STUDY AREA

This study evaluates the potential impacts of hypothetical borrow pits on sediment dynamics and Barataria Basin hydrodynamics (Figure 1). The Barataria Basin formed between two major Mississippi River distributaries: the abandoned Lafourche delta complex to the west and the Plaquemines/Modern (active) delta complex to the east (Fisk, 1944; Kolb & van Lopik, 1958). The Barataria Basin lost approximately 1,100 km^2 of wetlands between 1932 and 2016 due to a variety of natural and human-induced stressors, including sea level rise, subsidence, storms, insufficient sediment supply, and infrastructure for navigation and flood control (Couvillion et al., 2017; Penland et al., 2001). Between

1993 and 2016, global eustatic sea level rise (ESLR) amounted to 3.4 mm ± 0.4 mm/year (Sweet et al., 2017). Subsidence rates in the Barataria Basin range between 2 and 7 mm/year, with the highest rates occurring throughout Barataria Bay (Byrnes et al., 2019). According to the National Oceanic and Atmospheric Administration (NOAA), the Grand Isle gauge (8761724) experiences a relative sea level rise rate of 9.16 ± 0.37 mm/yr. Barataria Bay is classified as an ebb-dominant estuary, with a tidal prism that has been expanding as a result of increased bay area due to wetland loss (FitzGerald et al., 2004). Most of the Barataria Basin is connected to the Gulf of Mexico via five main tidal inlets, listed here from west to east: Caminada Pass, Barataria Pass, Pass Abel, Quatre Bayou Pass, and Pass Ronquille (Figure 1). The Barataria Basin is microtidal, with an average tidal range near the Gulf of Mexico of 0.35 m that increases to approximately 0.6 m during spring tides (FitzGerald et al., 2007; Das et al., 2012; Li et al., 2021). The tidal range decreases in a northward direction. CPRA has contracted the Institute to develop a sediment resources inventory for the Barataria and Terrebonne basins, and ongoing efforts have identified several potential buried deltaic paleochannel deposits that contain restoration-compatible sediment (Hollis et al., 2023), and informed the locations and geometry of borrow areas selected to evaluate.

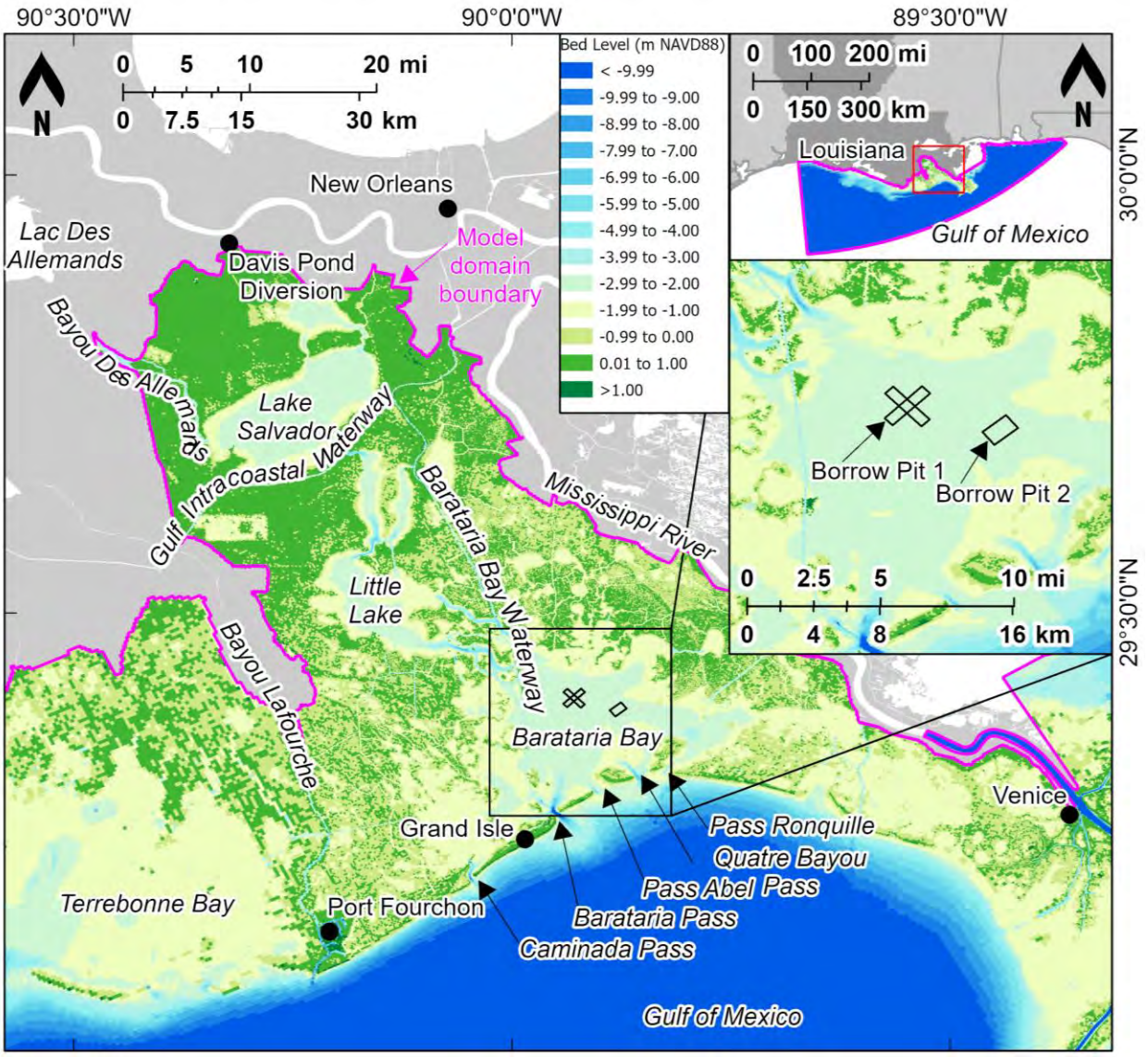

Figure 1. Study area map showing the topography and bathymetry of the numerical model domain (boundary depicted in magenta), along with geographic features of interest in this study. A version of this map focused on Barataria Bay and its surroundings can be found in Appendix A.2 (Figure A-3). The two hypothetical borrow pits evaluated in this study are also shown, i.e., Borrow Pit 1 in northwest-southeast and northeast-southwest orientation with a surface area of 1.65 km^2 (410 acres) and an excavation volume of ~10M m^3 (13M yd^3), and Borrow Pit 2 in northeast-southwest orientation with a surface area of 1.6 km^2 (400 acres) and an excavation volume of ~10M m^3 (13M yd^3). More details are provided in Table 2.

2.0 METHODS

2.1 MODEL SETUP AND DATA SYNTHESIS

This study leveraged a previously developed physics-based model (The Water Institute of the Gulf, 2022), which was updated, refined, and re-calibrated for use in this analysis (Appendix A). The model is based on the Delft3D Flexible Mesh (FM) modeling suite (Kernkamp et al., 2011) and includes coupled hydrodynamics (flow and waves), sediment transport, and morphology, using a mobile bed approach. The model domain, represented by an unstructured grid, includes the Barataria Basin extending north to Lake Des Allemands and extends east to the Mississippi River and west to Bayou Lafourche (Figure 1). The initial topography and bathymetry are based on the United States Geological Survey (USGS) digital elevation model (DEM) for the Northern Gulf of Mexico (Danielson et al., 2022), and are supplemented with data from Louisiana's System-Wide Assessment and Monitoring Program (SWAMP; Khalil et al., 2020). The model resolves the multiple tidal inlets fronting the basin, back-barrier lagoons and bayous, intertidal zones, and back-barrier marshes. Sediment transport and morphology are evaluated using six sediment fractions, consisting of fine sand, consolidated silt and clay, fluvial silt and clay, and organic mud. The model employs a spatially varying bed stratigraphy that is defined to independently represent the marshes, bay floor, and barrier islands (see Appendix A.4 for more details).

2.2 APPROACH AND MODEL FRAMEWORK

The modeling framework was set up to simulate morphological change over a 20-year period. The following representative conditions were simulated (Table 1): A) quiescent conditions in August 2015, which were selected based on a statistical analysis conducted using the methods described in Cobell et al. (2020); B) a period from October to March in 2015 that included the influence of cold fronts; and C) a 20-year storm sequence to include tropical cyclones. This storm sequence is derived from a synthetic 50-year storm sequence developed by Johnson & Geldner (2020; see Appendix A.3.2 for more details). Since it would have been computationally expensive to simulate hydrodynamics and morphodynamics for the full period of 20 years, a morphological time-scale factor was used to accelerate bed level change for the quiescent and cold front conditions. This factor allows for longer-term morphological changes to be obtained from shorter simulations of representative conditions, recognizing that morphological developments occur on much longer time scales than typical hydrodynamic changes. The approach was implemented and validated by Lesser et al. (2000; 2004) and has since been successfully used in coastal and deltaic applications by Roelvink (2006) and Li et al. (2018). These studies demonstrate that the application of acceleration methods does not significantly affect the simulated evolution of deltaic environments. The cold front season and quiescent conditions were upscaled by factors 10 and 60, respectively, while no upscaling was used for the tropical cyclones that were simulated sequentially at the end of each decade.

Table 1. Simulation set-up to represent a decade of mixed meteorological conditions. The offshore and riverine boundary conditions that were used force the model are presented in Appendix A.3.

Scenario	Simulation period	Morphological acceleration factor	Representative period
A) Quiescent conditions	August 2015	60	5 years
B) Cold fronts	October 2015–March 2016 (6 months)	10	5 years
C) Tropical cyclones	Individual storms from 2023 CMP synthetic tropical storm sequence (Johnson & Geldner, 2020)	1	< 1 month
TOTAL			10 years

The model included ESLR that is consistent with the "Lower" scenario used in the 2023 Louisiana CMP (White et al., 2021), which is based on NOAA's Intermediate scenario (Sweet et al., 2017) and ranged from 6 to 9 mm/yr over the 20-year simulation period. Subsidence was included using spatially variable rates which ranged from 2 to 7 mm/yr for the Barataria Basin (Applied Coastal Research and Engineering, 2018), with subsidence rates of approximately 7 mm/yr in the vicinity of the borrow areas in Barataria Bay. Marsh vertical accretion was assumed to keep pace with relative sea level rise (Kirwan et al., 2016), and dredging was implemented throughout the Barataria Bay Waterway (Figure 1) to maintain a navigable authorized depth of 3.65 m (12 ft).

To examine the influence of hypothetical borrow pit orientation on local to regional sediment dynamics, five scenarios (S1–S5, Table 2) were evaluated with different borrow area locations and orientations within Barataria Bay. Borrow Pit 1, which was evaluated with two different orientations, is situated in the northwest of Barataria Bay, approximately 5 km from the waterbodies that connect Barataria Bay to Little Lake. In contrast, Borrow Pit 2 is situated in the southeast of Barataria Bay, about 5 km from Quatre Bayou Pass and closer to the Gulf of Mexico but less proximal to inland marshes. Additionally, Borrow Pit 1 has a more elongate shape, with an aspect ratio (i.e., ratio of length and width) of approximately 4.5, while Borrow Pit 2 has an aspect ratio of 1.6. Both hypothetical borrow pits are situated in areas where there are indications of buried deposits of restoration-compatible sediments (Hollis et al., 2023).

Table 2. Evaluated borrow pit scenarios showing the orientation, pit dimensions, and resulting area and volume excavated for each scenario. The locations of the borrow pits are indicated in the inset of Figure 1.

Scenario	Description
S1	Future Without Action (FWOA), i.e., without borrow pits
S2	Borrow Pit 1 in northwest-southeast (NW-SE) orientation (2750×600×6 m^3/ 9000×2000×20 ft^3; 1.65 km^2/410 acres; Volume excavated ~10M m^3/13M yd^3)
S3	Borrow Pit 1 in northeast-southwest (NE-SW) orientation
S4	Borrow Pit 2 in northeast-southwest (NE-SW) orientation (1600×1000×6 m^3/ 5250×3200×20 ft^3; 1.6 km^2/400 acres; Volume excavated ~10M m^3/13M yd^3)
S5	Borrow Pit 1 in northwest-southeast (NW-SE) orientation and Borrow Pit 2 in northeast-southwest (NE-SW) orientation

2.3 MODEL CALIBRATION AND VALIDATION

The model was calibrated to ensure reasonable model skill in reproducing water levels, tidal phasing, tidal prism, wind waves, suspended sediment concentrations, and morphology. Water levels were calibrated using tidal harmonic analysis (Pawlowicz et al., 2002) performed at six stations across Barataria Basin (Appendix A.5, Figure A-15). At each location, the sum of tidal amplitudes between modeled and measured values for major diurnal constituents (K1, O1, P1, Q1) were compared, with differences ranging from 0.6 to 1.2 cm across stations. Non-tidal excursions were also captured reasonably well by the model (Appendix A.5, Figure A-16 through Figure A-21) with an average bias of -0.04 m and a root mean square error (RMSE) of 0.1 m. Based on guidance reported in Meselhe et al. (2017), all stations met the desired target of a %bias smaller than ±10% and %RMSE below ±15%. The correlation coefficients met the acceptable target as defined by Meselhe et al. (2017) with an average correlation coefficient of 0.83, with 5 out of 6 (83%) stations scoring above 0.8 (Appendix A.5, Table A-6). The largest disparities between measured and modeled data were observed at USGS station 073802516: Barataria Pass at Grand Isle. These discrepancies may be attributed to stratification effects caused by salinity gradients, which are not resolved in this depth-averaged model. However, there is significantly better agreement for the other USGS stations located in Barataria Bay, which are situated several kilometers away from the hypothetical borrow pits. A comparison of significant wave heights between modeled and measured values at two USGS stations in Barataria Bay (Appendix A.5, Figure A-26 through Figure A-29) also showed good agreement during higher energy events including Hurricane Laura in late August 2020 and during the passage of strong cold fronts in September of the same year. Simulated wave heights were overestimated during transitional conditions but exhibited good skill capturing both low and high energy events.

The combined cross-sectional area of the major tidal passes fronting the Barataria Bay (Caminada Pass, Barataria Pass, Pass Abel, Quatre Bayou Pass; Figure 1) was compared between the model and measured values reported in FitzGerald et al. (2007). Pass Ronquille was omitted from this comparison because of the absence of data for this specific pass in FitzGerald et al. (2007). In 2006 the cumulative tidal inlet cross-sectional area was 24,300 m^2 (262,000 ft^2, FitzGerald et al. 2007), while the model's initial cross-sectional area for the same tidal inlets in 2020 amounts to 26,600 m^2 (286,000 ft^2). The cross-sectional areas of individual inlets are also listed in Table A-7 (Appendix A.5.3). The discharge through the tidal inlets, as predicted by the model, was compared under comparable conditions for the major tidal passes fronting the Barataria Bay (Caminada Pass, Barataria Pass, Pass Abel, Quatre Bayou Pass, and Pass Ronquille; Appendix A.5.3). For example, the model predicted peak tidal discharges in Barataria Pass, ranging from up to 5,800 m^3/s during peak flood to 6,500 m^3/s during peak ebb, align with discharges observed during similar conditions by Li et al. (2011) and Ramatchandirane et al. (2019). These studies reported discharges ranging up to 6,500 m^3/s during peak flood and 7,500 m^3/s during peak ebb (Appendix A.5.3; Table A-8, Figure A-23A). These findings demonstrate that the model projections for Barataria Pass tend to be 10–15% lower compared to measurements. However, the model projections generally appear to be somewhat (~20%) larger for the other tidal passes, including Caminada Pass, Pass Abel, and Quatre Bayou Pass. When considering the major inlets combined, excluding Pass Ronquille, the combined peak ebb discharges is approximately 18,000 m^3/s as per model projections, closely resembling the value of 16,800 m^3/s found by Ramatchandirane et al. (2019; Appendix A.5.3, Table A-8). Flow velocity measurements through Barataria Pass were also compared with model predictions to assess model accuracy (Appendix A.5.3; Table A-9, Figure A-23B). Velocity measurements obtained from a 24-hour survey (Li et al., 2011) showed a range from 0.6 m/s near the channel bed to 1.3 m/s near the surface

at the center the channel. Additional velocity data from synoptic studies (Ramatchandirane et al., 2019) exhibited variations from 0.5 m/s near the banks to 1.0 m/s near the surface at the center of Barataria Pass. The model predictions for cross-sectional average flow velocity in Barataria Pass amounted to 0.75 m/s, which falls within the observed ranges by Li et al. (2011) and Ramatchandirane et al. (2019). Model-predicted peak velocities in Barataria Pass are approximately 30% larger compared to the other tidal passes. This aligns with the findings of FitzGerald et al. (2007), who compared Barataria Pass to the other tidal passes, and noted that it has a relatively small cross-sectional area considering its tidal prism. Despite the field flow measurements being taken at different times, when compared to the model predictions under similar environmental conditions, there is agreement between the model and measurements.

Suspended sediment concentrations collected during synoptic surveys in Barataria Pass (Li et al., 2011; Ramatchandirane et al., 2019) during tidal (quiescent) non-storm conditions compared favorably with model predictions, and typically range between 10–100 mg/L (Appendix A.5.3; Table A-10, Figure A-24 and Figure A-25). The modeled suspended sediment concentrations in Barataria Bay (Appendix B.1, Figure B-2e) were compared and calibrated against the bottom suspended sediment concentrations as measured by Li et al. (2021) over a period of four months during winter and spring in 2019. Model predictions of morphology along the shoreface of Caminada Headland and along the inlets of Barataria Bay were compared to previous studies of the geomorphic evolution of the Caminada Headland by Miner et al. (2009) and Beasley (2018). The model's morphology projections showed erosion on the order of 0.5 to 1 m at Barataria Pass and Pass Abel ebb-tidal deltas and flood deltas over the 20-year simulation period, more than 2 m at the tidal inlet throat, and on the order of 0.5 m of erosion along the eastern Caminada Headland shoreface. Observations along the same environments at a different period (1980–2006) by Miner et al. (2009) and Beasley (2018), showed shoreface change along the headland on the order of 1 m, and tidal inlet throat scour of the order of 2 m or more, and flood and ebb-tidal delta change on the order of 1 m. Moreover, the selected values of the parameters that describe sediment characteristics are consistent with typical literature values found in laboratory tests for systems with mud-sand mixtures as described by Van Rijn & Barth (2019). More information on the selected sediment parameters is provided in Appendix A.5.6.

3.0 RESULTS

3.1 HYDRODYNAMIC IMPACTS

For the baseline reference simulation without a borrow pit (S1; FWOA), the tidal prism for Barataria Basin is approximately 354 million m^3 by the end of the first decade (2020–2029), and increases by 12% in the second decade (2030–2039) to approximately 395 million m^3 (Table 3). The changes in tidal prism simulated by the model with borrow pits in place show similar results. Across the borrow pit scenarios examined, the simulated tidal prism is predicted to increase by approximately 0.01–0.03% during the first decade, and from 0.03–0.05% during the second decade. This constitutes a very small change that falls within the model's margin of error, and thus suggests that the modeled borrow pits have minimal to no influence on the tidal prism of the Barataria Basin over the 20-year simulation period (Table 3).

Table 3. Simulated average tidal prism for a 3-month period, combined for Caminada Pass, Barataria Pass, Pass Abel, Quatre Bayou Pass, and Pass Ronquille, across all borrow pit (BP) scenarios (S1 through S5). The numbers are depicted with a substantial number of significant digits, illustrating that the observed differences are well within the margin of error of the model.

Scenario	First decade (2020–2029)		Second decade (2030–2039)	
	Tidal Prism (million m^3)	Ref. to FWOA	Tidal Prism (million m^3)	Ref. to FWOA
S1: FWOA	353.60	-	394.74	-
S2: BP1, NW-SE	353.67	0.02%	394.86	0.03%
S3: BP1, NE-SW	353.51	-0.03%	394.69	-0.01%
S4: BP2, NE-SW	353.57	-0.01%	394.76	0.01%
S5: BP1 (NW-SE), BP2 (NE-SW)	353.64	0.01%	394.92	0.05%

In contrast to tidal prism results, local hydrodynamics are noticeably influenced by borrow pits (Figure 2). Water level response due to the passage of cold fronts ("meteorological tides") is typically characterized by pre-frontal southerly winds that increase water levels in Barataria Bay, followed by northerly winds after the passage of the cold front leading to a rapid lowering of water levels (Figure 2a; Feng & Li, 2010; Li et al., 2019). Water level excursions are noticeable during the simulation period, with excursion magnitudes ranging from 0.1–0.3 m during pre-frontal conditions, and from 0.3–0.5 m during post-frontal conditions (Figure 2), with corresponding sediment transport results that corroborate trends reported in Li et al. (2021) related to bay sediment redistribution and export from the Barataria Basin. Significant wave heights at the borrow pit site (Figure 2b) are consistently up to 15% higher with the pit present, regardless of the borrow pit configuration considered (Appendix B.1, Figure B-2). This increase was observed not only during cold fronts but also during tropical cyclones (Appendix B.1, Figure B-3 through Figure B-9). Flow velocities are lower within the pit during non-frontal conditions but can be significantly higher (0.2–0.3 m/s) during the peak of the cold front (Figure 2c, Figure 3).

In most, but not all, cases during both cold fronts and tropical cyclones, the smallest decrease in flow velocities occurs for Borrow Pit 1 in the NW-SE orientation (S2), while the largest decrease is observed for Borrow Pit 2 in the NE-SW orientation (S4; see Appendix B.1, Figure B-2b)..

High-energy events, such as cold fronts, can change the flow patterns in the vicinity of borrow pits, leading to an increase in flow velocities both at and around the borrow pits. During the pre-frontal southerly winds that occur several hours before the passage of a cold front, above-average northwesterly currents are typically observed in Barataria Bay. However, within Borrow Pit 1 (i.e., the western borrow pit) in NW-SE orientation, relatively strong currents in the opposite (southeastern) direction are present (Figure 3a). As the cold front passes and wind-driven water level set-up begins to decrease, stronger ebb currents occur (Figure 3b). During this time, Borrow Pit 1 appears to act as a funnel for the currents, resulting in higher flow velocities at and around the borrow pit when compared to the surrounding areas of Barataria Bay. The phenomenon of increased flow velocities within the pit is also observed for Borrow Pit 1 in NE-SW orientation, albeit on a smaller number of occasions and with a less significant increase in velocities compared to the same pit in NW-SE orientation. Borrow Pit 2 (in NE-SW orientation) experiences this phenomenon the least. For all borrow pit configurations, and under both cold front conditions and tropical cyclones, the corresponding wave-current bed shear stress (Figure 2d, Figure 3) is substantially lower within the borrow pit despite increases in wave heights and flow velocities (Figure 2b,c).

Detailed results and maps of the influence of high energy events such as cold fronts and tropical cyclones can be found in Appendix B.

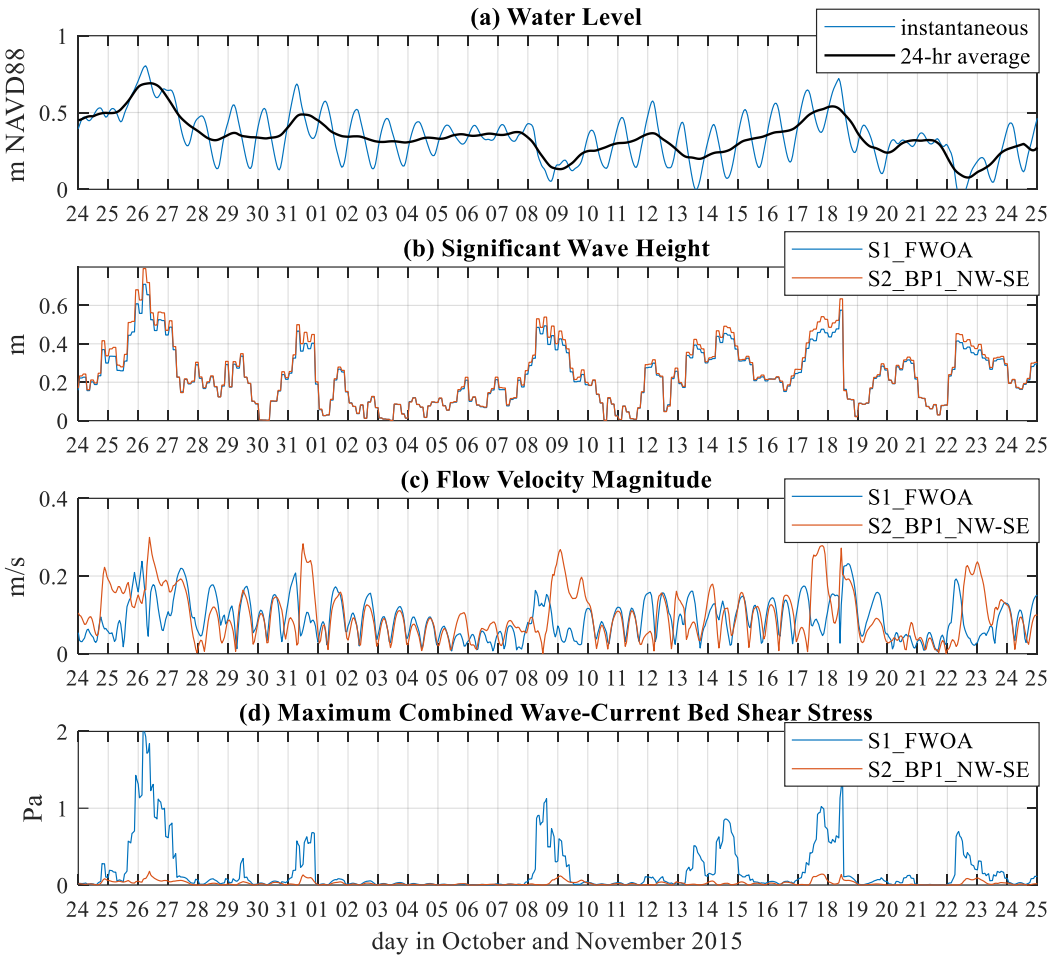

Figure 2. Simulated (a) water level, (b) significant wave height, (c) flow velocity magnitude, and (d) combined wave-current bed shear stress (at the center of Borrow Pit 1) for Scenario 1 (FWOA) and Scenario 2 (Borrow Pit 1 in NW-SE orientation) during the passage of several cold fronts between October 24 and November 25, 2015. Wave heights show a small difference (up to 15%), while the wave-current bed shear stresses are an order of magnitude lower, indicating a non-linear response. Appendix B.1 contains similar timeseries figures for the full 6-month simulation period, for all borrow pit configurations, and for the quiescent conditions and tropical cyclones.

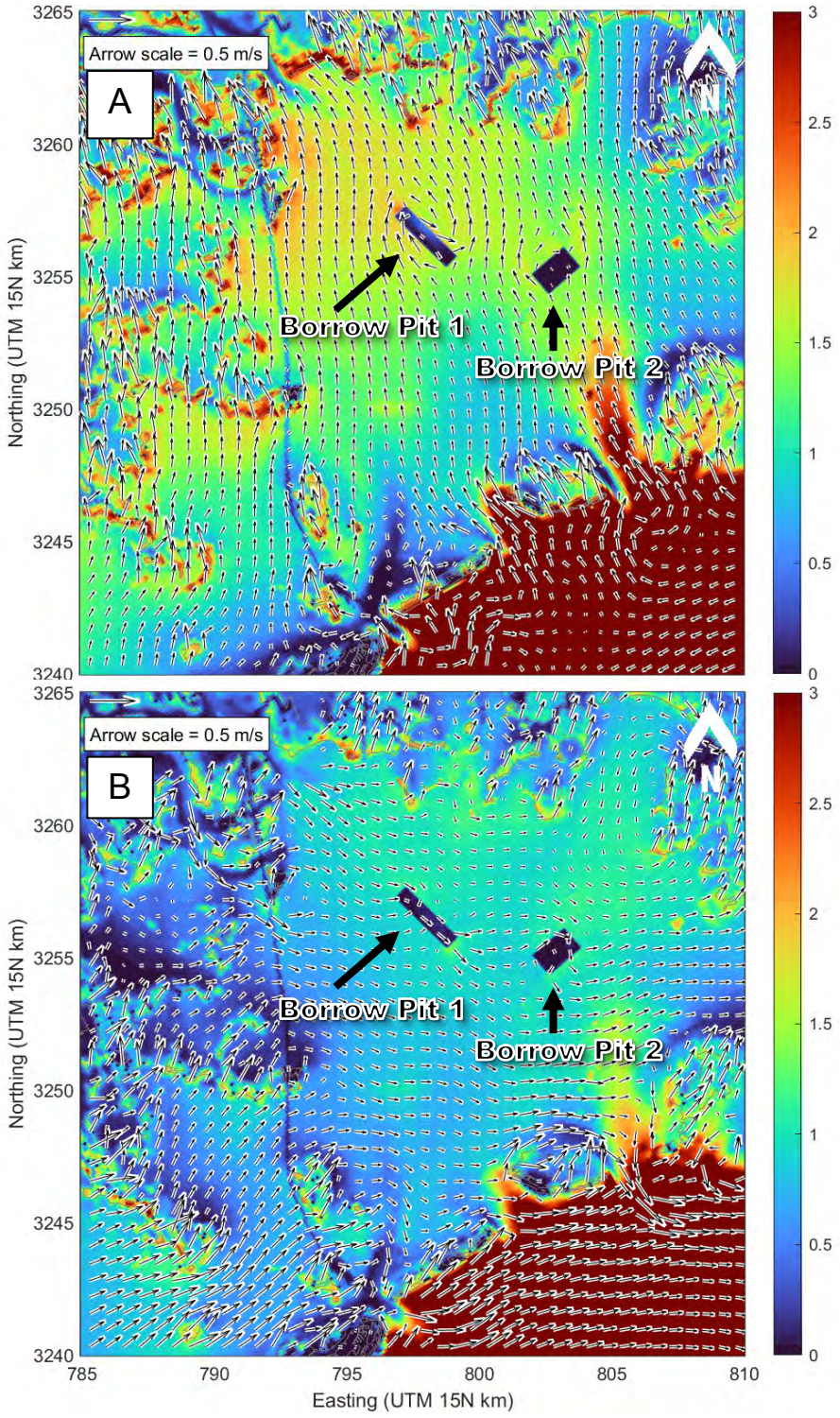

Figure 3. Instantaneous bed shear stress (Pa, combined wave+current) for Scenario 5 (Borrow Pit 1 in NW-SE orientation and Borrow Pit 2) on October 26, 2015, along with flow velocity vectors for Scenario 5, during relatively strong pre-frontal southerly winds several hours before the passing of a cold front (Figure A, at 6 am) and during the passing of the same cold front 12 hours later (Figure B, at 6 pm). Appendix B contains a larger version of these figures (Figure B-10 and Figure B-12) and supplemental figures (Figure B-11 and Figure B-13) that show the water level and wind vectors for the same area at the same points in time.

3.2 MORPHOLOGIC IMPACTS

3.2.1 Sediment Dynamics in Barataria Bay

Sediment concentrations in Barataria Bay (Figure 4a) increase at the onset of a passing cold front, especially when significant wave heights exceed 0.4 m. Model results indicate negligible differences in sediment concentrations in Barataria Bay with borrow pits present (Figure 4a), which is expected since the area occupied by the borrow pits is small compared to the area of the bay. Bed level change in Barataria Bay (Figure 4b) and within the borrow pits (Figure 4c) shows a punctuated response to high-energy events such as cold front passages and tropical cyclones. On a decadal timescale, model results show degradation and subsidence of the Barataria Bay floor that varies between 10–15 mm/year for all scenarios, of which approximately 6 mm/year can be attributed to subsidence alone (Appendix B.4). The presence of borrow pits increases erosion of the bay floor on the order of 10% compared to the no pit scenario. Borrow pit infilling takes place simultaneously with bay floor erosion, suggesting that sediment removed from the bay is likely to be captured by the borrow pits. The model indicates a net export of sediment from the Barataria Basin (Figure 4d), which is consistent with prior research that has characterized the basin as ebb-dominant (FitzGerald et al., 2004). Sediment export is enhanced during cold front passages due to the rigorous water and sediment volumes that are exchanged. The presence of borrow pits has minimal (<1%) influence on the export of sediment for the locations, pit dimensions, orientations, and conditions examined in this study (Figure 4d).

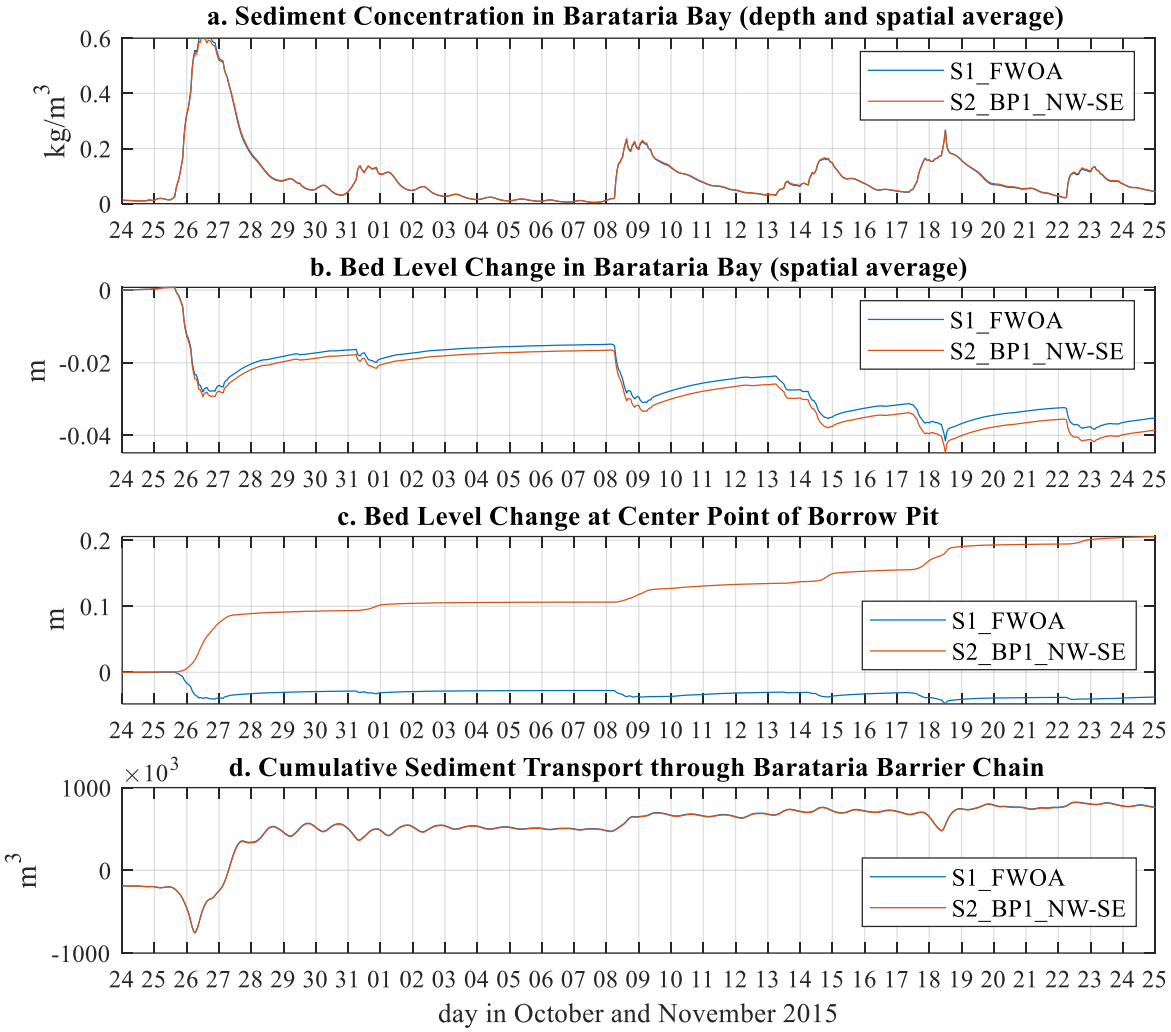

Figure 4. Modeled (a) sediment concentration, (b) upscaled bed level change, spatially averaged across Barataria Bay, (c) upscaled bed level change at the center of Borrow Pit 1, and (d) cumulative sediment transport (export = positive) through the Barataria Barrier Chain , i.e., Caminada Pass, Barataria Pass, Pass Abel, Quatre Bayou Pass, and Pass Ronquille, for S1 (FWOA) and S2 (Borrow Pit 1 in NW-SE orientation) during the passage of several cold fronts in between October 24 and November 25 of 2015. Appendix B.1 contains similar timeseries figures for the full 6-month simulation period, for all borrow pit configurations, and for the quiescent conditions and tropical cyclones.

3.2.2 Borrow Pit Infilling

Borrow pit infilling is of comparable magnitude across pit locations and orientations, resulting in infilling amounts ranging between 1.39 and 1.54 m after a period of 20 years (Table 4). This equates to an average infilling rate of approximately 0.75 m per decade or 0.075 m (0.25 ft) per year. When compared to the excavation volume of the borrow pits, estimated to be ~10M m^3 (13M yd^3, Table 2), the infilling rates represent ~12% of the initial excavation volume per decade. Borrow Pit 2 (S4 and S5) experiences infilling rates that are almost 6% higher than those in Borrow Pit 1 (S1 and S2). The influence of meteorological conditions on borrow pit infilling is shown in Table B-2 in Appendix B, revealing that the majority (>80%) of infilling occurs during cold fronts, while a significantly smaller portion (<20%) takes place during tropical storms. Minimal infilling (~2%) occurs during quiescent conditions. To verify the model, the simulated infilling rate (Table 5) of approximately 0.075 m (0.25 ft) per year was compared to

measured infilling rates that are described in the previous BAMM study by CB&I (2015). In the CB&I (2015) synthesis, in-bay borrow areas that are not exposed to significant sources of fluvial sediment were selected to compare with the model. One of these sites is located along the north shore of Lake Pontchartrain near Goose Point and experienced measured infilling of 0.12 m/year (0.4 ft/year), while the other two sites are located in Barataria Basin: Little Lake and the Barataria Basin Landbridge borrow areas and experienced infilling from 0.06 to 0.21 m/year (0.2 to 0.7 ft/year), respectively. Given this range of measured rates, especially those of Goose Point and Little Lake, the model agrees well with observations. More comprehensive information on the infilling rates from the BAMM synthesis can be found in Appendix C.

Table 4. Borrow pit infilling volumes and corresponding infilling rates after 20 years for all borrow pit (BP) scenarios (S1 through S5).

	Volume infilled after 20 years (million m^3)		Vertical infilling after 20 years (m)		Vertical infilling rate (m/year)	
Scenario	**Borrow Pit 1**	**Borrow Pit 2**	**Borrow Pit 1**	**Borrow Pit 2**	**Borrow Pit 1**	**Borrow Pit 2**
S1: FWOA	-	-	-	-	-	-
S2: BP1, NW-SE	2.32	-	1.41	-	0.070	-
S3: BP1, NE-SW	2.36	-	1.43	-	0.072	-
S4: BP2, NE-SW	-	2.47	-	1.54	-	0.077
S5: BP1 (NW-SE), BP2 NE-SW	2.30	2.44	1.39	1.53	0.070	0.076

Table 5. Comparison between modeled and measured infilling rates from previous BAMM study by CB&I (2015). The vertical infilling rates represent a spatial average for the entire borrow pit. Local infilling rates may vary across the pit and could be either higher or lower than the average. More details including the exact locations of the measured borrow areas can be found in Table C-1 in Appendix C.

Borrow area		Borrow pit surface area (km^2)	Vertical infilling rate	
			(m/year)	(ft/year)
Modeled in this study (more details in Table 4)	Borrow Pit 1	1.65	0.07	0.24
	Borrow Pit 2	1.60	0.08	0.26
Measured at comparable in-bay borrow areas (more details in Appendix C)	Little Lake (Barataria Basin)	5.2	0.06	0.2
	Barataria Basin Landbridge (just north of Little Lake)	0.8 to 1.5 for each the three pits (~4 km^2 combined)	0.21	0.7
	Goose Point (Lake Pontchartrain)	0.6	0.12	0.4

3.2.3 Regional Borrow Pit Impacts

During long-term simulations, the morphologic evolution of the basin is influenced by environmental forcing, such as sea level rise, subsidence, and other assumptions related to the dynamics of the marshes, making it difficult to isolate the influence of additional variables such as the presence of borrow pits. To isolate the influence of borrow pits alone, a baseline simulation (S1) was conducted using the same

environmental forcing but did not include the borrow pits. Borrow pit impacts, isolated from other morphological change driven by environmental conditions, were then obtained by subtracting bed level change between scenarios with and without pit (Figure 5). The borrow pits exhibited reworking of sediment around the pit perimeters as a response to the bathymetric transition between bay and pit, with erosion rates of more than 0.15 m extending up to 1 km from the pit perimeter. Centimeter-scale impacts extend more than 5 km away from the borrow pits at locations proximal to tidal inlets and marshes, and along the section of Barataria Bay Waterway that is located within the bay (Figure 5).

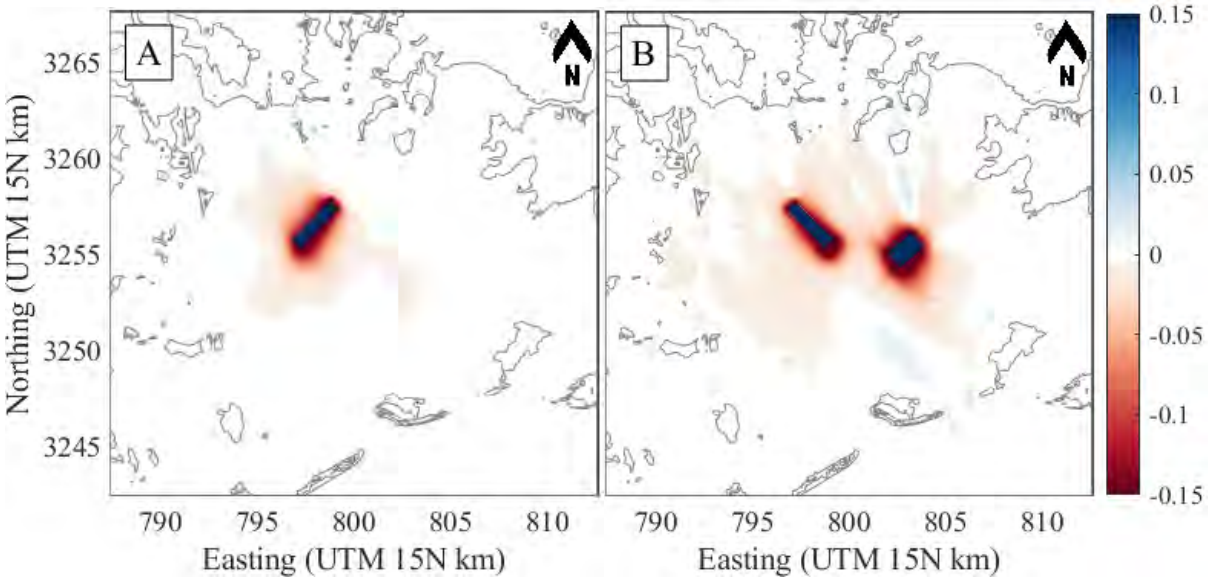

Figure 5. Modeled bed level change (m) differenced to FWOA for (A) S3 (Borrow Pit 1 in NE-SW orientation) and (B) S5 (Borrow Pit 1 in NW-SE orientation and Borrow Pit 2 in NE-SW orientation) after 10 years. Appendix B.5 contains larger maps for all scenarios with differenced bed level change after the full simulation period of 20 years.

Volumetric changes in the borrow pits and Barataria Bay were quantified for the entire 20-year simulation period (Table 6). Model results suggest that borrow pits exhibit differential infilling across scenarios (S2–S5; 2.3–2.5 million m^3 per borrow pit). The total volumetric changes in Barataria Bay outside of the borrow pit footprints (i.e., not considering the infilling that occurs within the borrow pits for scenarios where they are present) indicate sediment loss of 25 to 30 million m^3 (Table 6; column 1) which is at least ten times the volume captured by the borrow pits. Regardless of scenario, including the scenario without a borrow pit, the ongoing bay erosion is an order of magnitude larger than the additional erosion caused by the presence of a borrow pit. The net effect of borrow pits on Barataria Bay outside of pit footprints (Table 6; column 3) is of the same order as the borrow pit infilling volumes (Table 6; column 1), suggesting that most of the sediment that is captured by the borrow pits most likely originates from Barataria Bay.

Borrow pits do not adversely impact marshes peripheral to Barataria Bay, as evidenced by a volumetric analysis that assessed impacts beyond the bay (Table 6; columns 4 and 5). The scenarios with borrow pits (S2–S5) reduce the loss of sediment from the marshes by between 20,000 and 60,000 m^3 (Table 6; column 5) when compared to the baseline no pit simulation (S1). These volumes, however, are relatively

small, representing only 1–2% of the absolute loss of sediment volume for all scenarios (which ranges between 3.52–3.58 million m^3; Table 6; column 4).

Sediment export volumes driven by tidal and high-energy event-induced exchange through the basin's major tidal inlets were quantified to evaluate borrow pit impacts on sediment exchange (Table 6; columns 6 and 7). Model results show that the sediment exchange between Barataria Basin and Barataria Bight through the five major tidal inlets in the absence of borrow pits is approximately 91.4 million m^3, and varied marginally when borrow pits are present. Results also show that S2 increased sediment export by approximately 70,000 m^3, while S3, S4, and S5 decreased sediment export by 30,000 m^3, 250,000 m^3, and 240,000 m^3 respectively (Table 6, column 7). However, the difference in sediment export between the scenarios is small compared to the absolute volume of sediment export (~91.1–91.5 million m^3; Table 6, column 6). Moreover, the increase or decrease in sediment export volumes between scenarios is also small compared to borrow pit infilling volumes (~2.4 million m^3; Table 6, column 1). The largest reduction of sediment export volume is 250,000 m^3 for Borrow Pit 2 as tested in Scenario 4 (Table 6, column 7), which represents approximately 0.3% of the absolute export volumes (Table 6, column 6), and about 10% of the infilled volumes (Table 6, column 1).

Table 6. Volumetric changes over a 20-year period for all borrow pit (BP) scenarios (S1 through S5), including changes within the Borrow Pits (first column), Barataria Bay (second and third columns), the periphery of Barataria Bay (fourth and fifth columns), as well as sediment export volumes from the Barataria Basin (sixth and seventh columns). Figure 6 shows a map with indicators of the areas that were considered in this analysis.

	Volumetric Change (million m^3)					**Sediment Export Volume (million m^3)**	
	Borrow Pit(s) (i.e., infilling, more details in **Table 4**)	Barataria Bay Outside of Borrow Pit Footprint(s)		Periphery of Barataria Bay*		From Barataria Basin**	
		Absolute	Ref. to FWOA	Absolute	Ref. to FWOA	Absolute	Ref. to FWOA
Scenario	*Column 1*	*Column 2*	*Column 3*	*Column 4*	*Column 5*	*Column 6*	*Column 7*
S1: FWOA	-	-26.46	-	-3.58	-	91.43	-
S2: BP1, NW-SE	**2.32**	-28.89	**-2.43**	-3.56	**0.02**	91.50	**0.07**
S3: BP1, NE-SW	**2.36**	-28.83	**-2.37**	-3.56	**0.02**	91.39	**-0.03**
S4: BP2, NE-SW	**2.47**	-28.84	**-2.38**	-3.52	**0.06**	91.18	**-0.25**
S5: BP1 (NW-SE), BP2 (NE-SW)	**4.74**	-31.17	**-4.71**	-3.53	**0.05**	91.19	**-0.24**
* Area extending up to 10 km upland from the Barataria Bay Perimeter (Figure 6) ** Measured at Caminada Pass, Barataria Pass, Pass Abel, Quatre Bayou Pass, Pass Ronquille (Figure 6)							

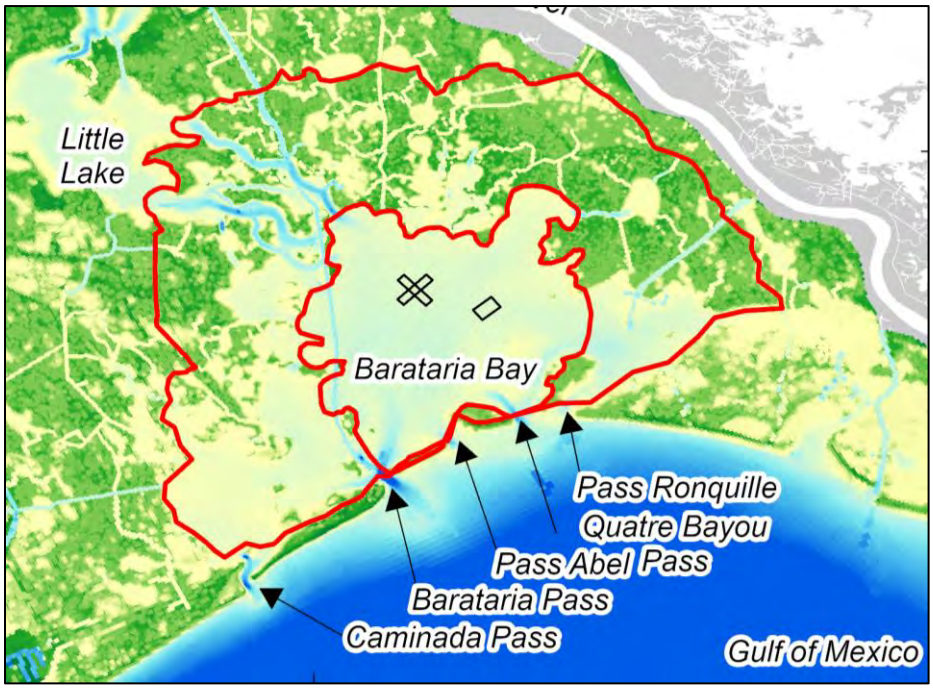

Figure 6. Map with polygons indicating the areas considered for the volumetric analysis in Table 6. The innermost red polygon represents Barataria Bay, while the periphery of Barataria Bay is represented by the area between the larger and smaller red polygons.

4.0 DISCUSSION, CONCLUSION, AND RECOMMENDATIONS

4.1 TIDAL PRISM

The study results suggest that the effect of in-bay sediment mining on the tidal prism of Barataria Bay is negligible (<<1%) and is within the model margin of error. Tidal prism is proportional to the bay surface area (D'Alpaos et al., 2010; Jarrett, 1976), hence the volume of water (and corresponding surface area) added to the basin through the excavation of the borrow pits does not influence the tidal prism since the bay surface area does not change. Moreover, the increase in depth caused by the excavation of the pits does not contribute to changing the bottom friction characteristics of the bay, except locally, in a way that would alter the tidal wave propagation, change tidal asymmetry, and increase tidal prism (Dronkers, 1986). This study evaluated two borrow pits in the middle of the bay, covering an area of approximately 1% of the total bay surface area. However, the study did not evaluate an exhaustive set of scenarios or multiple locations of borrow pits in which a more direct impact may occur.

4.2 LOCAL HYDRODYNAMICS

Regardless of their size, depth, and orientation, the borrow pits do influence local hydrodynamics, especially during higher energy events such as cold fronts and tropical cyclones. While the borrow pits do not influence local water levels, they cause an increase in wave heights of up to 15% locally; the increased water depth following the excavation of the pits supports larger waves over the pit. In turn, and despite the slight increase in wave heights, the increase in depth lessens the wave-driven bottom shear stress throughout the pits (Figure 3) and thus promotes deposition (Figure 4c). It should be noted that multiple pits spread across the bay floor could have a cumulative influence that extends beyond those observed at each pit, and might have potential regional impacts to the bay wave climate, circulation, and thus bay floor, that this study did not consider. Model results suggest that borrow pit orientation does not influence regional circulation; however, pit orientation does alter local circulation patterns during more energetic events such as cold fronts and tropical cyclones. One example that describes the anticipated change in the local circulation occurs during the peak of the storms. During pre-frontal or pre-storm conditions, winds from the southeast cause water level to set up along the northern region of the Barataria Bay perimeter, leading to a southerly directed return flow through the pits generating higher flow conditions through the pit with increased velocity (Figure 2c, Figure 3a). Pit orientations where the pit length aligns with the direction of the return flow funnel water more efficiently through the pit during these conditions. In contrast, pit orientations where the width is aligned with the general direction of the return flow are less likely to develop higher velocity conditions. However, despite these less favorable conditions for deposition, the borrow pits remain depositional during the storm and continue to infill (Figure 4c). It should be noted that excavation of multiple borrow pits across the bay may influence regional circulation patterns, the cumulative impacts of which this study did not consider.

4.3 BORROW PIT INFILLING

The borrow pits evaluated in this study infill at a rate of approximately 120,000 m^3/year (Table 4), and the results suggest that there are small differences in infilling of less than 7% among the different borrow pit

configurations tested. Specifically, Borrow Pit 1 (in NW-SE orientation) displayed the lowest infilling rates, while Borrow Pit 2 (NE-SW) showed the highest infilling rate within an approximate difference of 7 %. Borrow Pit 2 is rectangular but has a lower aspect ratio of width to length than Borrow Pit 1, which may partly explain the higher infilling rate. Borrow Pit 2, however, is located closer to the tidal inlets, and thus the large sediment exchange between the bay and Barataria Bight may also be the reason infilling is higher. Simulated vertical infilling rates for the borrow pits evaluated are approximately 0.075 m/year (0.25 ft/year) which is of the same order as measured rates of infilling that vary between 0.06 to 0.21 m/year (0.2 to 0.7 ft/year) for comparable in-bay borrow areas that are not exposed to significant sources of fluvial sediment (Table 5). One of the pits with similar environmental conditions is located in Lake Pontchartrain, near Goose Point; the fetch in the vicinity of Goose Point is higher compared to Barataria Bay, but with a similar depth, the wave energy arriving at this borrow pit could be similar to the ones studied here in Barataria Bay. Moreover, Goose Point is sheltered from northerly winds, which can be stronger post storm, and aid in directing sediment already in suspension toward the borrow pit. Goose Point, unlike the evaluated hypothetical borrow pits located in the middle of Barataria Bay, is located near the northern rim of Lake Pontchartrain, where wind driven currents along the lake perimeter are swift and in excess of 0.2 m/s (Georgiou & McCorquodale, 2000; Haralampides et al., 2000; Huang et al., 2020), can transport sediment entrained from the onset of a storm toward the borrow pit, maximizing the opportunity for sediment deposition. Model results suggest that cold fronts are the dominant (>80%) driver of borrow pit infilling, while tropical cyclones make a lesser contribution to infilling (<20%). During periods of heightened storm activity, the contribution to infilling from tropical cyclone activity might increase. However, given the frequency of cold fronts, tropical cyclones are not expected to become the dominant driver of infilling even during active hurricane seasons.

4.4 REGIONAL SEDIMENT DYNAMICS

The sediment captured by the borrow pits is mainly (>90%) sourced from the Barataria Bay floor, specifically the areas proximal to the borrow pit excavation footprint, where the model predicts decimeter-scale erosion (Figure 5). Model results also suggest that all but one of the evaluated borrow pits contribute to reduced sediment export from the bay overall, because they serve as a sediment sink for the system which traps sediment that would otherwise be exported to the Gulf (Table 6). For example, Borrow Pit 2 is the most effective in reducing sediment export at tidal inlets; over the 20-year simulation period, the reduction in sediment export is approximately 250,000 m^3, corresponding to 0.3% of the absolute sediment export volume (which is of the order of 91 million m^3) or 10% of the sediment volume captured by the borrow pit. Similarly, Borrow Pit 1 slightly increases or decreases sediment export depending on the orientation, suggesting that orientation is a relevant factor. However, the difference in sediment export between the two orientations of Borrow Pit 1 is small (~100,000 m^3 over 20 years), on the order of 0.1% of the absolute sediment export volumes, or less than 4% of the sediment volume captured by the borrow pit (~2.4 million m^3). Overall, this response suggests that while borrow pits do slightly change (i.e., decrease for most pit configurations) sediment export from the Barataria Bay system, the changes in sediment volumes are only a small fraction (<1%) of the absolute sediment volumes that are being exported via tidal inlets.

Sediment trapping by the borrow pits evaluated in this study does not adversely impact marshes peripheral to Barataria Bay. A volumetric analysis conducted to evaluate sediment fluxes at the marsh-bay interface shows a negligible net influx of sediment to the marsh (Table 6). This suggests that the

borrow pits do not change present-day conditions and attendant sediment exchange between the bay and the marsh. Recognizing that this study did not evaluate borrow pits proximal to the marsh edge, it is prudent to note that if pits are situated at locations different from those evaluated in this study, the results may change and thus produce a different outcome. Similarly, the evaluated borrow pits have little to no influence on other distal environments, such as the tidal inlets fronting the bay (Figure 5). However, more significant impacts on inlet morphology and sediment exchange are expected when placing borrow pits proximal to the tidal inlets. Additionally, each of the investigated pits covers only 0.5% of the total surface area of Barataria Bay. Therefore, additional simulations and analysis are therefore necessary to evaluate other borrow pit locations and orientations beyond the scenarios evaluated during this study.

4.5 RECOMMENDATIONS ON BORROW PIT GEOMETRIC DESIGN AND SITING

- When planning and designing borrow pits, it is important to consider the effect of pit orientation. The retention capacity and sediment-reducing ability of a borrow pit differs between the two orientations of Borrow Pit 1. The NE-SW oriented version of Borrow Pit 1 exhibited a higher infilling rate, resulting in a small reduction of sediment exported from the Barataria Basin. Contrastingly, Borrow Pit 1 in the NW-SE orientation had a somewhat lower infilling rate and caused a small increase in sediment export. This difference may be due to the orientation of Borrow Pit 1 in NW-SE which is in alignment with the direction of the tidal currents in Barataria Bay, which also flows in the NW-SE direction, leading to flow funneling within the borrow pit, especially during high-energy conditions. Borrow Pit 2 was only evaluated in the NE-SW orientation and experienced the greatest infilling rates, making it the most effective at reducing sediment export. This improved performance could be partially attributed to its location, but also due to its orientation and a more square design. Theoretically, borrow pits that approach the dimensions of a square might have a higher potential to capture sediment, as they receive a broader spectrum of flow and incoming wave energy, which can create conditions that are conducive to sedimentation.
- It is recommended to locate borrow pits at a considerable distance, i.e., several kilometers away, from proximal marshes and tidal inlets. Over the 20-year period projected in the study, the borrow pits had noticeable impacts, albeit at a centimeter-scale, extending over 5 km from the pit location. These impacts could be more significant when borrow pits are situated closer to proximal marshes or tidal inlets than evaluated in this study. For instance, borrow pits that are close to tidal inlets or near flood tidal deltas could influence the propagation of the tidal wave and thus could influence the tidal prism. Similarly, borrow pits (or multiple borrow pits combined) situated in areas where they could influence conveyance of the incoming tide, thus influence tidal range, may have the potential to influence tidal prism. Furthermore, placing borrow pits proximal to marsh shorelines may have a different outcome. For instance, even if morphological changes are similar in magnitude to those predicted for pits positioned in the bay center (Figure 5), the predicted footprint of change would suggest that some marsh-shoreline impacts could be expected. Therefore, it is recommended to conduct further studies exploring additional pit configurations to gain a better understanding of the distances from proximal marshes or tidal inlets at which pits may begin to adversely impact these areas.

- The design of multiple borrow pits within the same bay should consider potential cumulative regional impacts that extend beyond what was found in this study. Examples include changes to the bay wave climate, circulation, and thus morphology of the bay floor, tidal inlets, or proximal marshes.

4.6 RECOMMENDATIONS ON MONITORING

Based on the analysis conducted in this report to evaluate the consequences of using borrowed sediment from inter-distributary bays, the following recommendations are proposed:

- Additional field investigations and monitoring is recommended to improve understanding of the hydrodynamics within and around borrow pits, consistent with recommendations made previously by CB&I (2015). This recommendation is due to the complex flow patterns around borrow pits, which can result in three-dimensional flow conditions and intricate wave transformation across the abrupt bathymetric transitions that occur near the borrow pits. These field conditions challenge numerical models, and additional observations will help close the gap and allow for model ground truthing, improved model skill, and insights into these complex processes.
- To understand sediment transport mechanics and short-term morphological changes in the bay floor during higher energy events like cold fronts and tropical storms, targeted monitoring and research are necessary. Current observations of suspended sediment concentrations in Barataria Bay during such events are limited. The study conducted by Li et al. (2021) provided valuable insights into near-bottom suspended sediment concentrations, but additional measurements of suspended sediment throughout the water column (using hydroacoustic/backscatter sensors or automatic samplers) and at multiple locations within interior bays would benefit the BAMM program. These expanded observations would enhance the understanding of the dynamic processes of sediment entrainment, transport, and deposition during high energy conditions. These high energy events, as indicated by model results, play a significant role in sediment erosion and deposition, which directly affect bay erosion and borrow pit infilling processes.
- Cost effective repeat bathymetry collection at annual to sub-decadal timescales in Barataria Bay, or within similar interior bays that may contain potential borrow pits, would provide insight into the processes that influence long-term subaqueous morphological evolution of the bay floor. Widely spaced single beam surveys spanning the bays can still be useful for evaluating bay floor evolution, especially if repeated along re-occupied transects. These observations would further support predictions of long-term future changes of interior bays, and simultaneously document the potential impact of anthropogenic activities resulting from these changes.
- The current understanding of borrow pit infilling dynamics and the origin of infilled sediment is limited. Model results suggest that 90% of infilled sediment originates from erosion of the Barataria Bay floor, but the source of the infilled sediment may vary for borrow pits located in other areas. Moreover, the source of the sediment may change after the construction and operation of the Mid-Barataria Sediment Diversion. Repeat hydrographic surveys (bathymetry) at annual and inter-annual timescales would elucidate processes and conditions that lead to infilling and provide field-derived infilling rates during the cold front season. These higher frequency

datasets would provide insights into the role of cold fronts and tropical cyclones on infilling and a more comprehensive evaluation of volumetric rates at those timescales. Finally, seismic surveys, vibracoring, and radioisotope dating could be considered to obtain more conclusive evidence on the origin of the infilled sediment. These recommendations build upon previous recommendations by CB&I (2015) to enhance bathymetric data collection and improve the understanding of the composition of the bay floor and borrow pit infilled sediment.

5.0 REFERENCES

Allison, M. A., Demas, C. R., Ebersole, B. A., Kleiss, B. A., Little, C. D., Meselhe, E. A., Powell, N. J., Pratt, T. C., & Vosburg, B. M. (2012). A water and sediment budget for the lower Mississippi–Atchafalaya River in flood years 2008–2010: Implications for sediment discharge to the oceans and coastal restoration in Louisiana. *Journal of Hydrology*, *432–433*, 84–97.

Applied Coastal Research and Engineering. (2018). *Determining recent subsidence rates for Barataria Basin, Louisiana: Implications for engineering and design of coastal restoration projects* (Final Report prepared for Louisiana Coastal Protection and Restoration Authority. Contract 4400009020, Task 3.) (p. 70).

Ardaman & Associates. (2017). *Field and laboratory data collection phase: West Fourchon Marsh Creation & Nourishment (TE-134)* (Draft) (p. 176). Lafourche Parish: Ardaman & Associates. Prepared for Coastal Protection and Restoration Authority.

Ardaman & Associates. (2018). *Caminada Headlands Back Barrier Marsh Creation Increment l (BA-171): Marsh fill settlement re-evaluation* (Geotechnical Engineering Report No. 17- 2810B) (p. 42). Lafourche & Jefferson parishes, Louisiana: Ardaman & Associates. Prepared for Coastal Protection and Restoration Authority.

Beasley, B. (2018). *Coupled barrier island shoreline and shoreface dynamics*. University of New Orleans, New Orleans, LA.

Blum, M. D., & Roberts, H. H. (2009). Drowning of the Mississippi Delta due to insufficient sediment supply and global sea-level rise. *Nature Geoscience*, *2*(7), 488–491.

Booij, N., Ris, R. C., & Holthuijsen, L. H. (1999). A third-generation wave model for coastal regions: 1. Model description and validation. *Journal of Geophysical Research: Oceans*, *104*(C4), 7649–7666.

Byrnes, M. R., Britsch, L. D., Berlinghoff, J. L., Johnson, R., & Khalil, S. (2019). Recent subsidence rates for Barataria Basin, Louisiana. *Geo-Marine Letters*, *39*(4), 265–278.

Caldwell, R. L., & Edmonds, D. A. (2014). The effects of sediment properties on deltaic processes and morphologies: A numerical modeling study. *Journal of Geophysical Research: Earth Surface*, *119*(5), 961–982.

CB&I. (2015). *Louisiana Borrow Area Management and Monitoring (BAMM) Program* (p. 30). Boca Raton, Florida: CB&I Government Solutions.

Cobell, Z., Sable, S., & Rose, K. A. (2020). *Calcasieu Ship Channel Salinity Control Measures Project (CS-0065): Larval Transport Modeling* (No. CS-0065) (p. 106). Baton Rouge, LA: The Water Institute of the Gulf. Produced for and funded by the Coastal Protection and Restoration Authority.

Couvillion, B. (2017). *2017 Coastal Master Plan Modeling: Attachment C3-27: Landscape Data. Version Final*. (pp. 1–84). Baton Rouge, LA: Coastal Protection and Restoration Authority.

Couvillion, B. R., Beck, H., Schoolmaster, D., & Fischer, M. (2017). *Land area change in coastal Louisiana from 1932 to 2016* (U.S. Geological Survey Scientific Investigations Map No. 3381) (p. 16). Reston, VA: U.S. Geological Survey.

CPRA. (2023). *Louisiana's Comprehensive Master Plan for a Sustainable Coast* (4th Edition, Draft Plan Release) (p. 100). Baton Rouge, LA: Louisiana Coastal Protection and Restoration Authority, the State of Louisiana.

D'Alpaos, A., Lanzoni, S., Marani, M., & Rinaldo, A. (2010). On the tidal prism–channel area relations. *Journal of Geophysical Research*, *115*(F1).

Dalyander, P. S., Miner, M. D., Khalil, S., Lee, D. M., Leblanc, W., Newman, A., Cameron, C., & Leonardo, D. D. (2021). *Barrier Island System Management (BISM): A holistic system-approach to adaptively manage Louisiana's barrier islands and headlands* (p. 115). Baton Rouge, LA: The Water Institute of the Gulf. Produced for and funded by the Coastal Protection and Restoration Authority (Task Order 73).

Danielson, J. J., Tyler, D. J., Cushing, W. M., Barras, J. A., Poppenga, S., Beverly, S. D., & Shogib, M. R. I. (2022). Topobathymetric model of the northern Gulf of Mexico, 1885 to 2021. U.S. Geological Survey.

Das, A., Justic, D., Inoue, M., Hoda, A., Huang, H., & Park, D. (2012). Impacts of Mississippi River diversions on salinity gradients in a deltaic Louisiana estuary: Ecological and management implications. *Estuarine, Coastal and Shelf Science*, *111*, 17–26.

Deltares. (2019). *D-Flow Flexible Mesh Suite: User Manual* (Version 1.5.0) (p. 412). Netherlands: Deltares.

Dronkers, J. (1986). Tidal asymmetry and estuarine morphology. *Netherlands Journal of Sea Research*, *20*(2), 117–131.

Egbert, G. D., & Erofeeva, S. Y. (2002). Efficient inverse modeling of barotropic ocean tides. *American Meteorological Society*, *19*, 183–204.

Eustis Engineering Services, LLC. (2015). *Final Geotechnical Exploration State of Louisiana Coastal Protection and Restoration Authority Caminada Headlands Back Barrier Marsh Creation Project Offshore Work* (No. Contract No. 2503-13-14, Task No.1, Amendment No.1) (p. 134). Lafourche Parish, LA: Eustis Engineering Services, LLC. Prepared for Coastal Protection and Restoration Authority.

Feng, Z., & Li, C. (2010). Cold-front-induced flushing of the Louisiana Bays. *Journal of Marine Systems*, *82*(4), 252–264.

Fisk, H. N. (1944). *Geological investigations of the alluvial valley of the lower Mississippi River: US Army Corps of Engineers.* Vicksburg, MS: Mississippi River Commission.

FitzGerald, D. M., Kulp, M. A., Hughes, Z. J., Georgiou, I. Y., Miner, M. D., Penland, S., & Howes, N. C. (2007). Impacts of rising sea level to backbarrier wetlands, tidal inlets, and barrier islands: Barataria coast, Louisiana. In *Coastal Sediments '07* (pp. 1179–1192). New Orleans, Louisiana, United States: American Society of Civil Engineers.

FitzGerald, D. M., Kulp, M. A., Penland, S., Flocks, J., & Kindinger, J. L. (2004). Morphologic and stratigraphic evolution of muddy ebb-tidal deltas along a subsiding coast: Barataria Bay, Mississippi River Delta. *Sedimentology*, *51*(6), 1157–1178.

Flocks, J. G., Ferina, N. F., Dreher, C., Kindinger, J. L., FitzGerald, D. M., & Kulp, M. A. (2006). High-resolution stratigraphy of a Mississippi subdelta-lobe progradation in the Barataria Bight, north-central Gulf of Mexico. *Journal of Sedimentary Research*, *76*(3), 429–443.

Fugro. (2018). *LNG plant borings - Fugro data sheets* (p. 42).

Gahagan & Bryant Associates, Inc. (2013). *Caminada Moreau Subsidence Study Phases 1-3 Project Report* (p. 467). Lafourche Parish, LA.

GeoEngineers. (2010). *Geotechnical Data Collection Report Caminada Headland Beach and Dune Restoration Project (BA-45). LaFourche and Jefferson parishes, Louisiana.* (Geotechnical Data Collection Report No. 16715- 012– 00) (p. 415). Lafourche Parish, LA: GeoEngineers. Prepared for Taylor Energy, Inc.

GeoEngineers. (2017). *Desktop Geotechnical Evaluation and Phase 2 Scoping: Federal Navigation Improvements-Port Fourchon* (No. 22642- 001– 00) (p. 118). Lafourche Parish, LA: GeoEngineers. Prepared for GIS Engineering, Inc.

Georgiou, I., & McCorquodale, A. (2000). Salinity stratification from a navigation canal into a shallow lake.

Georgiou, I. Y., & Trosclair, K. J. (2013). *Measurements of lateral flow from the Mississippi River at Mardi Gras Cut using synoptic ADCP near the Bohemia Spillway* (Preliminary field report) (pp. 1–4). The Lake Pontchartrain Basin Foundation.

Georgiou, I. Y., Yocum, T. E., Amos, M. L., Kulp, M. A., & Flocks, J. (2019). *Louisiana Barrier Island Comprehensive Monitoring Program 2015-2019 coastal surface-sediment characterization analysis: Methods and results.* (p. 38). New Orleans, LA: Prepared for the Louisiana Coastal Protection and Restoration Authority (CPRA), Pontchartrain Institute for Environmental Sciences, University of New Orleans.

GIS Engineering, LLC. (2019). *Port Fourchon Belle Pass Channel Deepening Project* (No. 22642- 001– 00).

Hajek, E. A., & Wolinsky, M. A. (2012). Simplified process modeling of river avulsion and alluvial architecture: Connecting models and field data. *Sedimentary Geology*, *257–260*, 1–30.

Hanegan, K., & Georgiou, I. Y. (2014). Tidal modulated flow and sediment flux through Wax Lake Delta distributary channels: Implications for delta development. In *Proceedings of the International Association of Hydrological Sciences* (Vol. 367, pp. 391–398). New Orleans, LA: IAHS.

Haralampides, K., Georgiou, I. Y., & McCorquodale, A. J. (2000). Water quality impacts on the Lake Pontchartrain estuarine system. Presented at the Water Environment Federation 73rd Annual Conference & Exposition on Water Quality and Wastewater Treatment.

Henry, K. M., & Twilley, R. R. (2013). Soil development in a coastal Louisiana wetland during a climate-induced vegetation shift from salt marsh to mangrove. *Journal of Coastal Research*, *29*(6), 1273–1283.

Hollis, R., Swartz, J., Khalil, S., Raynie, R., & Miner, M. D. (2023). Sediment inventory in a mud-dominated deltaic plain: Implementation of the Louisiana Sediment Management Plan. In *Coastal Sediments 2023* (pp. 2805–2818). World Scientific.

Huang, W., Li, C., White, J. R., Bargu, S., Milan, B., & Bentley, S. (2020). Numerical Experiments on Variation of Freshwater Plume and Leakage Effect From Mississippi River Diversion in the Lake Pontchartrain Estuary. *Journal of Geophysical Research: Oceans*, *125*(2), e2019JC015282.

Jarrett, J. T. (1976). *Tidal prism-inlet area relationships* (Vol. 3). US Department of Defense, Department of the Army, Corps of Engineers ….

Johnson, D. R., & Geldner, N. (2020). *Storm Selection for the ICM - Updates & Improvements* (p. 10). Baton Rouge, Louisiana: Purdue University; Prepared for Coastal Protection and Restoration Authority.

Jung, H., Messina, F., Moss, L., Baustian, M. M., Duke-Sylvester, S., & Roberts, H. H. (2019). *TO51: Vegetation Model and Integration Framework for Mid-Breton Outfall Management Model.* (Funded by the Coastal Protection and Restoration Authority under Task Orders 51). The Water Institute of the Gulf.

Kernkamp, H. W. J., Van Dam, A., Stelling, G. S., & de Goede, E. D. (2011). Efficient scheme for the shallow water equations on unstructured grids with application to the Continental Shelf. *Ocean Dynamics*, *61*(8), 1175–1188.

Khalil, S., Forrest, B., & Haywood, E. (2022). Strategic approaches to sediment management for restoration of a deltaic plain. *Shore & Beach*, 39–49.

Khalil, S., Forrest, B., Lowiec, M., Suthard, B., Raynie, R., Haywood, E., Robertson, Q., & Andrews, J. (2020). Overview of statewide geophysical surveys for ecosystem restoration in Louisiana. *Shore & Beach*, 102–109.

Khalil, S. M. (2019). *General guidelines: Exploration for sediment resources for coastal restoration* (No. Version_VIII). Baton Rouge, LA: Coastal Protection and Restoration Authority.

Khalil, S. M., Finkl, C. W., Roberts, H. H., & Raynie, R. C. (2010). New approaches to sediment management on the inner continental shelf offshore coastal Louisiana. *Journal of Coastal Research*, *26*(4), 591–604.

Khalil, S. M., Freeman, A. M., & Raynie, R. C. (2018). Sediment management for sustainable ecosystem restoration of coastal Louisiana. *Shore & Beach*, *86*(1), 12.

Kirwan, M. L., Temmerman, S., Skeehan, E. E., Guntenspergen, G. R., & Fagherazzi, S. (2016). Overestimation of marsh vulnerability to sea level rise. *Nature Climate Change*, *6*(3), 253–260.

Kolb, C. R., & van Lopik, J. R. (1958). *Geology of the Mississippi River Deltaic Plain, Southeastern Louisiana Waterways Experiment Station* (Technical Report No. 3–483) (p. 120). Vicksburg, Mississippi: U. S. Army Corps of Engineers.

Kolker, A. S., & Weathers, H. D. (2022). *Discharge study at Bayou Tortillon* (Technical Report). Louisiana Universities Marine Consortium and Delta Geo-Marine.

Kulp, M. A., Penland, S., Flocks, J. G., Kindinger, J. L., Dreher, C., & Ferina, N. (2002). Regional geology, coastal processes, and sand resources in the vicinity of East Timbalier Island.

Legates, D. R., & McCabe, G. J. (1999). Evaluating the use of "goodness-of-fit" measures in hydrologic and hydroclimatic model validation. *Water Resources Research*, *35*(1), 233–241.

Leonardi, N., Canestrelli, A., Sun, T., & Fagherazzi, S. (2013). Effect of tides on mouth bar morphology and hydrodynamics. *Journal of Geophysical Research: Oceans*, *118*(9), 4169–4183.

Lesser, G., Kester, J., & Roelvink, J. (2000). On-line sediment transport within Delft3D-FLOW.

Lesser, G. R., Roelvink, J. A. v, Van Kester, J. A. T. M., & Stelling, G. S. (2004). Development and validation of a three-dimensional morphological model. *Coastal Morphodynamic Modeling*, *51*(8–9), 883–915.

Li, C., Huang, W., & Milan, B. (2019). Atmospheric cold front–induced exchange flows through a microtidal multi-inlet bay: Analysis using multiple horizontal ADCPs and FVCOM simulations. *Journal of Atmospheric and Oceanic Technology*, *36*(3), 443–472.

Li, C., White, J. R., Chen, C., Lin, H., Weeks, E., Galvan, K., & Bargu, S. (2011). Summertime tidal flushing of Barataria Bay: Transports of water and suspended sediments. *Journal of Geophysical Research: Oceans*, *116*(C4), 1–15.

Li, G., Xu, K., Xue, Z. G., Liu, H., & Bentley, S. J. (2021). Hydrodynamics and sediment dynamics in Barataria Bay, Louisiana, USA. *Estuarine, Coastal and Shelf Science*, *249*, 107090.

Li, L., Storms, J. E. A., & Walstra, D. J. R. (2018). On the upscaling of process-based models in deltaic applications. *Geomorphology*, *304*, 201–213.

Liang, M., Meselhe, E., Messina, F., & Ortals, C. (2016). *Sediment Diversions: Optimization of the Operation Plans* (No. Task Order 41). Baton Rouge, LA: The Water Institute of the Gulf.

Liu, K., Chen, Q., Hu, K., Xu, K., & Twilley, R. R. (2018). Modeling hurricane-induced wetland-bay and bay-shelf sediment fluxes. *Coastal Engineering*, *135*, 77–90.

Long, J., Dalyander, P. S., Poff, M., Spears, B., Borne, B., Thompson, D., Mickey, R., Dartez, S., & Grandy, G. (2020). Event and decadal-scale modeling of barrier island restoration designs for decision support. *Shore & Beach*, 49–57.

Luijendijk, A. P., Ranasinghe, R., de Schipper, M. A., Huisman, B. A., Swinkels, C. M., Walstra, D. J. R., & Stive, M. J. F. (2017). The initial morphological response of the Sand Engine: A process-based modelling study. *Coastal Engineering*, *119*, 1–14.

Marciano, R., Wang, Z. B., Hibma, A., de Vriend, H. J., & Defina, A. (2005). Modeling of channel patterns in short tidal basins. *Journal of Geophysical Research: Earth Surface*, *110*(F1).

McCorquodale, A., Georgiou, I. Y., Davis, M. D., & Pereira, J. (2010). *Hydrology and hydrodynamic modeling of the Mississippi River in southeast Louisiana*. New Orleans, LA: Pontchartrain Institute for Environmental Studies, University of New Orleans.

Melby, J. A., Diop, F., Nadal-Caraballo, N. C., Green, D., & Gonzalez, V. (2015). Coastal Hazards System. In *Coastal Structures and Solutions to Coastal Disasters 2015* (pp. 219–229). Boston, Massachusetts: American Society of Civil Engineers.

Meselhe, E., Costanza, K., Jung, H., Ainsworth, C. H., Simpson, E., Chagaris, D., Addis, D., Rodrigue, M., & Smits, J. (2017). *Model performance assessment for the LCA Mississippi River Hydrodynamic and Delta Management Study (TO-5)* (p. 58). Baton Rouge, LA.

Miner, M. D., Kulp, M. A., FitzGerald, D. M., Flocks, J. G., & Weathers, H. D. (2009). Delta lobe degradation and hurricane impacts governing large-scale coastal behavior, South-central Louisiana, USA. *Geo-Marine Letters*, *29*(6), 441–453.

Moriasi, D. N., Arnold, J. G., Van Liew, M. W., Bingner, R. L., Harmel, R. D., & Veith, T. L. (2007). Model evaluation guidelines for systematic quantification of accuracy in watershed simulations. *Trans. ASABE*, *50*(3), 885–900.

Nadal Caraballo, N. C., Yawn, M., Gonzalez, V., Torres, M., Melby, J., & Taflanidis, A. (2020). Coastal Hazards System: A Probabilistic Coastal Hazard Analysis Framework. *Journal of Coastal Research*, *95*, 1211.

Nardin, W., Mariotti, G., Edmonds, D. A., Guercio, R., & Fagherazzi, S. (2013). Growth of river mouth bars in sheltered bays in the presence of frontal waves. *Journal of Geophysical Research: Earth Surface*, *118*(2), 872–886.

NOAA. (n.d.). Sea Level Trends - NOAA Tides & Currents.

Nyman, J. A., DeLaune, R. D., Roberts, H. H., & Patrick, W. H. (1993). Relationship between vegetation and soil formation in a rapidly submerging coastal marsh. *Marine Ecology Progress Series*, *96*(3), 269–279.

Partheniades, E. (1965). Erosion and deposition of cohesive soils. *Proceedings of the American Society of Civil Engineers*, *91, Part 1*, 105–139.

Pawlowicz, R., Beardsley, B., & Lentz, S. (2002). Classical tidal harmonic analysis including error estimates in MATLAB using T_TIDE. *Computers and Geosciences*, *28*.

Penland, S., Wayne, L., Britsch, L. D., Williams, S. J., Beall, A. D., & Butterworth, V. C. (2001). *Geomorphic classification of coastal land loss between 1932 and 1990 in the Mississippi River delta plain, southeastern Louisiana* (Open-File Report No. 00–417) (p. 1). Washington, D.C.: U.S. Geological Survey.

Ramatchandirane, C. G., Courtois, A., Di Leonardo, D. R., Eckland, A. C., Miner, M. D., & Yocum, T. E. (2019). *Investigation of flow and water constituent fluxes through the tidal inlets of the Barataria Basin* (No. Task Order 55) (p. 91). Baton Rouge, LA: The Water Institute of the Gulf. Prepared for and funded by the Coastal Protection and Restoration Authority.

Robichaux, P., Xu, K., Bentley, S. J., Miner, M. D., & Xue, Z. G. (2020). Morphological evolution of a mud-capped dredge pit on the Louisiana shelf: Nonlinear infilling and continuing consolidation. *Geomorphology*, *354*, 107030.

Roelvink, J. A. (2006). Coastal morphodynamic evolution techniques. *Coastal Engineering*, *53*(2–3), 277–287.

Stockdon, H. F., Holman, R. A., Howd, P. A., & Sallenger, A. H. (2006). Empirical parameterization of setup, swash, and runup. *Coastal Engineering*, *53*(7), 573–588.

Sullivan, J. C., Torres, R., Garrett, A., Blanton, J., Alexander, C., Robinson, M., Moore, T., Amft, J., & Hayes, D. (2015). Complexity in salt marsh circulation for a semienclosed basin. *Journal of Geophysical Research: Earth Surface*, *120*(10), 1973–1989.

Swarzenski, C. M., & Perrien, S. M. (2015). *Discharge, suspended sediment, and salinity in the Gulf Intracoastal Waterway and adjacent surface waters in South-Central Louisiana, 1997–2008* (USGS Numbered Series No. 2015–5132). *Discharge, suspended sediment, and salinity in the Gulf Intracoastal Waterway and adjacent surface waters in South-Central Louisiana, 1997–2008* (Vol. 2015–5132, p. 30). Reston, VA: U.S. Geological Survey.

Sweet, W. (William V., Kopp, R., E., Weaver, C. P., Obeysekera, J. T. B., Horton, R. M., Thieler, E. R. (Edward R., 1965-, & Zervas, C. E., 1957-. (2017). *Global and regional sea level rise scenarios for the United States* (Technical Report NOS CO-OPS ; 83). National Oceanic and Atmospheric Administration.

The Water Institute of the Gulf. (2022). *Partnership for Our Working Coast: A community-informed transdisciplinary approach to maximizing benefits of dredged sediment for wetland restoration planning at Port Fourchon, Louisiana*. Baton Rouge, LA: The Water Institute of the Gulf. Prepared for and funded by The National Fish and Wildlife Foundation, Shell, Chevron, Danos, and the Greater Lafourche Port Commission.

Turner, R. E., Lee, J. M., Milan, C. S., & Swenson, E. M. (2021). Phosphorus concentrations into a subtropical lake strongly influence nitrogen accumulation, nitrogen export, and Chl a concentrations. *Hydrobiologia*, *848*(20), 4787–4800.

Underwood, S. (2012). *Louisiana Sediment Management Plan (LASMP): Recommendations for an Implementation Strategy* (Final Report) (p. 30). Applied Coastal Engineering, Inc. Prepared for Louisiana Coastal Protection and Restoration Authority.

van Rijn, L. C. (1993). *Principles of sediment transport in rivers, estuaries and coastal seas*. Amsterdam: Aqua Publications.

van Rijn, L. C. (2020). Literature review of critical bed-shear stresses for mud-sand mixtures. *Technical Note. Www. Leovanrijn-Sediment. Com*.

van Rijn, L. C., & Barth, R. (2019). Settling and consolidation of soft mud–sand layers. *Journal of Waterway, Port, Coastal, and Ocean Engineering*, *145*(1), 04018028.

Weathers, H. D., Allison, M., Ramatchandirane, C., & Yuill, B. (2016). Water and sediment dynamics in the fort St. Philip Crevasse during the 2016 highwater event. Presented at the State of the Coast 2016, New Orleans, LA.

White, E. D., Fitzpatrick, C., Freeman, A., Jankowski, K. L., & Pahl, J. W. (2021). *2023 Coastal Master Plan Modeling: ICM Boundary Conditions* (Forthcoming). Coastal Protection and Restoration Authority.

Willemsen, P. W. J. M., Smits, B. P., Borsje, B. W., Herman, P. M. J., Dijkstra, J. T., Bouma, T. J., & Hulscher, S. J. M. H. (2022). Modeling decadal salt marsh development: variability of the salt marsh edge under influence of waves and sediment availability. *Water Resources Research*, *58*(1).

Wilson, C. A., & Allison, M. A. (2008). An equilibrium profile model for retreating marsh shorelines in southeast Louisiana. *Estuarine, Coastal and Shelf Science*, *80*(4), 483–494.

APPENDICES

APPENDIX A. NUMERICAL MODEL

This appendix contains a comprehensive description of the numerical model used in the study "Assessing the Impact of In-Bay Borrow Pits on Estuarine Sediment Dynamics, Barataria Bay, Louisiana," covering the model setup, input data, boundary conditions, calibration, and sensitivity analysis. The model used is a physics-based coupled hydro-morphodynamic Delft3D FM model (Kernkamp et al., 2011), consisting of D-Flow FM for hydrodynamics, D-Morphology for sediment transport and morphology, and the coupled wave module D-Wave, which includes the effects of surface waves and wave-current interactions with the third-generation spectral wave model SWAN (Booij et al., 1999). Delft3D has been widely used in numerous studies investigating sediment transport and morphology in natural systems (Caldwell & Edmonds, 2014; Hajek & Wolinsky, 2012; Leonardi et al., 2013; Lesser et al., 2004; Luijendijk et al., 2017; Marciano et al., 2005; Nardin et al., 2013). The model has also been extensively utilized to simulate flow and wave propagation in coastal and wetland environments, including fine-scale circulation and over-marsh flow in saltmarsh or mangrove systems (Caldwell & Edmonds, 2014; Hanegan & Georgiou, 2014; Liu et al., 2018; Sullivan et al., 2015; Willemsen et al., 2022).

A.1 MODEL COMPUTATIONAL DOMAIN

The numerical model was developed to represent hydrodynamics, sediment transport, and morphology throughout the area of interest (i.e., Barataria Bay) and in the surrounding areas (as shown in Figure 1). The model domain covers most of the Barataria Basin, extending north to include Lake Cataouatche and the tidal connection to Lac Des Allemands, the Terrebonne Basin to the west, and a portion of the Lower Mississippi River, the modern delta, and major distributaries. The model extends seaward to include the Barataria Bight and the shelf along the northern Gulf of Mexico up to about 100 km offshore.

An unstructured grid with varying spatial resolution consisting of triangular and quadrilateral elements was developed for the hydrodynamics, sediment transport, and morphology model components (Figure A-1). The grid resolution ranges from 50 m around the borrow pits, to 100 m throughout Barataria Bay and proximal environments, and to 200 m in the rest of the Barataria Basin. The resolution throughout Terrebonne Basin and along the proximal shelf is 400 m, exponentially decreasing to 3.5 km along the offshore open boundary.

The wave model domain employed a structured curvilinear grid (Figure A-2) with spatially varying resolution, ranging from 6 km near the offshore boundary to 150–200 m throughout Barataria Bay and proximal environments.

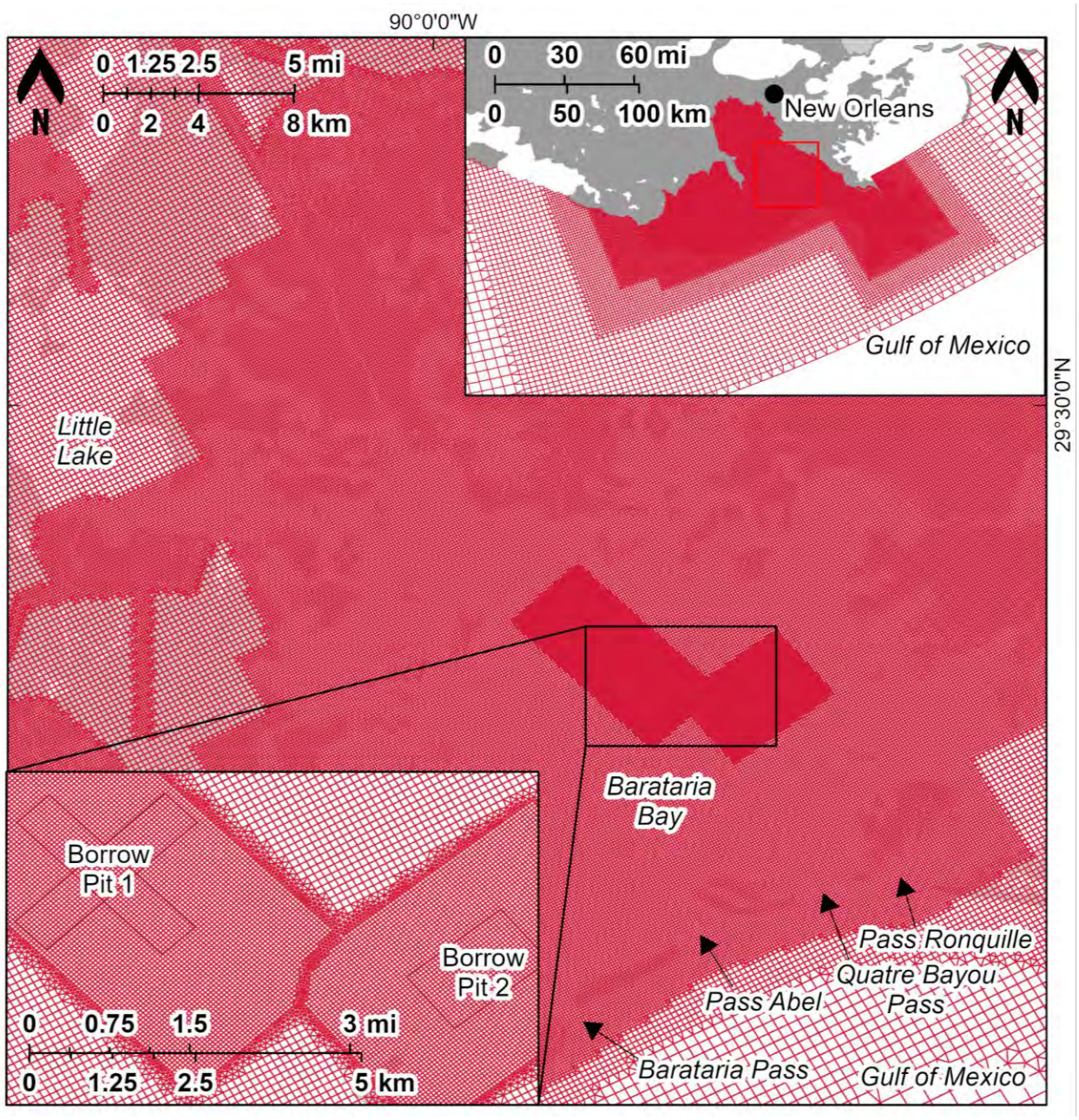

Figure A-1. Map of the unstructured D-Flow Flexible Mesh grid.

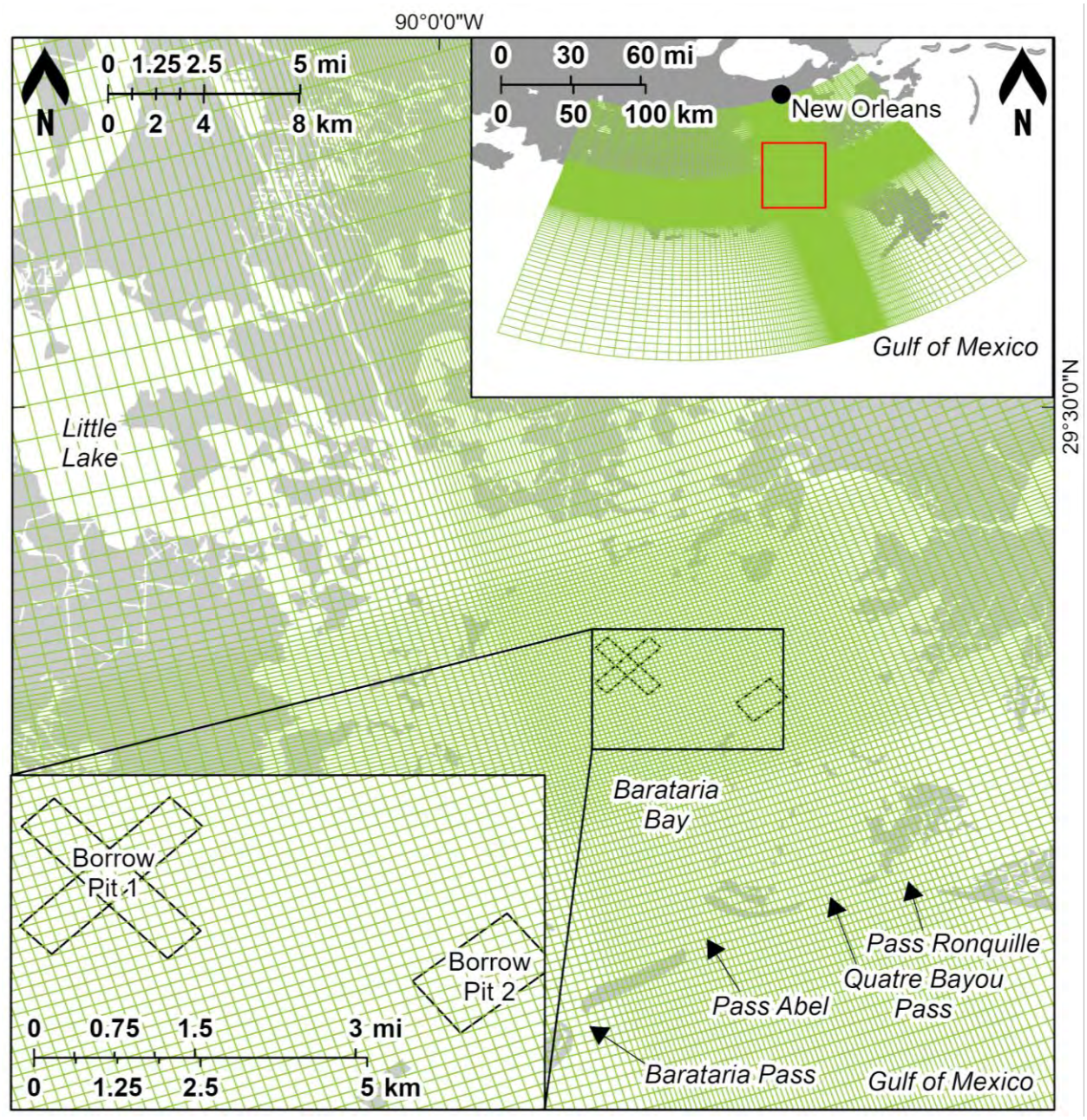

Figure A-2. Map of the structured (SWAN-based) D-Wave grid.

A.2 TOPOGRAPHY AND BATHYMETRY

The model's topography and bathymetry (Figure A-3) are based on a comprehensive Digital Elevation Model (DEM) developed by the United States Geological Survey (USGS) to support the Lowermost Mississippi River Management Program (LMRMP; Danielson et al., 2022). The dataset was supplemented with more recent data—where available—from Louisiana's System-Wide Assessment and Monitoring Program (SWAMP; Khalil et al., 2020), and inspected for accuracy along the tidal inlets fronting Barataria Bay as well as throughout Barataria Bay. Shortcomings in the original DEM were corrected by manual editing of the bathymetry. For instance, along the perimeter of Barataria Bay, near the transition from the bay to the peripheral marshes, manual edits were made to the model bathymetry and topography informed by recent aerial photography to ensure that hydraulic connections between Barataria Bay and the back-barrier marshes were accurately represented in the model. This included small channels, canals, and bayous that were not represented due to interpolation onto the model domain. These corrections ensured a more precise representation of the hydrodynamics, sediment transport, and morphology of the area.

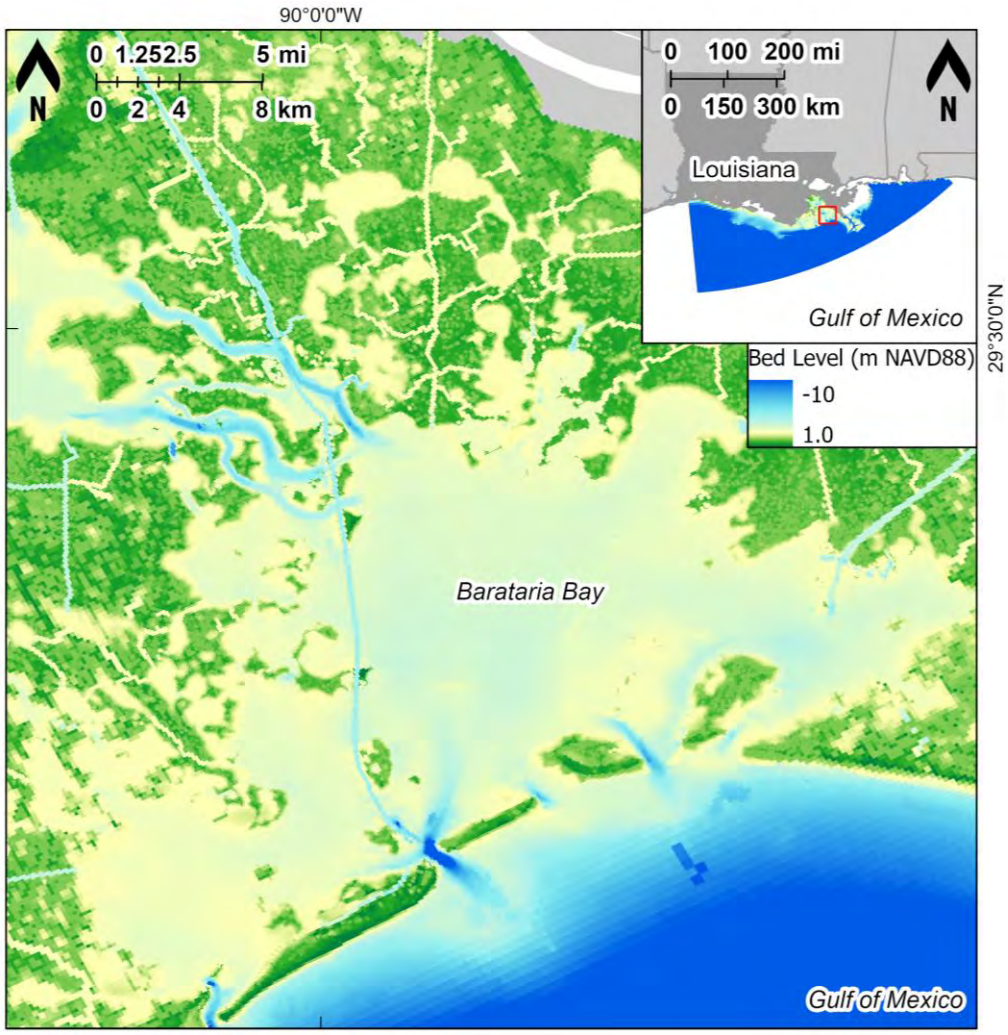

Figure A-3. Topobathymetric map of the model in and around Barataria Bay (Danielson et al., 2022; Khalil et al., 2020). This is a more detailed version of Figure 1.

The impact of vegetation on bottom roughness, and thus flow velocity, was incorporated by utilizing the *trachytopes* approach. This approach incorporates the drag from plants on the flow field and a corresponding increase in local roughness, accomplished by using plant physical parameters such as vegetation height, stem diameter, and stem density. For this study, vegetation parameters originated from a 2014 land use land cover map with a 30 m resolution (Couvillion, 2017). The model utilized five habitats and a total of eight wetland vegetation taxa (Table A-1). Jung et al. (2019) provided the initial vegetation parameters, such as vegetation height, stem diameter, and stem density, for each vegetation type, as well as recommended calibration settings.

Table A-1. Eight wetland vegetation taxa, which represent habitats in the model domain, along with the vegetation heights and densities that were used in the model, based on Jung et al. (2019).

Habitat	Wetland Vegetation Taxa	Vegetation height h_v (m)	Vegetation density n (1/m) [i.e., number of stems per square meter multiplied by stem diameter]
Fresh Marsh	*Sagittaria latifolia*	0.8	0.77
	Zizaniopsis miliacea	2.1	1.50
Intermediate Marsh	*Typha* spp.	2.3	0.14
	Phragmites spp.	3.2	0.13
	Sagittaria lancifolia	0.9	0.42
Brackish Marsh	*Spartina patens*	1.3	0.02
Saline Marsh	*Spartina alterniflora*	1.0	0.05
Mangrove Forest	*Avicennia germinans*	1.3	0.02

A.3 BOUNDARY CONDITIONS

A.3.1 Offshore Boundary Conditions

Tidal constituents derived from the TOPEX/Poseidon Global database (Egbert & Erofeeva, 2002) were used at the open boundary of the model domain to the south. The boundary was divided into 11 sections, each with a length of approximately 50–70 km. To the west of the model domain, a Neumann boundary condition (Deltares, 2019) was applied. Eight astronomic tidal constituents (M2, S2, N2, K2, K1, O1, P1, Q1) were used to force the model for each segment. Seasonal fluctuations in water level in the Gulf of Mexico were included at the open boundary using mean monthly water levels from the NOAA Grand Isle station l, gauge number 8761724. (Figure A-4).

ESLR rates (Figure A-5) are consistent with the "Lower" scenario used in the 2023 Louisiana Coastal Master Plan (White et al., 2021), which is based on NOAA's Intermediate scenario (Sweet et al., 2017)

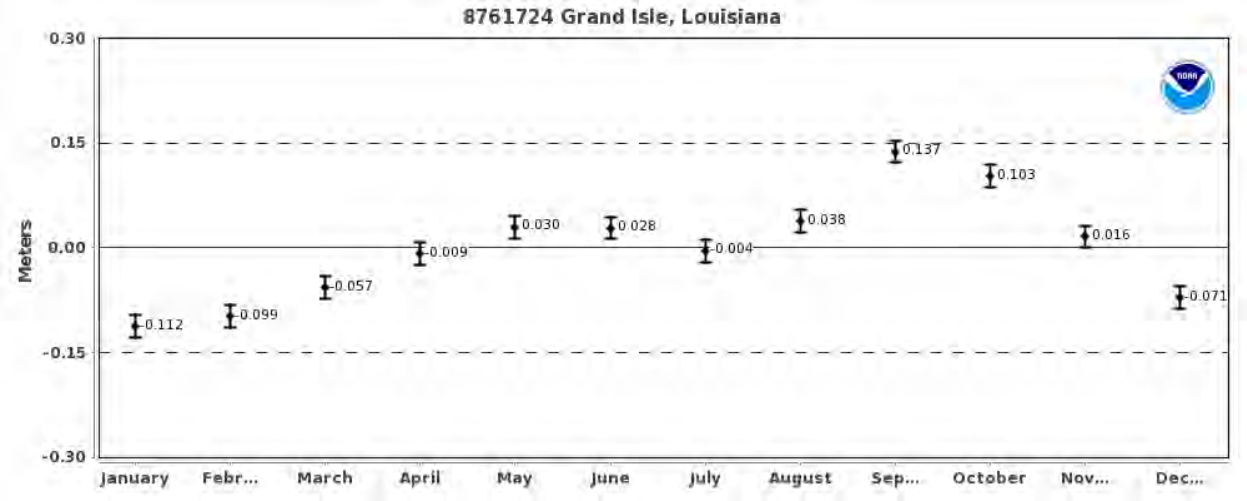

Figure A-4. Monthly mean sea levels at Grand Isle (points) and the monthly upper and lower 95% (bars; NOAA, n.d.). Note the annual variation in mean sea level varies by approximately 0.25 m during the year. Figure taken from https://tidesandcurrents.noaa.gov/sltrends/sltrends_station.shtml?plot=seasonal&id=8761724

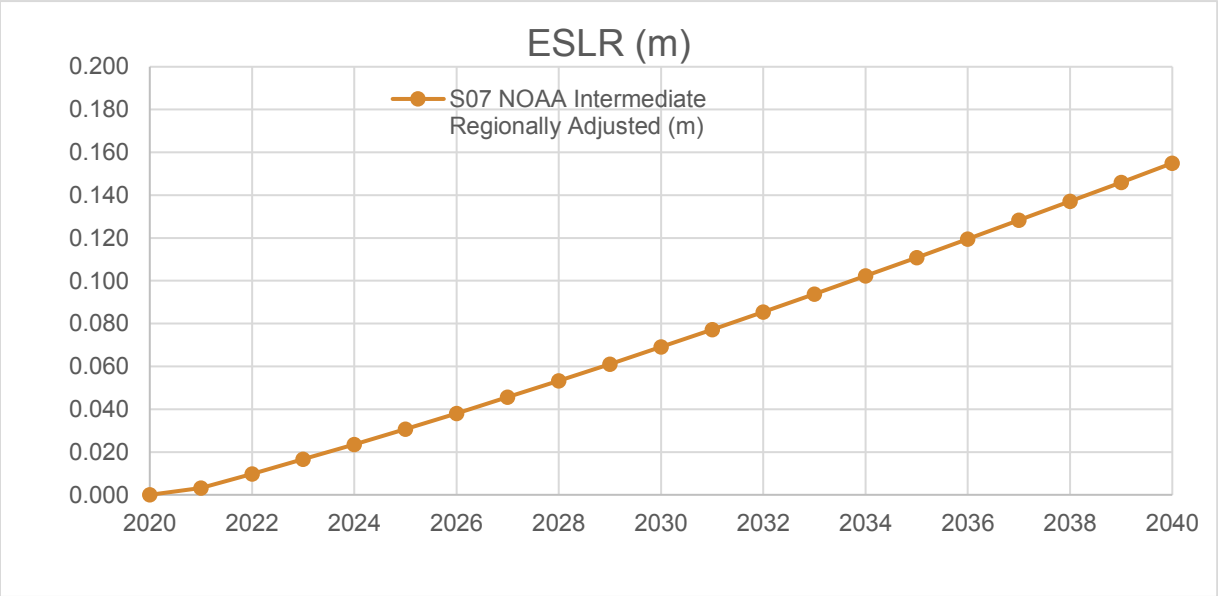

Figure A-5. ESLR rates between 2020 and 2040 based on Scenario S07 NOAA Intermediate Regionally Adjusted from Louisiana's 2023 CMP (White et al., 2021)

A.3.2 Tropical Cyclones

The simulated 20-year sequence of synthetic tropical storms is derived from a 50-year sequence generated by Johnson & Geldner (2020). This 50-year sequence was selected from a suite of synthetic storms developed for the USACE Coastal Hazards Systems (Melby et al., 2015; Nadal Caraballo et al., 2020). The selection of the 50-year sequence was performed by Johnson & Geldner (2020) using a heuristic optimization routine, which aimed to balance the impacts across Louisiana's coastal region and across diverse return periods. This optimization routine was designed to maximize sequence diversity irrespective of sample size. While a subsample of the resulting sequence is unlikely to strictly maximize sequence diversity due to the random sequencing of storms, it can be expected to have similar levels of sequence diversity to the original sample. For this reason, given scope and budget constraints, the 20-year period between year 10 and 30 of the 50-year sequence was used (Johnson & Geldner, 2020). Another way to approach upscaling would be to run the full sequence with a MORFAC of 0.4 (20/50) which would downscale the impacts to a 20-year time period. However, due to computational limitations and because of the way the rest of the year was upscaled (i.e., cold fronts and quiescent conditions), it was not feasible to simulate all 61 storms. Instead, a subset of 11 synthetic storms representing the years 1980 to 1999 were chosen for the 20-year period considered in this study (Table A-2).

Following selection of the sequence, weaker storms that were not anticipated to have any impacts on Barataria Bay were removed from the sequence, using a previously developed methodology detailed in a study by The Water Institute of the Gulf (2022), which focused on developing landscape and ecosystem evolution models to simulate future landscape changes near Port Fourchon, Louisiana. The methodology involved the removal of storms that were deemed unlikely to impact or overtop the barrier islands due to their distal proximity from the study area or their relatively weak intensity, resulting in minimal impacts to the barrier island system. Although the primary focus of the current study is not on barrier island evolution, the selected approach was considered appropriate due to the proximity of Port Fourchon to Barataria Bay. It is assumed that storms with minimal impacts on the barrier islands would also have

minimal impacts on Barataria Bay. A total of 4 of the original 11 storms in the 20-year sequence selected were excluded from the analysis, leaving a 7-storm sequence (Figure A-6 through Figure A-12) to be modeled within the framework (Table A-2). The analysis was conducted by comparing the total water level (TWL)—i.e., the combined contribution of wave run-up and storm surge—to a benchmark representing the berm and dune maximum elevation, following a similar methodology as presented in Long et al. (2020).TWL was calculated by adding the storm surge to the 2% probability of wave runup exceedance calculated using the Stockdon empirical formulation, which requires significant wave height and wave period at 20 m depth offshore along with beach slope (Stockdon et al., 2006). Significant wave height, wave period, and storm surge were extracted for each of the synthetic storms from the ADvanced CIRCulation model (ADCIRC) output at two locations offshore of Port Fourchon at 28.867°N, 90.483°W and at 29.101°N, 89.978°W. Beach slope was estimated by taking the mean slope of 30 beach profiles taken from the Louisiana Coastal Master Plan's barrier island model (ICM-BI; Dalyander et al., 2021) at approximately 50 m spacing along the Caminada Headland. Beach slopes were calculated from manual extraction of the location and elevation of the dune (or berm) toe and the shoreline; the mean slope for these profiles was calculated as 0.0389. A value of 2.0 m was chosen as the threshold for storm exceedance based on dune and berm elevations along the Caminada Headland. Storms with a TWL that was below this level for the two nearshore locations where waves and water levels were extracted were excluded from the sequence (predicted TWL for the two locations was similar and generally varied by less than 0.25 m).

Each storm consisted of time varying wind and pressure fields throughout the model domain, and offshore boundary conditions for water level, wave height, period, and direction. Waves were imposed at the offshore boundary of the wave grid (Figure A-2) to account for incoming waves during more energetic conditions during tropical storms. Waves during storms were forced at the open boundary every 20 minutes, and included significant wave heights, wave periods, and wave directions. The wave data used for the tropical cyclones were obtained from simulations produced with ADCIRC. The spatially varying boundary information is provided at eight equidistant locations along the boundary, each 40 km apart.

Table A-2. 20-year tropical storm sequence including the synthetic storm ID, storm central pressure, significant wave height (Hs), peak wave period (Tp), water level (WSE), wind velocity (WVEL), and total water level (TWL). Oceanographic data and wind speed values are provided for two locations (ST1 and ST2). Storms that were omitted from the sequence based on the TWL threshold are blacked out in the table.

	Storm ID	Central Pressure	year	ST1 Hs (m)	ST1 Tp (s)	ST1 WSE (m)	ST1 WVEL (m/s)	ST1 TWL (m)	ST2 Hs (m)	ST2 Tp (s)	ST2 WSE (m)	ST2 WVEL (m/s)	ST2 TWL (m)
1	357	965.25	1982	5.52	12.9	0.76	18.52	2.73	5.37	13.5	0.68	16.89	2.70
2	102	955.25	1984	3.90	14.7	0.64	19.27	2.52	2.91	7.5	0.68	20.96	1.51
3	*256*	*975.25*	*1985*	*3.43*	*10.7*	*0.53*	*13.09*	*1.83*	*2.97*	*10.3*	*0.48*	*11.15*	*1.63*
4	584	985.25	1985	5.46	10.6	0.63	22.20	2.22	4.82	10.0	0.55	19.13	1.97
5	600	985.25	1986	5.06	11.4	0.77	21.80	2.43	5.96	11.6	0.86	24.83	2.69
6	*349*	*965.25*	*1987*	*4.12*	*10.6*	*0.62*	*14.92*	*2.01*	*3.85*	*10.7*	*0.59*	*13.86*	*1.94*
7	298	975.25	1988	5.26	15.2	0.66	17.40	2.90	5.72	15.3	0.71	20.88	3.07
8	*125*	*985.25*	*1989*	*2.89*	*10.1*	*0.59*	*12.09*	*1.70*	*2.67*	*10.8*	*0.55*	*11.13*	*1.69*
9	*30*	*965.25*	*1989*	*2.90*	*6.3*	*0.41*	*20.46*	*1.10*	*3.71*	*6.3*	*0.67*	*31.92*	*1.45*
10	508	955.25	1992	6.85	14.7	1.53	31.14	4.01	7.30	14.9	1.43	31.02	4.03
11	544	975.25	1995	5.42	16.2	0.65	12.40	3.08	5.73	16.1	0.65	13.14	3.14

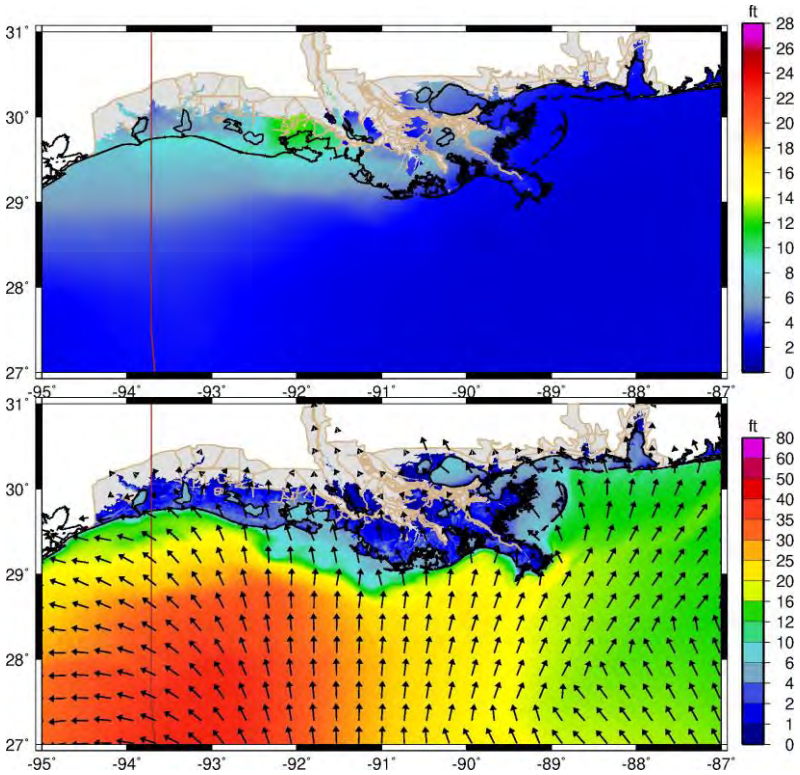

Figure A-6. Synthetic storm ID357 (track indicated in red): maximum surge elevation (upper panel) and maximum significant wave height (lower panel).

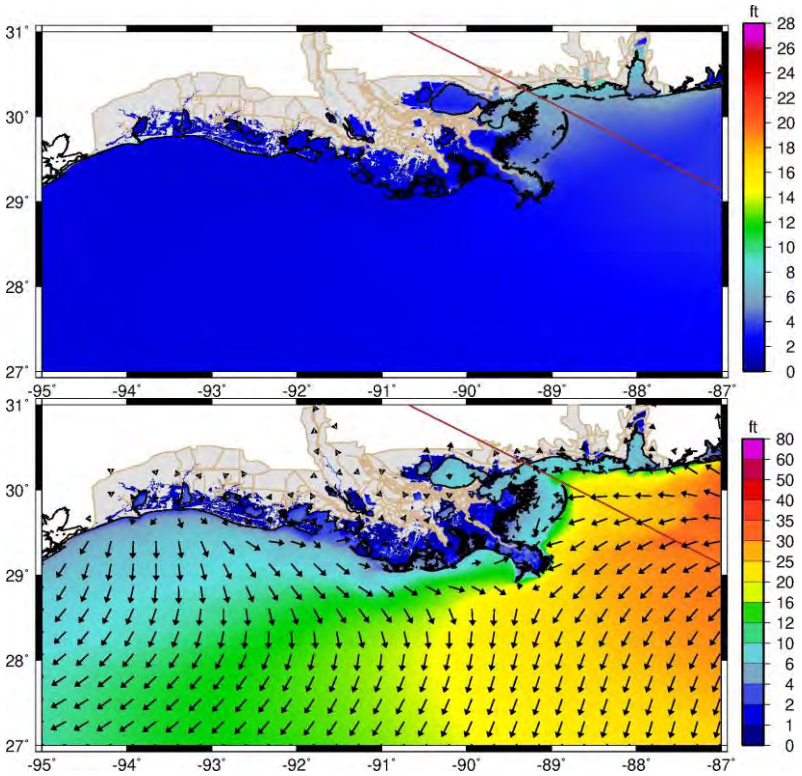

Figure A-7. Synthetic storm ID102 (track indicated in red): maximum surge elevation (upper panel) and maximum significant wave height (lower panel).

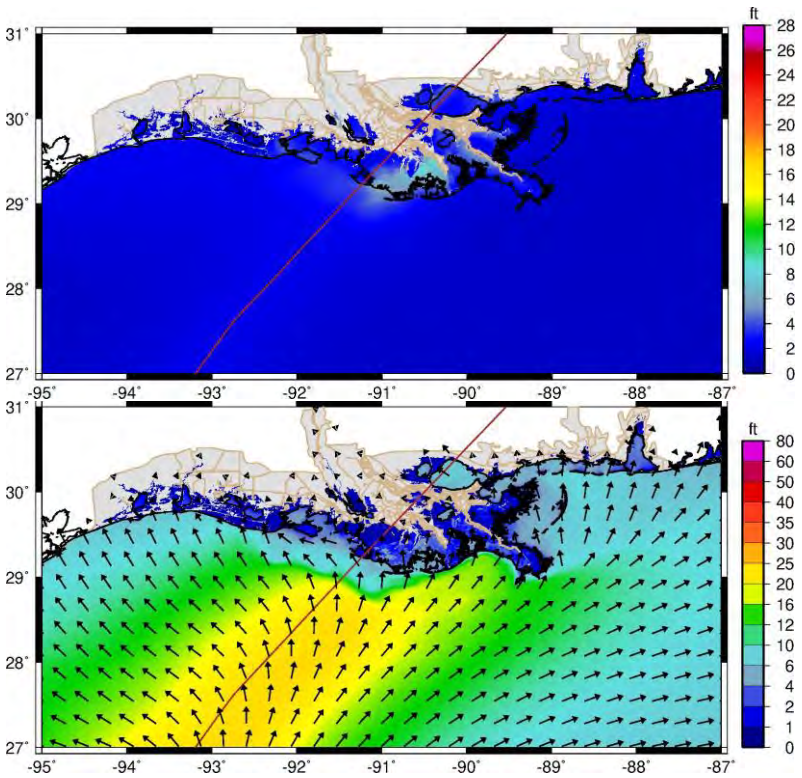

Figure A-8. Synthetic storm ID584 (track indicated in red): maximum surge elevation (upper panel) and maximum significant wave height (lower panel).

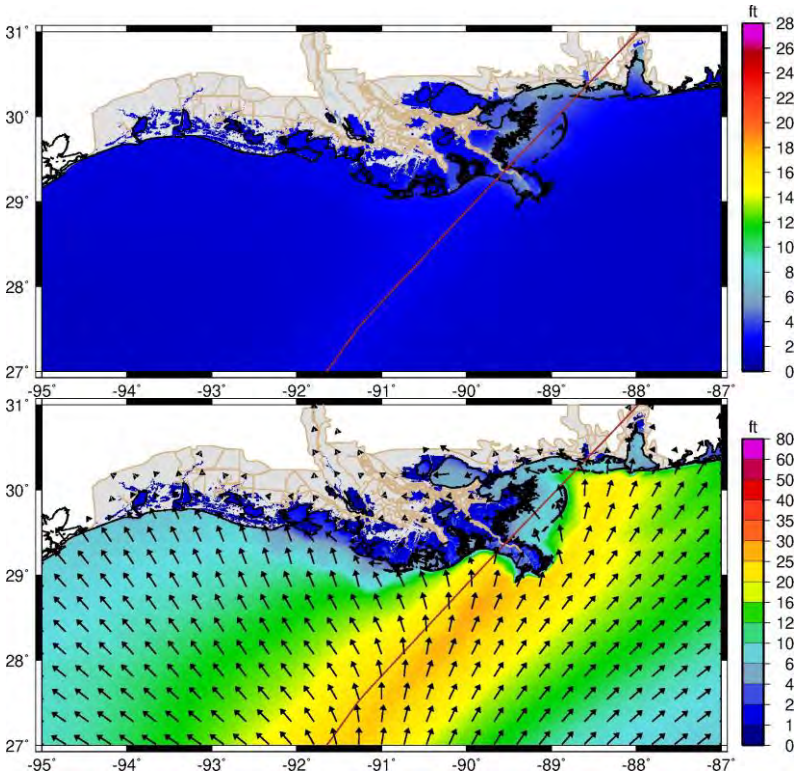

Figure A-9. Synthetic storm ID600 (track indicated in red): maximum surge elevation (upper panel) and maximum significant wave height (lower panel).

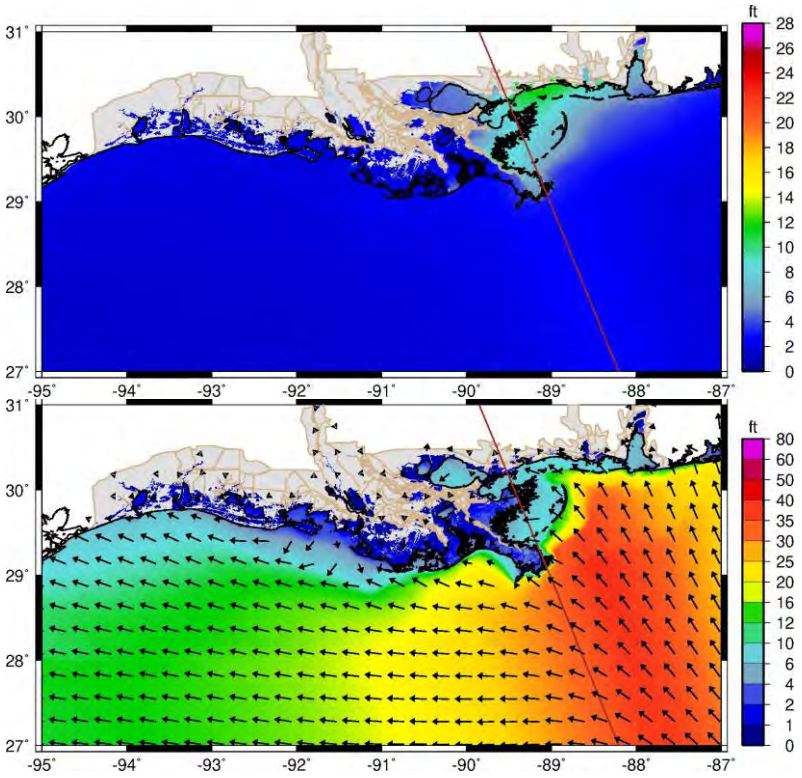

Figure A-10. Synthetic storm ID298 (track indicated in red): maximum surge elevation (upper panel) and maximum significant wave height (lower panel).

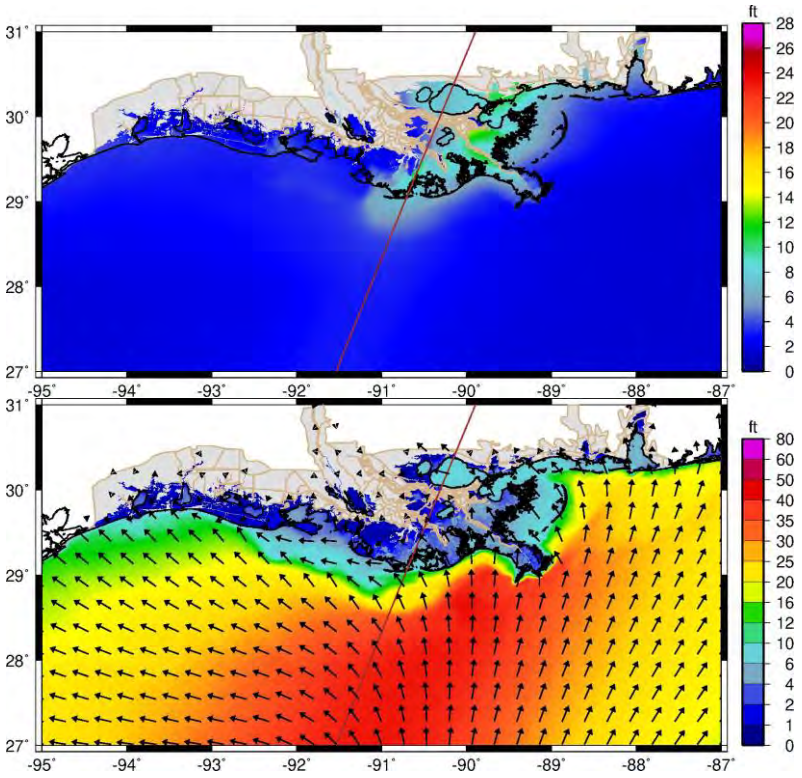

Figure A-11. Synthetic storm ID508 (track indicated in red): maximum surge elevation (upper panel) and maximum significant wave height (lower panel).

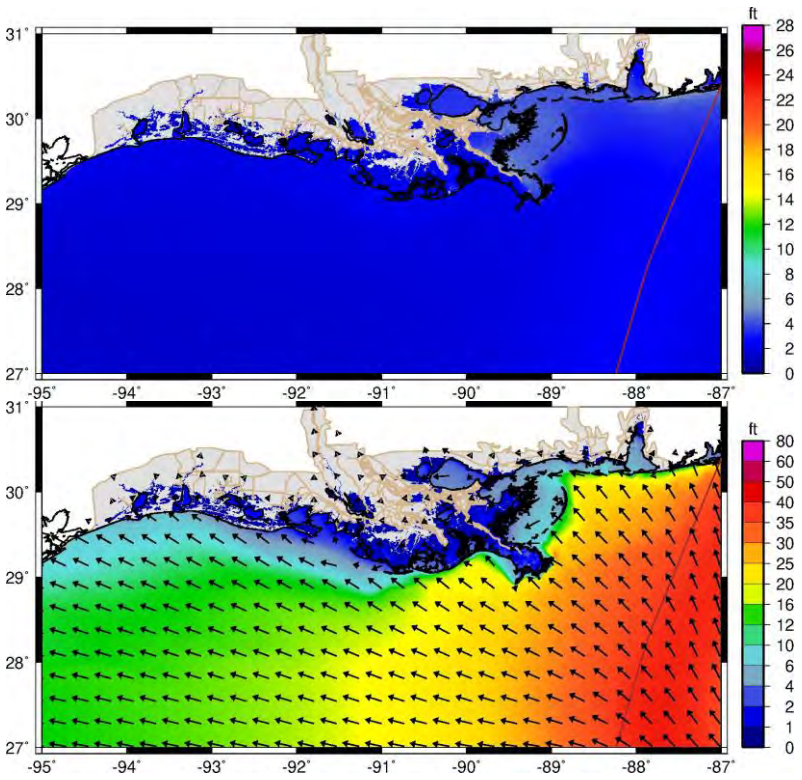

Figure A-12. Synthetic storm ID544 (track indicated in red): maximum surge elevation (upper panel) and maximum significant wave height (lower panel).

A.3.3 Riverine Boundary Conditions

The following riverine inflows are included in the model (Figure A-13):

- Gulf Intracoastal Waterway (GIWW) east of Larose, Louisiana: The discharge and sediment concentration timeseries are based on a USGS study of the GIWW (Swarzenski & Perrien, 2015)
- Bayou Des Allemands (for which no discharge records are available): Simulation output from CPRA's Integrated Compartment Model (ICM) from the 2017 CMP were used to compile a monthly discharge timeseries. This was done by correlating modeled discharges to precipitation in the local catchment area as observed during the simulation period. Suspended sediment concentrations are based on observations in Lac Des Allemands by Turner et al. (2021).
- Davis Pond Diversion: Instantaneous discharge based on measurements at the local USGS station (Station ID: 295501090190400).
- Naomi Siphon and West Pointe a la Hache Siphon: Daily discharge based on records kept by CPRA.
- Mississippi River (at Venice): Based on discharge data from the USGS station at Belle Chasse (07374525). A reduction of 20% was applied as an approximation of the loss of discharge between Belle Chasse and Venice caused by leakage through Mardi Gras Pass, Neptune Pass, and crevasses in the Fort St. Philip area. The approximated reduction is based on previous studies into the discharge distribution in the lowermost Mississippi River (Allison et al., 2012; Georgiou & Trosclair, 2013; McCorquodale et al., 2010) and more recent measured data, including synoptic ADCP surveys collected by the U.S. Army Corps of Engineers (USACE) New Orleans District, Olga Revetment discharge data provided by Dave Ramirez (USACE), and survey data in Neptune Pass and the Fort St. Philip reach (Kolker & Weathers, 2022; Weathers et al., 2016). The following passes and distributaries downstream of Venice are represented within the model grid:
    - Baptiste Collette
    - Cubit's Gap and Main Pass
    - Pass a Loutre
    - South Pass
    - Southwest Pass
    - West Bay Sediment Diversion
    - Grand Pass and Tiger Pass

The suspended sediment concentrations in the Mississippi River, the Davis Pond Diversion, and the Naomi and West Pointe a la Hache siphons, were estimated using a hysteresis rating curve previously developed for the Belle Chasse location for fine sediment (Liang et al., 2016). The curve estimates total fine sediment, of which 75% is assumed to be silt and 25% clay based on grain size analysis of suspended sediment conducted by USGS at the Belle Chasse station. Sand was not included at the fluvial input locations to avoid adding more sediment classes in the model, with the assumption that these fluvial input

sources are distal to Barataria Bay, and any sand entering the basin at these locations would deposit prior to reaching the bay and would constitute a negligible portion of the suspended sediment concentration.

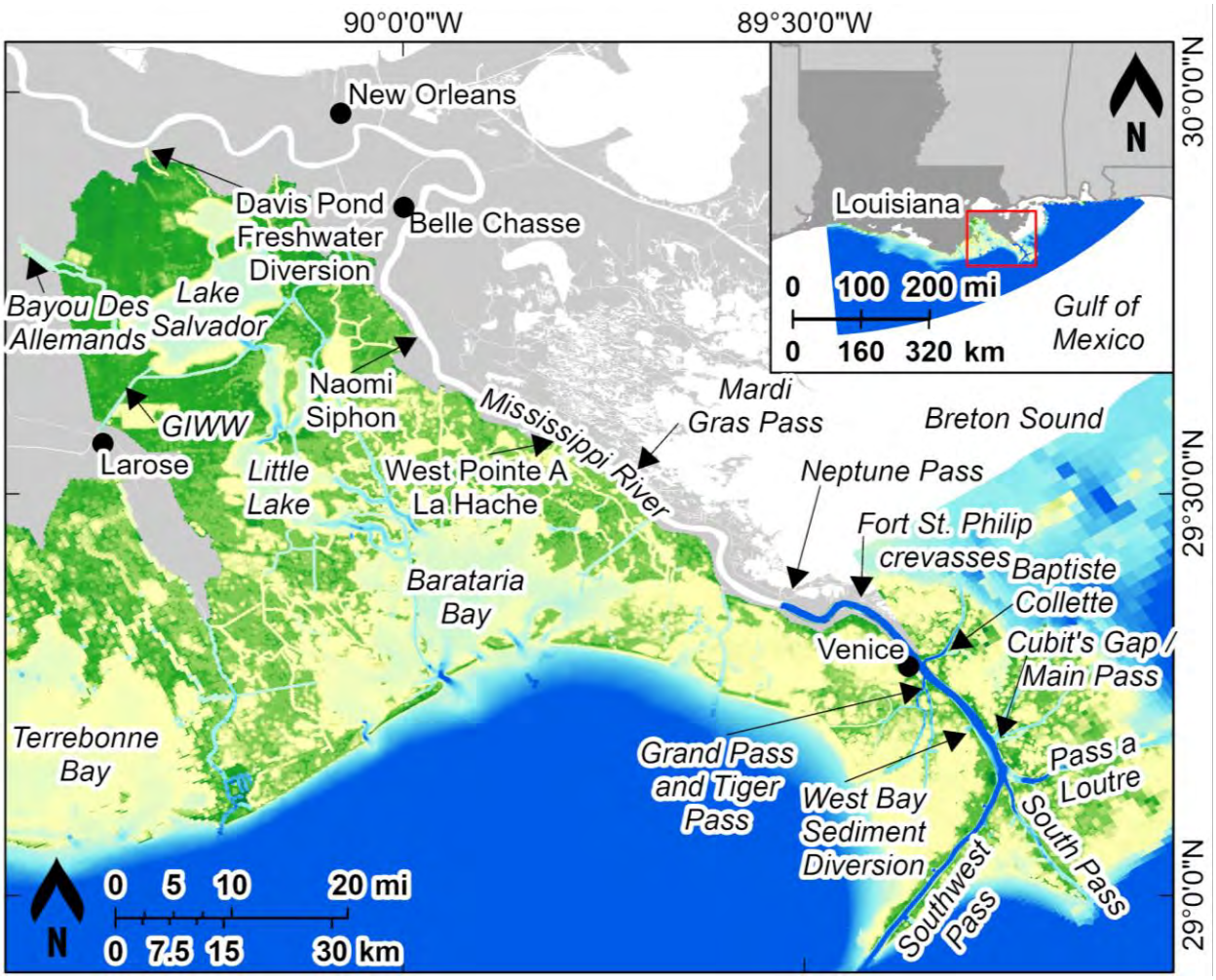

Figure A-13. Topobathymetric map of the model domain, showing all features that represent or are related to boundary conditions.

A.4 SEDIMENT TRANSPORT AND MORPHOLOGY

A.4.1 Sediment Fractions and Bed Composition

This model is composed of six sediment fractions, including fine sand, two silt fractions (consolidated and unconsolidated), two clay fractions (consolidated and unconsolidated), and organic marsh soil (Table A-3). The bed composition is spatially varying both horizontally and vertically (Table A-4 and Figure A-14). The upper shoreface and barrier islands are sandy and located above -3 m NAVD88. The bay floor and lower shoreface are muddy and located below -1 m NAVD88 in the bay and below -3 m NAVD88 at the barrier islands. The marshes, which have high organic soil content, are located above -1 m NAVD88.

This schematization is based on a previous literature review (The Water Institute of the Gulf, 2022) of numerous previous studies (Ardaman & Associates, 2017, 2018; Eustis Engineering Services, LLC, 2015; Flocks et al., 2006; Fugro, 2018; Gahagan & Bryant Associates, Inc., 2013; GeoEngineers, 2010, 2017; Georgiou et al., 2019; GIS Engineering, LLC, 2019; Henry & Twilley, 2013; Kulp et al., 2002; Liu et al., 2018; Nyman et al., 1993; Wilson & Allison, 2008).

Table A-3. Sediment fractions used within the model, along with their most important characteristics.

Sediment fraction	D50 (i.e., median diameter; µm)	Settling velocity (m/s)	Critical shear stress for erosion (Pa)	Comments
Sand (fine)	130	~	~	Natively present in bay
Silt (consolidated)	30	8.5E-4	0.5	Natively present in bay
Clay (consolidated)	4	1.44E-5	0.5	Natively present in bay
Silt (fluvial)	30	8.5E-4	0.15	Introduced by Mississippi River, other tributaries
Clay (fluvial)	4	1.44E-5	0.15	Introduced by Mississippi River, other tributaries
Organic	~	2.5E-4	4	Natively present at marshes

Table A-4. Stratified bed layers defined within the model, along with their sediment composition.

Stratified bed layers	Sand	Silt (consolidated)	Clay (consolidated)	Organic	Elevation range
Barrier, upper shoreface, tidal deltas	100%	~	~	~	Above −1 m NAVD88
Bay floor, lower shoreface	15%	50%	35%	~	Below −1 m NAVD88 in bay, below −3 m NAVD88 at barrier and upper shoreface
Marshes (saline)	14%	42%	24%	20%	Above −1 m NAVD88
Marshes (brackish)	9%	26%	15%	50%	Above −1 m NAVD88

Figure A-14. Map with spatial delineation of sediment layers. See Table A-3 and Table A-4 for sediment layer classification by grain size. From north to south: brackish wetland (purple), saline wetland (teal), barrier (yellow), upper shoreface (blue), and lower shoreface (green). Note. Reprinted from previous study by The Water Institute of the Gulf (2022).

A.4.2 Sediment Transport Formula

The Van Rijn sediment transport formulations (Van Rijn, 1993) were used to predict sand transport which includes separate treatment of the suspended sediment transport and bedload transport. The computation of cohesive sediments, i.e., clay and silt, was based on the Partheniades-Krone formulation (Partheniades, 1965), which depends on user-defined critical shear stress values for erosion and deposition for sediment flux to and from the bed (listed in Table A-3). To determine the values of these parameters, several sensitivity tests were performed, as described in Appendix A.5.6. The final model calibration factors are listed in Table A-5.

Table A-5. Key model calibration factors for sediment transport and morphology.

Parameter	Value
Current-related suspended sediment transport factor	0.2
Current-related bedload transport factor	0.2
Wave-related suspended sediment transport factor	0.2
Wave-related bedload sediment transport factor	0.2
Streamwise bed gradient factor for bed load transport	1
Transverse bed gradient factor for bed load transport	1.5

A.4.3 Morphological Evolution

The 20-year morphological evolution is divided into two 10-year "cycles." Morphological upscaling (Table 1) is employed for simulations that represent either quiescent conditions or cold fronts, using factors of 40 and 10, respectively. No morphological upscaling was applied to simulations that represent tropical cyclones. Before completing each cycle, adjustments were made outside of the Delft3D FM modeling suite to the bathymetry and topography to account for processes that the model does not directly simulate, such as subsidence (from Byrnes et al., 2019), marsh accretion (which is assumed to keep up with sea level rise), and dredging of the Barataria Bay Waterway (to a navigable depth of 4 m [~14 ft], location indicated in Figure 1). The subsidence in the Barataria Basin varied between 2–7 mm/year, with Barataria Bay experiencing a relatively high rate of subsidence at approximately 7 mm/year.

A.5 MODEL CALIBRATION

The model hydrodynamics were calibrated for the entire year of 2020 using six USGS gauges spread across the Barataria Basin (Figure A-15). Water level calibration results are shown in Figure A-16 through Figure A-21 and Table A-6 in Section A.5.1. A comparison between modeled and measured tidal ranges is depicted in Figure A-22 in Section A.5.2. Wave calibration results are represented by Figure A-26 through Figure A-29 in Section A.5.4. Lastly, calibration results of the discharge distribution in the Mississippi River bird's foot delta are listed in Table A-11 in Section A.5.5.

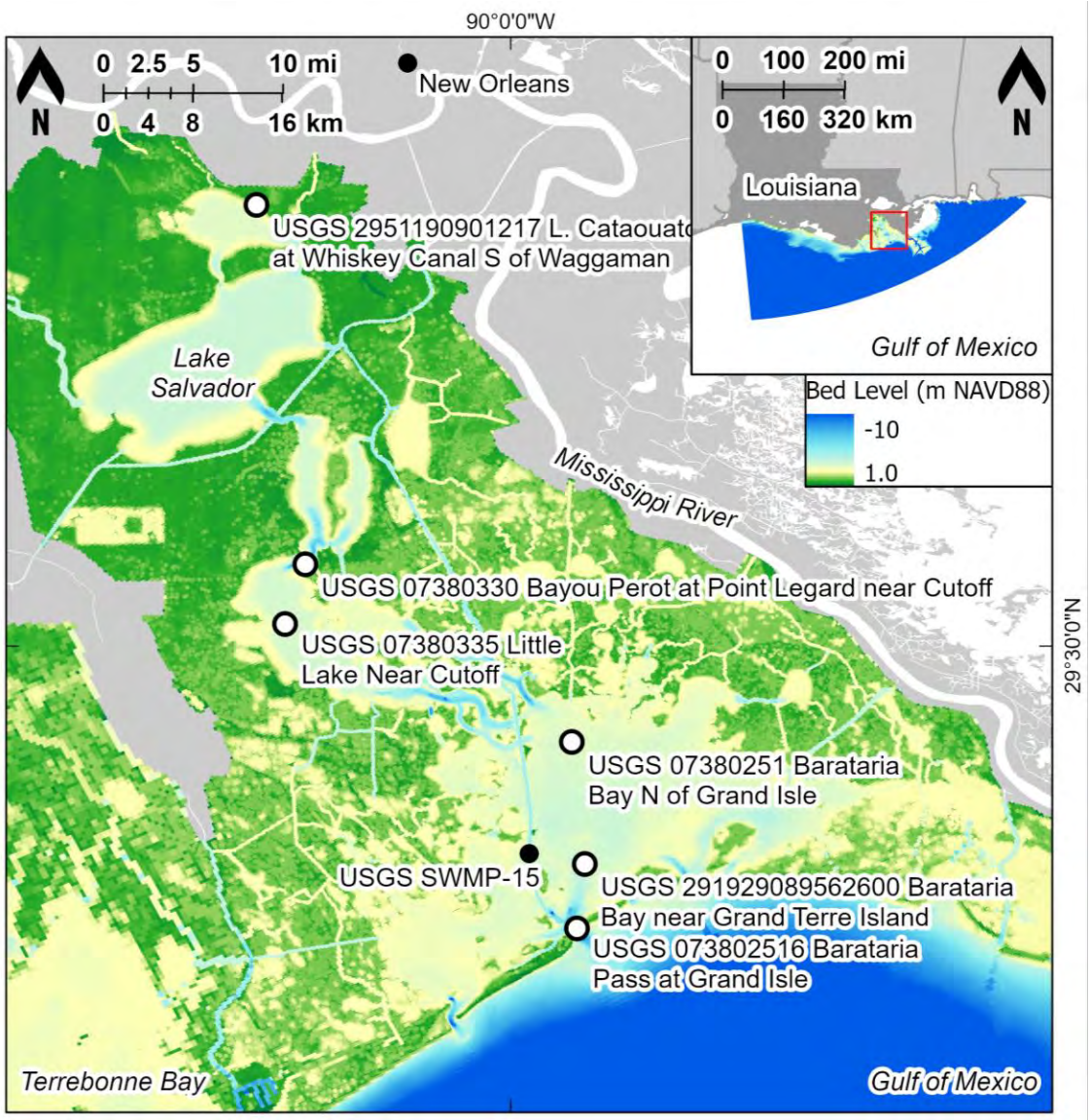

Figure A-15. Topobathymetric map of the model domain with the USGS stations used for model calibration.

A.5.1 Water Level

Model results were calibrated using USGS stations that have long-term records in various open-water locations in the Barataria Basin (Figure A-15). Comparisons between modeled and observed water levels are presented in Figure A-16 through Figure A-21. To assess the model's performance, statistical measures were calculated following guidance provided by Meselhe et al. (2017). The statistics presented in Table A-6 include the bias, root mean square error (RMSE), and the Pearson product-moment correlation coefficient. The model bias indicates whether the model tends to overestimate or underestimate the water level compared to the observed data. Ideally, this value should be as close to 0 as possible, indicating that the model predictions closely align with the observations (Meselhe et al., 2017; Moriasi et al., 2007). The RMSE represents the variation of the modeled data relative to the observed data. A lower RMSE indicates that the model's predictions are in close agreement with the actual measurements, with the ideal value being as close to 0 as possible (Legates & McCabe, 1999; Meselhe et al., 2017). The Pearson correlation coefficient measures the linear relationship between the modeled and observed water levels. A correlation coefficient of 1 indicates a perfect correlation between the model and the observations, signifying that the model accurately captures the variations in water levels seen in the real data (Legates & McCabe, 1999; Meselhe et al., 2017).

The guidance provided by Meselhe et al. (2017) defines the targets for water depth as follows:

- Percent bias: The desired target is <10% for all stations, and the acceptable target is <10% for 80% of the stations.
- Percent RMSE: The desired target is <15% for all stations, and the acceptable target is <15% for 80% of the stations.
- Pearson correlation coefficient: The desired target is >0.9 for all stations, and >0.8 for 80% of the stations.

The results in Table A-6 indicate that the model performs well in terms of the bias and RMSE targets, and it is considered acceptable for the Pearson correlation coefficient target. The largest disparities between measured and modeled data are evident when considering the Pearson correlation coefficient at station USGS 073802516, located in Barataria Pass at Grand Isle. In contrast, the two other USGS stations in Barataria Bay, namely USGS 07380251 (Barataria Bay North of Grand Isle) and USGS 291929089562600 (Barataria Bay near Grand Terre Island), exhibit correlation coefficients that are much closer to 1. These discrepancies, as well as some of the disparities in bias and RMSE, can possibly be attributed to stratification effects caused by salinity gradients. The depth-averaged model does not resolve these stratification effects, which may be influencing the accuracy of the model's predictions in these specific areas.

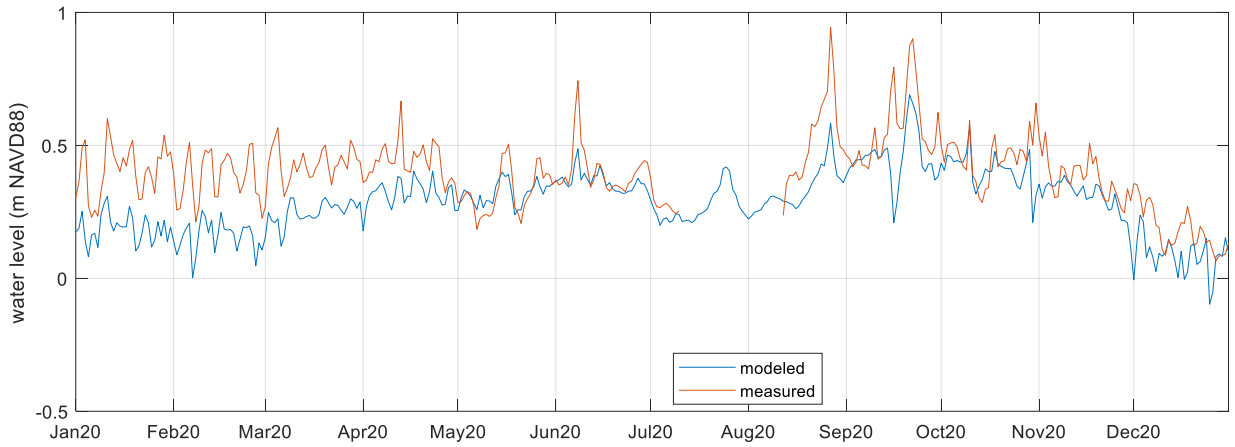

Figure A-16. Daily averaged water level comparison between model and observation at USGS 073802516 Barataria Pass at Grand Isle (see Figure A-15 for location).

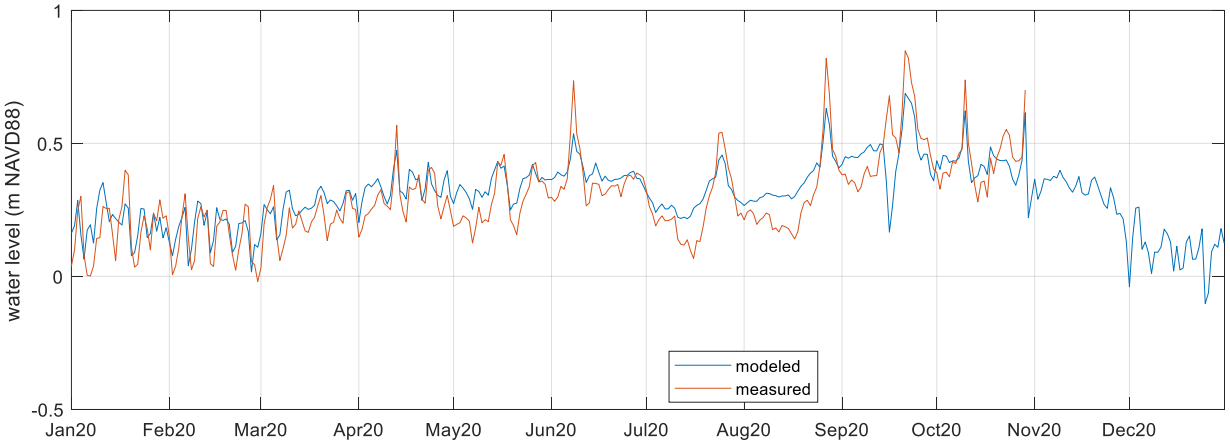

Figure A-17. Daily averaged water level comparison between model and observation at USGS 291929089562600 Barataria Bay near Grand Terre Island (see Figure A-15 for location).

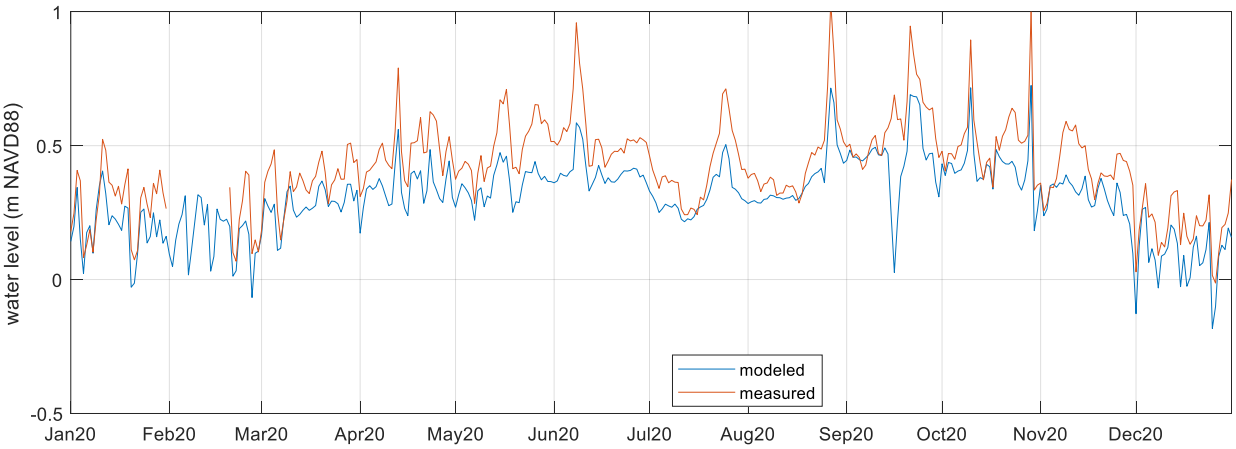

Figure A-18. Daily averaged water level comparison between model and observation at USGS 07380251 Barataria Bay N of Grand Isle (see Figure A-15 for location).

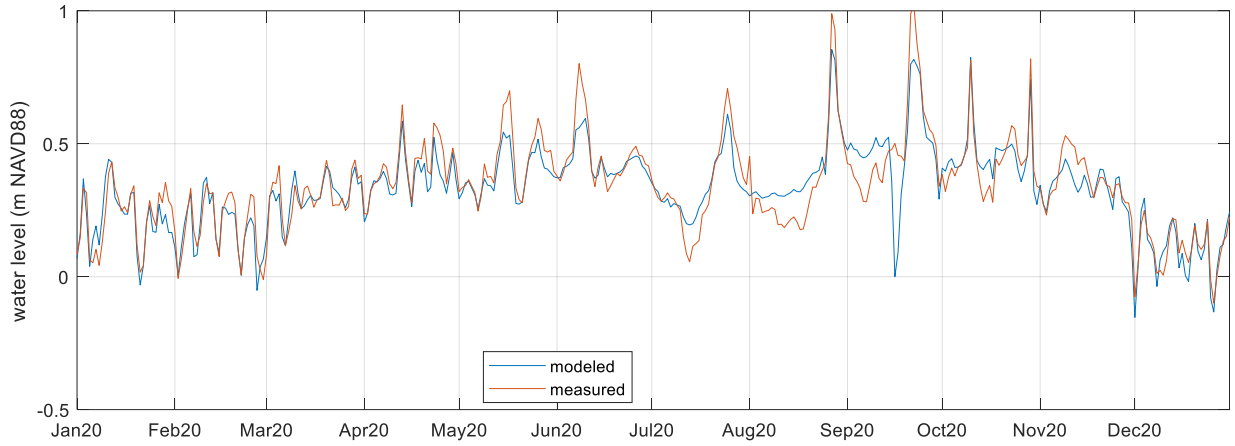

Figure A-19. Daily averaged water level comparison between model and observation at USGS 07380335 Little Lake Near Cutoff (see Figure A-15 for location).

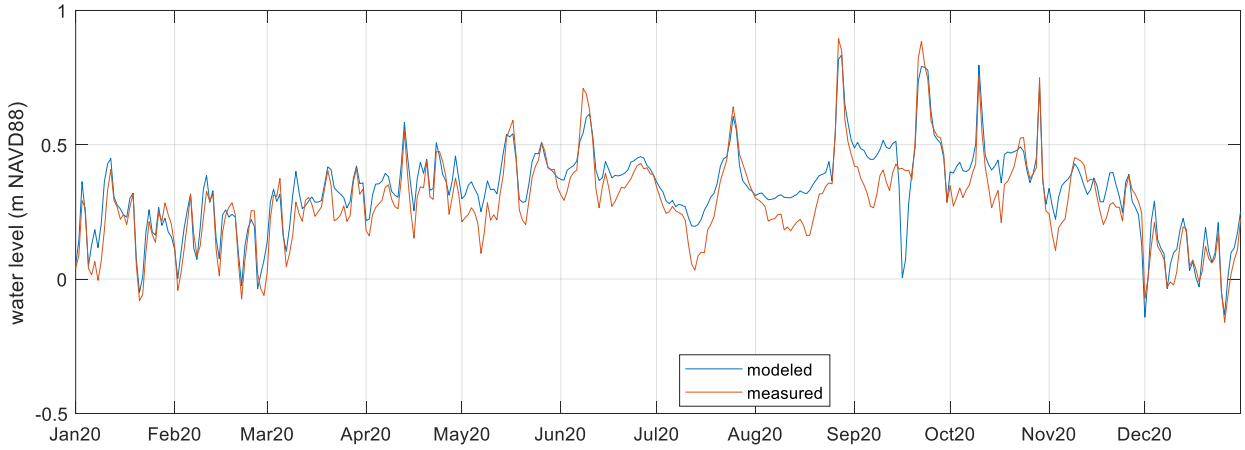

Figure A-20. Daily averaged water level comparison between model and observation at USGS 07380330 Bayou Perot at Point Legard near Cutoff (see Figure A-15 for location).

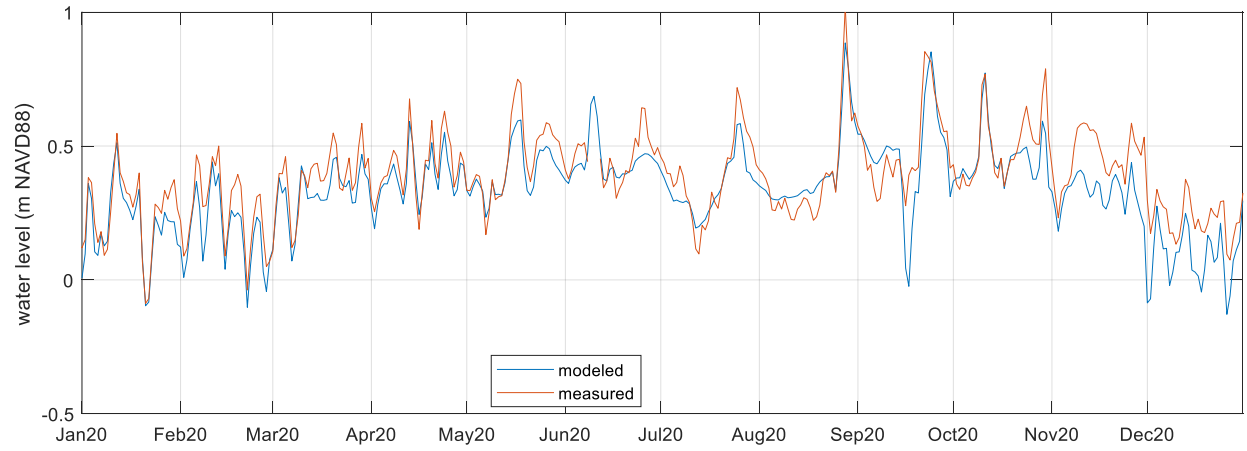

Figure A-21. Daily averaged water level comparison between model and observation at USGS 2951190901217 L. Cataouatche at Whiskey Canal S of Waggaman (see Figure A-15 for location).

Table A-6. Water level calibration statistics at the USGS stations shown in Figure A-15. Because of variation of water depth from grid cell to grid cell, a water depth of 2 m was assumed when calculating the percentages for the bias and RMSE.

Station Name	Bias (m)	Bias (% of water depth)	RMSE (m)	RMSE (% of water depth)	Correlation coefficient R (-)
USGS 073802516 Barataria Pass at Grand Isle, LA (depth below NAVD88 = 3.70 m)	-0.12	-3.2%	0.16	4.3%	0.56
USGS 291929089562600 Barataria Bay near Grand Terre Island (depth below NAVD88 = 2.47 m)	0.03	1.1%	0.09	3.6%	0.84
USGS 07380251 Barataria Bay N of Grand Isle (depth below NAVD88 = 2.20 m)	-0.11	-5.0%	0.14	6.1%	0.86
USGS 07380335 Little Lake Near Cutoff (depth below NAVD88 = 2.44 m)	-0.01	-0.3%	0.08	3.2%	0.89
USGS 07380330 Bayou Perot at Point Legard near Cutoff (depth below NAVD88 = 7.00 m)	0.04	0.6%	0.08	1.1%	0.91
USGS 2951190901217 L. Cataouatche at Whiskey Canal S of Waggaman (depth below NAVD88 = 1.43 m)	-0.04	-2.6%	0.08	5.4%	0.90

A.5.2 Tidal Range

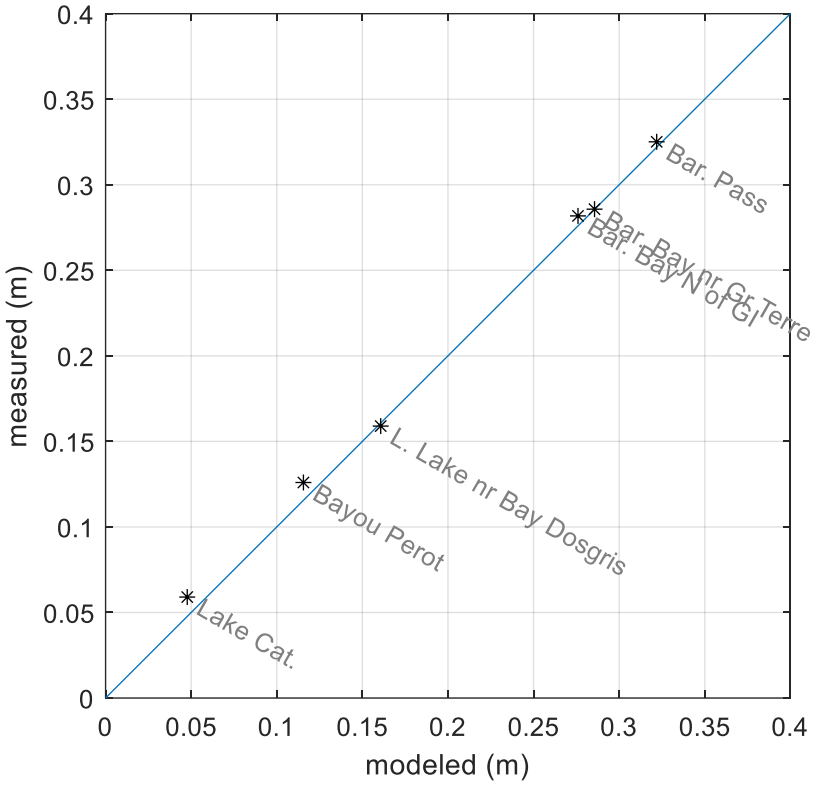

Figure A-22. Sum of amplitudes of major diurnal constituents K1, O1, P1, Q1, comparison between modeled and measured water levels, at the USGS stations in Figure A-15. The blue line represents the 1:1 line.

A.5.3 Tidal Inlets

Model results from the tidal inlets were assessed, encompassing cross-sectional areas (Table A-7), peak discharges (

Table A-8, Figure A-23A), flow velocities (

Table A-9, Figure A-23B), and total suspended sediment concentrations (Table A-10, Figure A-24, Figure A-25). These results were compared to findings from prior studies that used field data acquired through ADCPs and turbidity sensors (FitzGerald et al., 2007; Li et al., 2011; Ramatchandirane et al., 2019). Instead of running the model using the exact temporal parameters as the data collection instances, the analysis involved contrasting peak values and ranges between the measured and modeled data. The model demonstrates good agreement when assessing these peak values and ranges. Disparities can be partly attributed to the fact that some of the studies use older data, as well as the variations in discharges, velocities, and concentrations depending on the conditions when the data was collected (such as high energy or quiescent conditions, spring or neap tides). Additionally, disparities arise due to slight differences in measurement locations, or whether data was averaged across the whole inlet or derived from specific locations across the width or depth of the inlet.

Table A-7. Comparison of tidal inlet cross-sectional areas between historical records compiled by FitzGerald et al. (2007) and modeled values for the initial bathymetry in the numerical model. The modeled areas represent yearly averages for 2020, as instantaneous cross-sectional areas exhibit variability based on the water level.

		Inlet cross-sectional area (m^2)						
	Year	Caminada Pass	Barataria Pass	Pass Abel	Quatre Bayou Pass	Pass Ronquille	**Total (excluding Pass Ronquille)**	Total (including Pass Ronquille)
Historical records from Fitzgerald et al. (2007)	**1880**	809	3,996	0	133	N/A	**4,938**	N/A
	1930	1,353	7,079	395	2,590	N/A	**11,417**	N/A
	1980	1,532	8,712	4,193	3,777	N/A	**18,214**	N/A
	2006	3,372	7,541	6,669	6,726	N/A	**24,308**	N/A
Modeled (based on initial bathymetry in 2020)	**2020**	4,371	8,966	5,210	8,055	3,453	**26,602**	30,055

Table A-8. Comparison of peak tidal inlet discharges compared between historical records (FitzGerald et al., 2007; Li et al., 2011; Ramatchandirane et al., 2019) derived from ADCP measurements, and modeled values. The modeled values are derived from the entire year of 2020 (also see Figure A-23A). All positive values indicate flow toward the Gulf of Mexico (ebb tide), while negative discharges indicate flow toward Barataria Bay (flood tide).

		Inlet cross-sectional discharge (m^3/s)					
		Caminada Pass	Barataria Pass	Pass Abel	Quatre Bayou Pass	Pass Ronquille	**Combined (excluding Pass Ronquille)**
Fitzgerald et al. (2007), Figure 6: Two diurnal cycles, paper does not disclose information on when ADCP data was collected	**Peak flood**	N/A	~ -3,400	~ -1,400	~ -1,700	N/A	**N/A**
	Peak ebb	~ 1,700	~ 5,100	~ 1,700	~ 2,300	N/A	**10,800**
Li et al. (2011), Figure 6a: Full diurnal cycle on July 31st to August 1st in 2008 (spring tide conditions)	**Peak flood**	N/A	~ -6,500	N/A	N/A	N/A	**N/A**
	Peak ebb	N/A	~ 7,500	N/A	N/A	N/A	**N/A**
Ramatchandirane et al. (2019), Appendix A: Discharge based on various ADCP deployments between January and September 2019	**Peak flood**	N/A	N/A	N/A	-2,465	N/A	**N/A**
	Peak ebb	1,987	7,264	2,392	3,534	1,582	**16,759**
Modeled (entire year of 2020)	**1st percentile (i.e., near-peak flood)**	-2,213	-5,808	-3,030	-4,402	-1,718	**-17,171**
	5th percentile	-1,850	-4,891	-2,439	-3,693	-1,443	**-14,316**
	95th percentile	2,035	5,543	2,298	3,582	1,534	**14,992**
	99th percentile (i.e., near-peak ebb)	2,390	6,510	2,807	4,409	1,841	**17,957**

Table A-9. Comparison of tidal inlet velocities compared between historical records (Li et al., 2011; Ramatchandirane et al., 2019) derived from ADCP measurements, and modeled values. The modeled values are derived from the entire year of 2020 (also see Figure A-23B). All positive values indicate flow toward the Gulf of Mexico (ebb tide), while negative discharges indicate flow toward Barataria Bay (flood tide).

		Inlet velocity (m/s)				
		Caminada Pass	Barataria Pass	Pass Abel	Quatre Bayou Pass	Pass Ronquille
Li et al. (2011), Figure 3: Full diurnal cycle on July 31st to August 1st in 2008 (spring tide conditions)	**Peak flood**	N/A	N/A	N/A	N/A	N/A
	Peak ebb	N/A	0.6 m/s near bed and banks, up to 1.3 m/s near surface at channel center	N/A	N/A	N/A
Ramatchandirane et al. (2019), Figures 10 and 21: Velocities based on ADCP deployments between January and September 2019	**Peak flood**	N/A	N/A	N/A	N/A	N/A
	Peak ebb	N/A	- May 22, 2019, during near-spring tide conditions: 0.5 m/s near bed and banks, up to 1.0 m/s near surface at channel center - September 10, 2019, also during near-spring tide conditions, average velocity up to 0.8 m/s	N/A	N/A	N/A
Modeled (cross-sectional averages, from entire year of 2020)	**1st percentile (i.e., near-peak flood)**	-0.48	-0.63	-0.52	-0.52	-0.46
	5th percentile	-0.41	-0.53	-0.44	-0.44	-0.39
	95th percentile	0.48	0.64	0.48	0.47	0.49
	99th percentile (i.e., near-peak ebb)	0.57	0.75	0.58	0.57	0.58

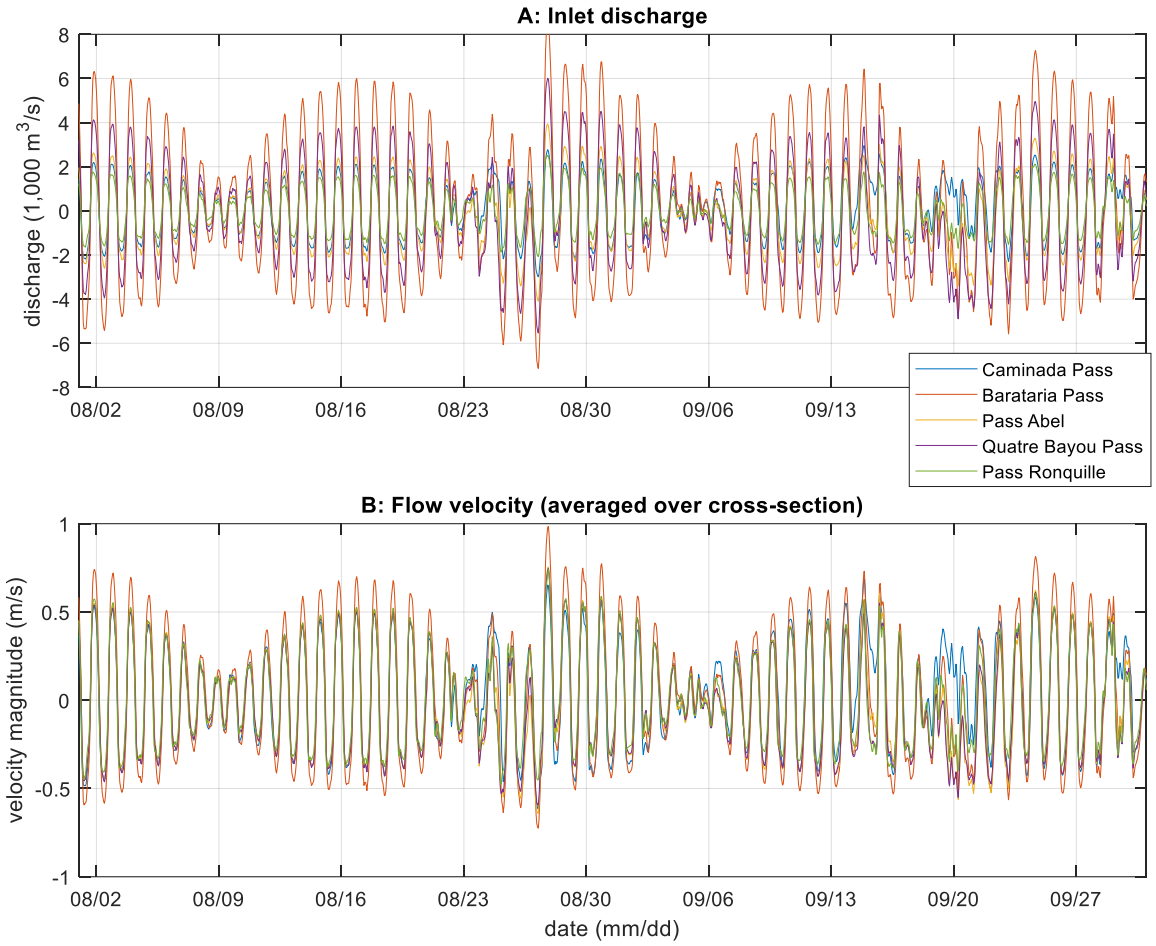

Figure A-23. Modeled tidal inlet discharges (A) and cross-section averaged velocities (B) for the months of August and September of year 2020 across the major tidal inlets (Caminada Pass, Barataria Pass, Pass Abel, Quatre Bayou Pass, and Pass Ronquille).

Table A-10. Comparison of suspended sediment concentrations at the tidal inlets, compared between historical records (Li et al., 2011; Ramatchandirane et al., 2019), and modeled values. The modeled values are derived from simulations representing quiescent conditions (Figure A-24) and cold front conditions (Figure A-25).

	Suspended sediment concentrations (mg/L)
Li et al. (2011), Figure 5 (Barataria Pass): Full diurnal cycle on July 31st to August 1st in 2008 (spring tide conditions)	10–450
Ramatchandirane et al. (2019), Appendix C (all tidal inlets): Concentrations based on turbidity sensor deployments between January and September 2019	10–190
Modeled (all tidal inlets, concentrations derived at center of inlet during quiescent and cold front conditions)	5– ~600

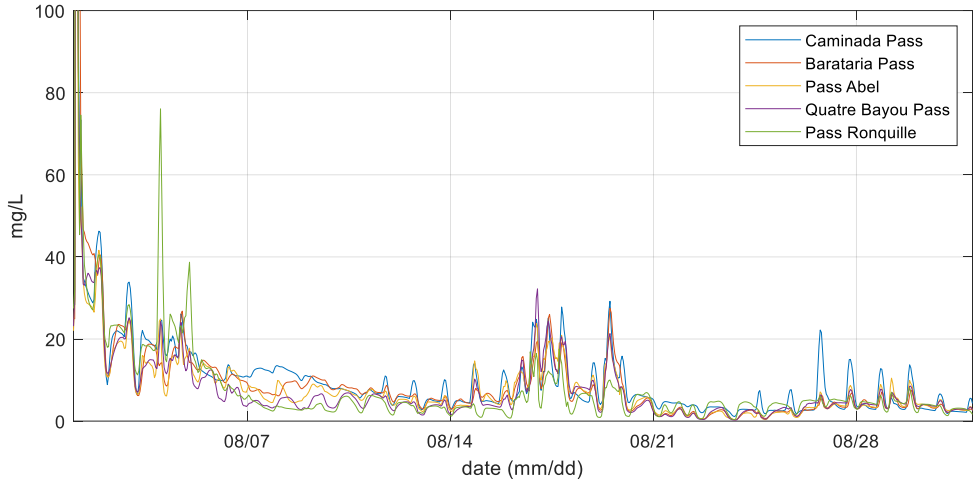

Figure A-24. Modeled suspended sediment concentrations across the major tidal inlets (Caminada Pass, Barataria Pass, Pass Abel, Quatre Bayou Pass, and Pass Ronquille) during quiescent conditions in August 2016.

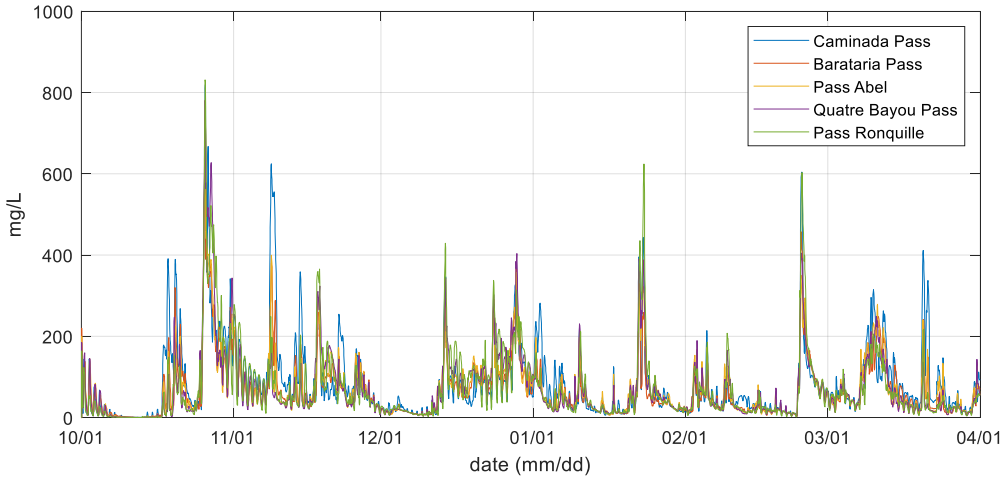

Figure A-25. Modeled suspended sediment concentrations across the major tidal inlets (Caminada Pass, Barataria Pass, Pass Abel, Quatre Bayou Pass, and Pass Ronquille) during cold front conditions in late 2015 and early 2016.

A.5.4 Waves

The model demonstrates satisfactory agreement for significant wave heights larger than 0.2 m (Figure A-27B and Figure A-29B). During transitional conditions, simulated wave heights are overestimated, but the model performs well in capturing both low- and high-energy events (Figure A-26 and Figure A-28). However, there is limited agreement for waves below 0.2 m (Figure A-27A and Figure A-29A), possibly due to shortcomings in the NAM wind data at low wind speeds. Considering that sediment resuspension only occurs during high-energy events when in-bay significant wave heights exceed 0.3 m, the model's performance was deemed acceptable for the specific objectives of this study.

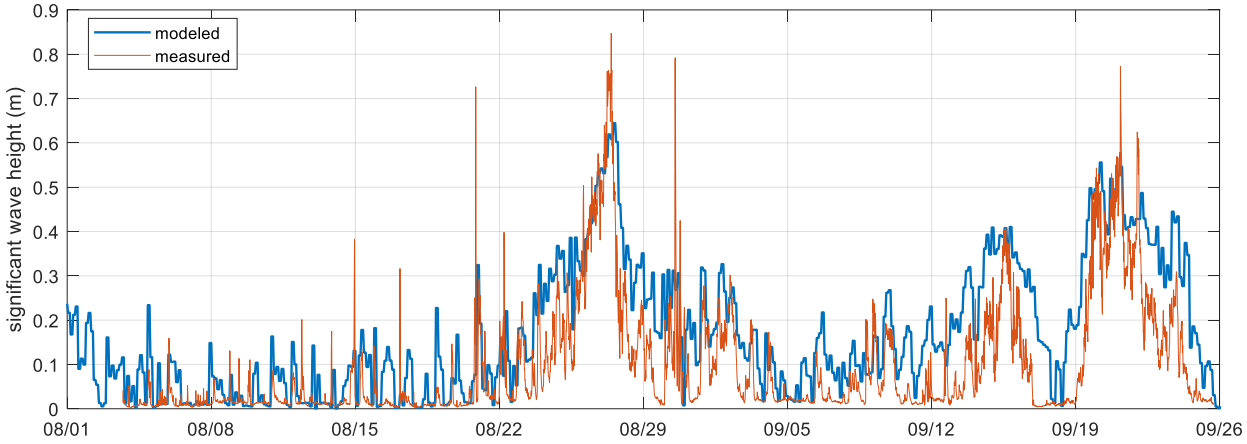

Figure A-26. Significant wave height timeseries comparison between model results and with observations at USGS 07380251 Barataria Bay N of Grand Isle (see Figure A-15 for location) in August and September 2020. Wave data were obtained from Matt Hyatt (LSU) and were supported by the Systemwide Assessment Monitoring Program (SWAMP).

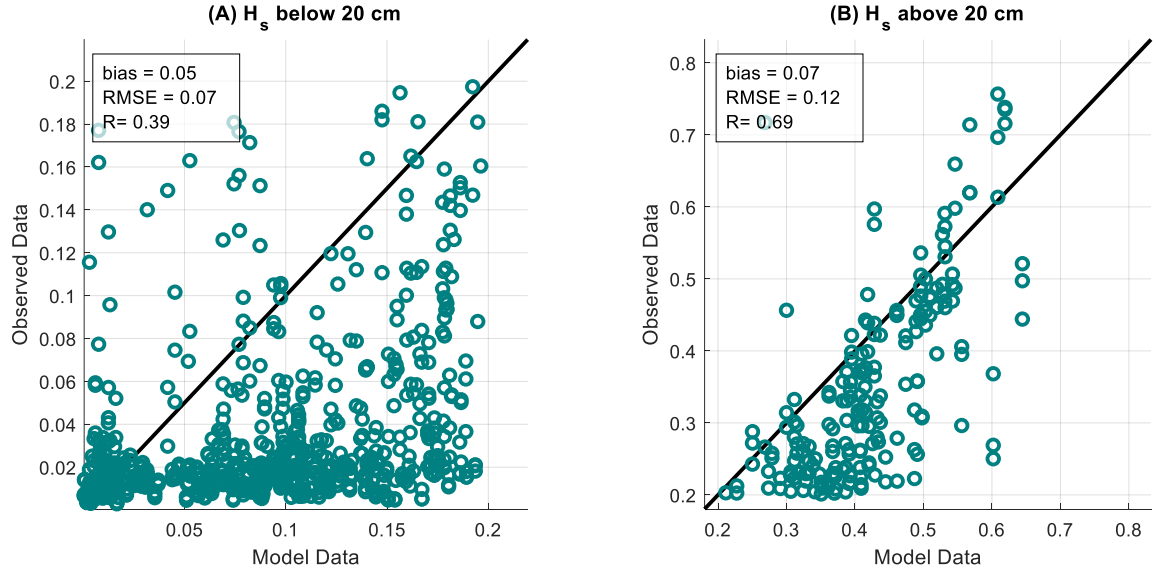

Figure A-27. Significant wave height (m) scatter plot comparison between model results and observations at USGS 07380251 Barataria Bay N of Grand Isle in August and September 2020 (see Figure A-15 for location). The left panel (A) exclusively displays waves below 20 cm, while the right panel (B) exclusively shows waves above 20 cm. The black line represents the 1:1 line. Wave data were obtained from Matt Hiatt (LSU) and were supported by the Systemwide Assessment Monitoring Program (SWAMP). Statistics are provided as bias (m), root mean square error (RMSE, m), and correlation coefficient R (-).

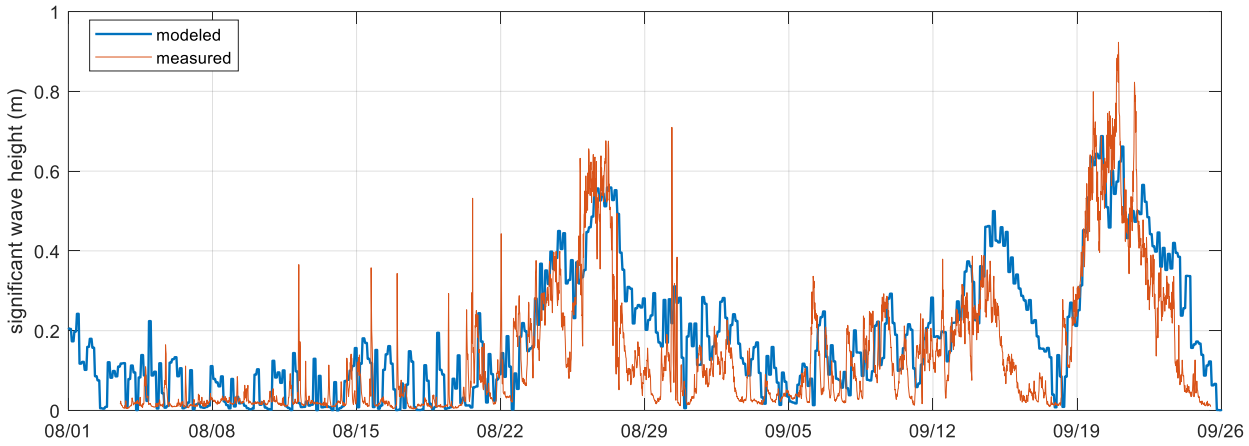

Figure A-28. Significant wave height timeseries comparison between model results and with observations at USGS SWMP-15 in August and September 2020 (see Figure A-15 for location). Wave data were obtained from Matt Hyatt (LSU) and were supported by the Systemwide Assessment Monitoring Program (SWAMP).

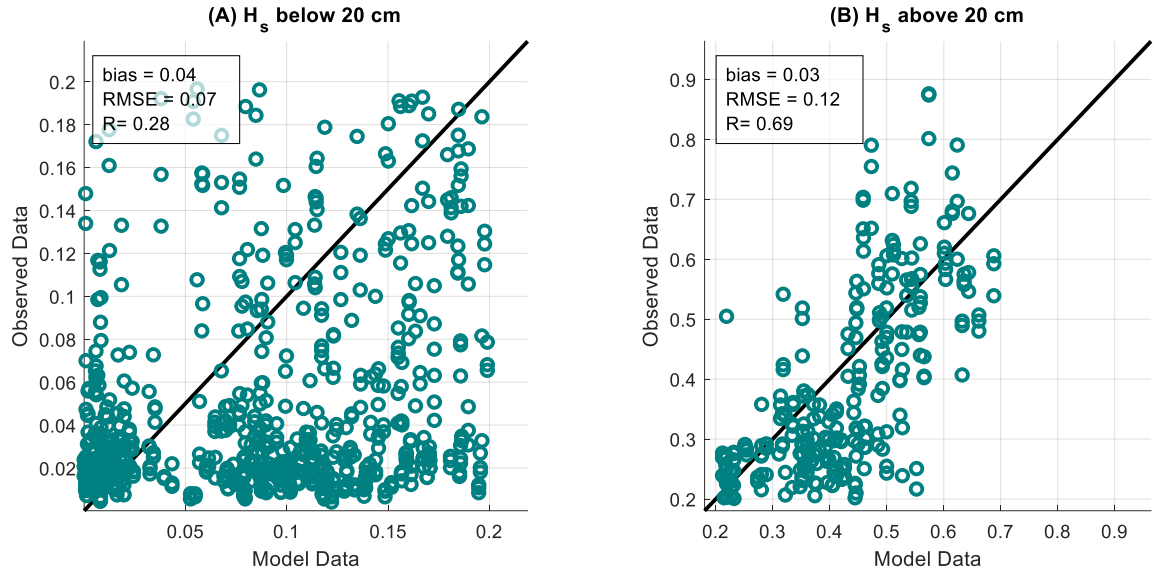

Figure A-29. Significant wave height (m) scatter plot comparison between model results and observations at USGS SWMP-15 in August and September 2020 (see Figure A-15 for location). The left panel (A) displays waves below 20 cm, while the right panel (B) shows waves above 20 cm. The black line represents the 1:1 line. Wave data were obtained from Matt Hyatt (LSU) and were supported by the Systemwide Assessment Monitoring Program (SWAMP). Statistics are provided as bias (m), root mean square error (RMSE, m), and correlation coefficient R (-).

A.5.5 Mississippi River Flow Distribution

Table A-11. Flow distribution rates through the modern delta of the Mississippi River downstream of Venice, as reported in literature and modeled. The literature-based rates are derived from McCorquodale et al. (2010) and Allison et al. (2012).

Distributary pass	Flow as percentage of total discharge at Venice		
	Literature (McCorquodale et al., 2010)	**Literature** (Allison et al., 2012)	**Modeled**
Baptiste Collette	10%	11%	10%
Grand Pass (including Tiger Pass)	12%	12%	12%
Main Pass (Cubit's Gap)	12%	12%	10%
Pass A Loutre	11%	10%	9%
South Pass	11%	10%	11%
Southwest Pass	36%	36%	37%
West Bay Sediment Diversion	6%	7%	6%

A.5.6 Sediment Transport and Morphology

The model utilized in this study is a modified version of a previous model developed by The Water Institute of the Gulf (2022). During the development of that model, the calibration of sediment transport was focused on assessing the trends of sediment transport along the shoreface, tidal inlets, and back barrier bays. Morphology was calibrated by comparing the erosional and depositional rates, trends, and patterns in the upper shoreface and bay floors. Given the limited availability of field observations with which to calibrate sediment transport and morphology models, the predictions of morphology were compared to previous studies of the geomorphic evolution of the Caminada Headland by Miner et al. (2009). The performance of the model was assessed by visually inspecting maps that display sediment transport rates and bed level changes through a series of iterative model tests. The modeled suspended sediment concentrations were compared and calibrated against the bottom suspended sediment concentrations reported by Li et al. (2021). However, it should be noted that the model results were depth-averaged, while the measurements taken by Li et al. (2021) were obtained near the bed. An overview of the key parameters that were adjusted during the calibration and sensitivity testing of the model is given in Table A-12. The selected values of the parameters that describe sediment characteristics are in line with typical literature values found in laboratory tests for systems with mud-sand mixtures as described by (Van Rijn & Barth, 2019). For example, dry bulk densities of sand-mud mixtures typical range from 400–1000 kg/m^3 after the primary (short-term) consolidation process (Van Rijn & Barth, 2019). For this study, a dry bulk density of 600 kg/m^3 was selected. Critical bed shears stress for surface erosion of consolidated mud-sand mixtures generally ranges between 0.2 and 1 Pa, while 0.5 Pa was selected for this study (Van Rijn, 2020).

Table A-12. Key sediment characteristics and calibration parameters used in the calibration and sensitivity testing of the modeled sediment transport and morphology.

Category	Parameter	Values (final selected values are underlined)
Sediment characteristics	Sand median grain size (D50)	110, 120, 130 µm
	Settling velocity (silt fraction)	0.30, 0.15, 0.085 mm/s (velocities correspond to D50s of 60, 40, 30 µm, respectively)
	Settling velocity (clay fraction)	0.0050, 0.0025, 0.00144, 0.00036 mm/s (velocities correspond to D50s of 7.5, 5, 4, 2 µm, respectively)
	Critical shear stress for erosion of consolidated mud (i.e., silt and clay)	0.2, 0.5, 0.75, 1, 1.5 Pa
	Dry bed (or bulk) density of consolidated mud (i.e., silt and clay)	1720, 600 kg/m^3
	Dry bed (or bulk) density of sand	1720 kg/m^3
Sediment transport	Suspended sediment transport factor: current-related	0.2, 0.5, 1
	Suspended sediment transport factor: wave-related	0.2, 0.5, 1
	Bedload transport factor: current-related	0.2, 0.5, 1
	Bedload transport factor: wave-related	0.2, 0.5, 1
Morphology	Mobile bed composition in Barataria Bay	8% sand / 14% silt / 78% clay 8% sand / 28% silt / 64% clay 15% sand / 50% silt / 35% clay
	Morphological scale factor (MorFac) for cold-front simulations	1, 5, 10, 20
	Dry cell erosion factor	0.5, 1

APPENDIX B. ADDITIONAL MODEL RESULTS

This appendix contains additional model results, presented in six sections. Section B.1 provides timeseries figures showing the response of Barataria Bay and the hypothetical borrow pits to various meteorological conditions (i.e., quiescent conditions, cold fronts, tropical cyclones). Sections B.2 and B.3 provide several examples demonstrating the hydrodynamic response of the system and borrow pits to high-energy events such as a tropical storms and cold fronts, respectively. In Section B.4, figures display bed level changes after 20 years for all evaluated scenarios. Section B.5 includes figures that isolate borrow pit impacts from other morphological changes driven by environmental conditions by subtracting bed level changes between scenarios with and without pits. Section B.6 contains tables with a breakdown of borrow pit infilling for each of the simulation meteorological conditions.

B.1 TIMESERIES: SYSTEM RESPONSE IN BAY AND BORROW PITS

This section contains detailed timeseries figures of the response of Barataria Bay and the hypothetical borrow pits to various meteorological conditions. In Chapter 3.0, Figure 2 in Section 3.1 and Figure 4 in Section 3.2 showed partial results of the simulation representing the cold fronts for Scenarios 1 and 2. The following figures (Figure B-1 through Figure B-9) show the results for all borrow pit configurations (S1 through S4) for all meteorological conditions, including quiescent conditions (Figure B-1), the entire 6-month cold front simulation (Figure B-2), the five tropical cyclones simulated for the first decade (Figure B-3 through Figure B-7), and the two tropical cyclones simulation for the second decade (Figure B-8 and Figure B-9).

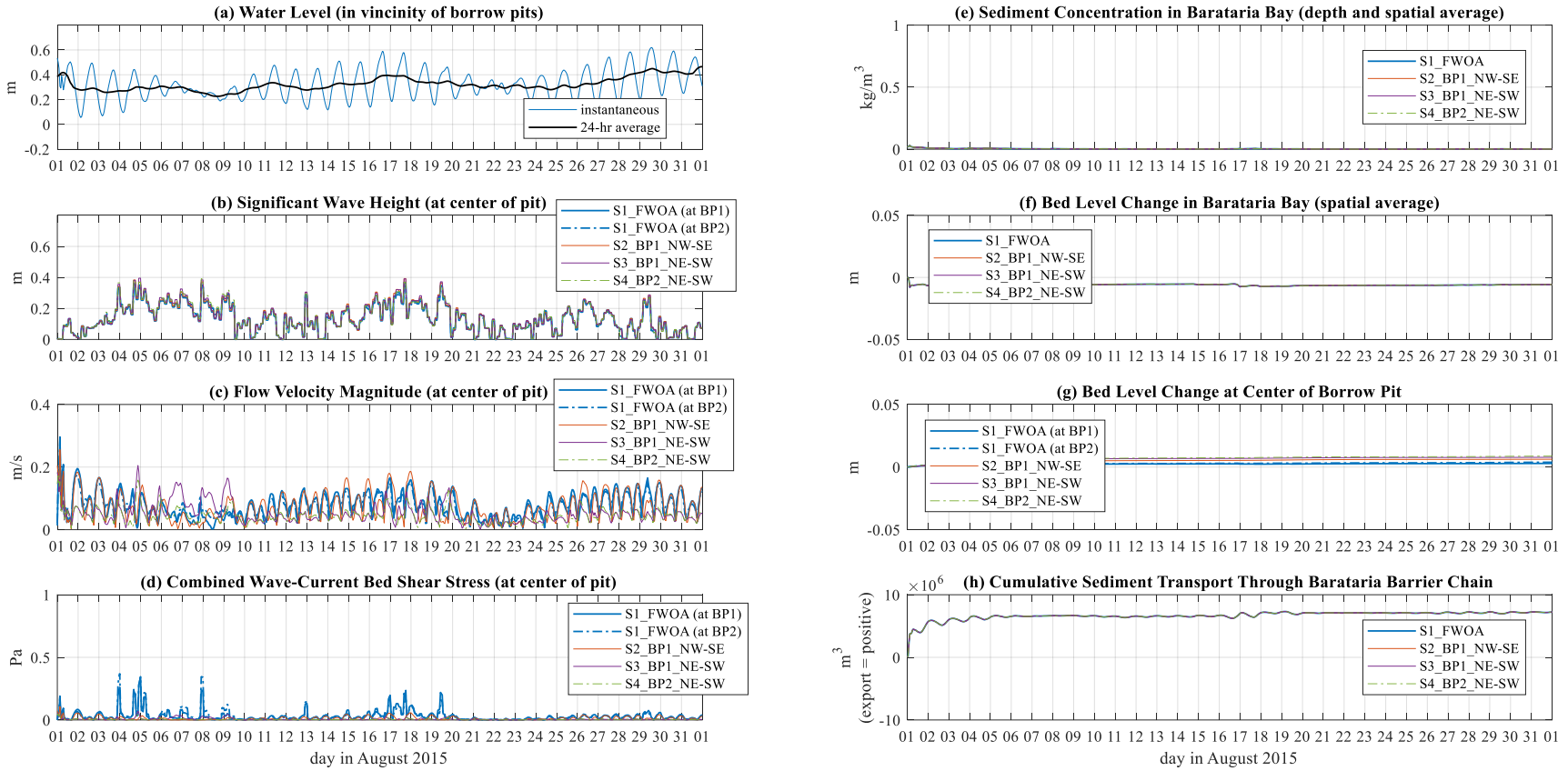

Figure B-1. Quiescent conditions (August 2015, simulation results from the first decade): simulated (a) water level (in vicinity of both borrow pits), (b) significant wave height (at center of borrow pit), (c) flow velocity magnitude (at center of borrow pit), (d) combined wave-current bed shear stress (at center of borrow pit), (e) sediment concentration (spatially and depth-averaged across Barataria Bay), (f) upscaled bed level change (spatially averaged across Barataria Bay), (g) upscaled bed level change at the center of the borrow pit, and (h) cumulative sediment transport (export = positive) through the Barataria Barrier Chain, i.e., Caminada Pass, Barataria Pass, Pass Abel, Quatre Bayou Pass, and Pass Ronquille. The S1_FWOA (Scenario 1 Future Without Action) results in subfigures (b), (c), (d), and (g) are taken from the location where Borrow Pit 1 would be situated in Scenario 2 and 3 (solid line), and where Borrow Pit 2 is situated in Scenario 4 (dashed line).

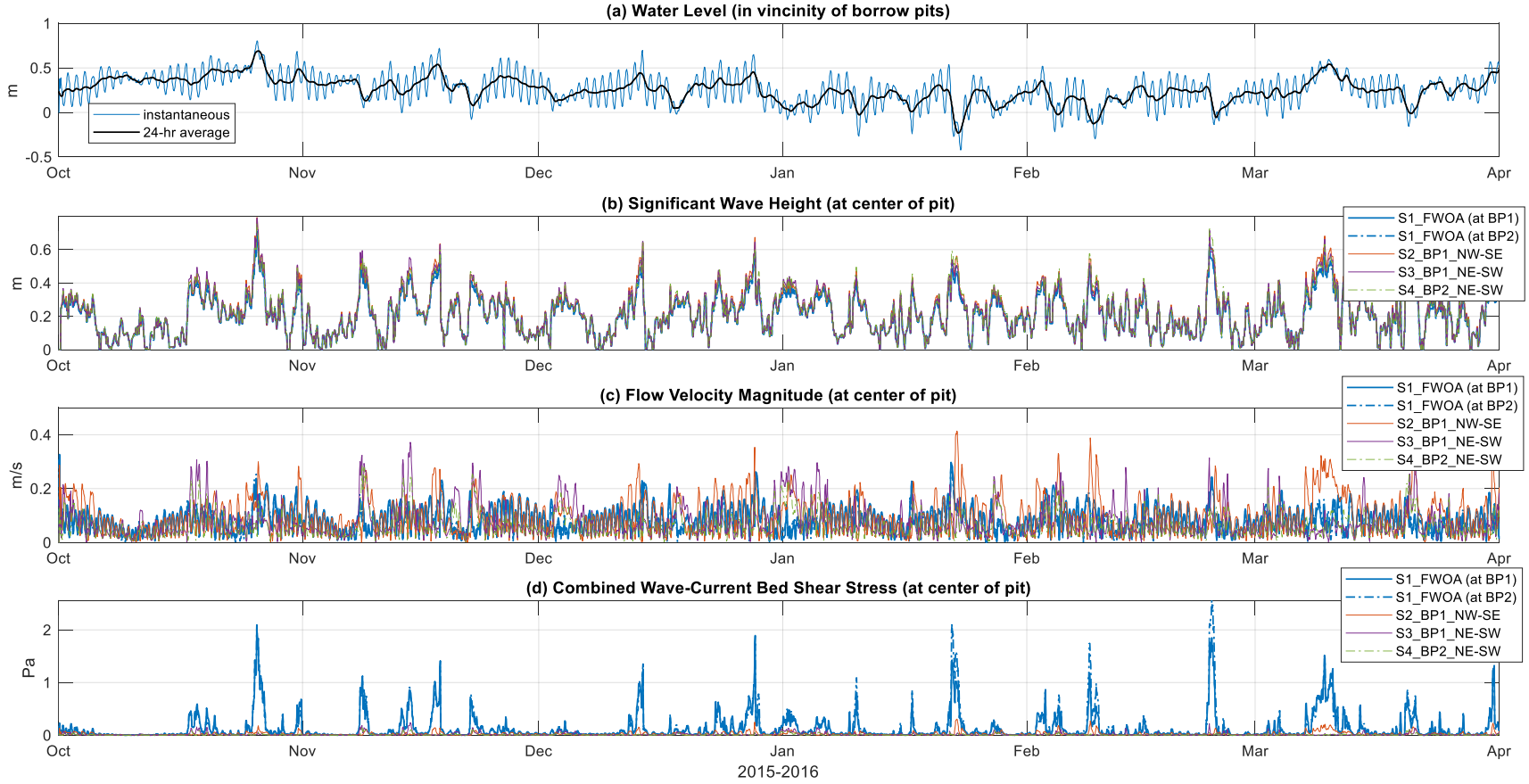

(figure continued on next page)

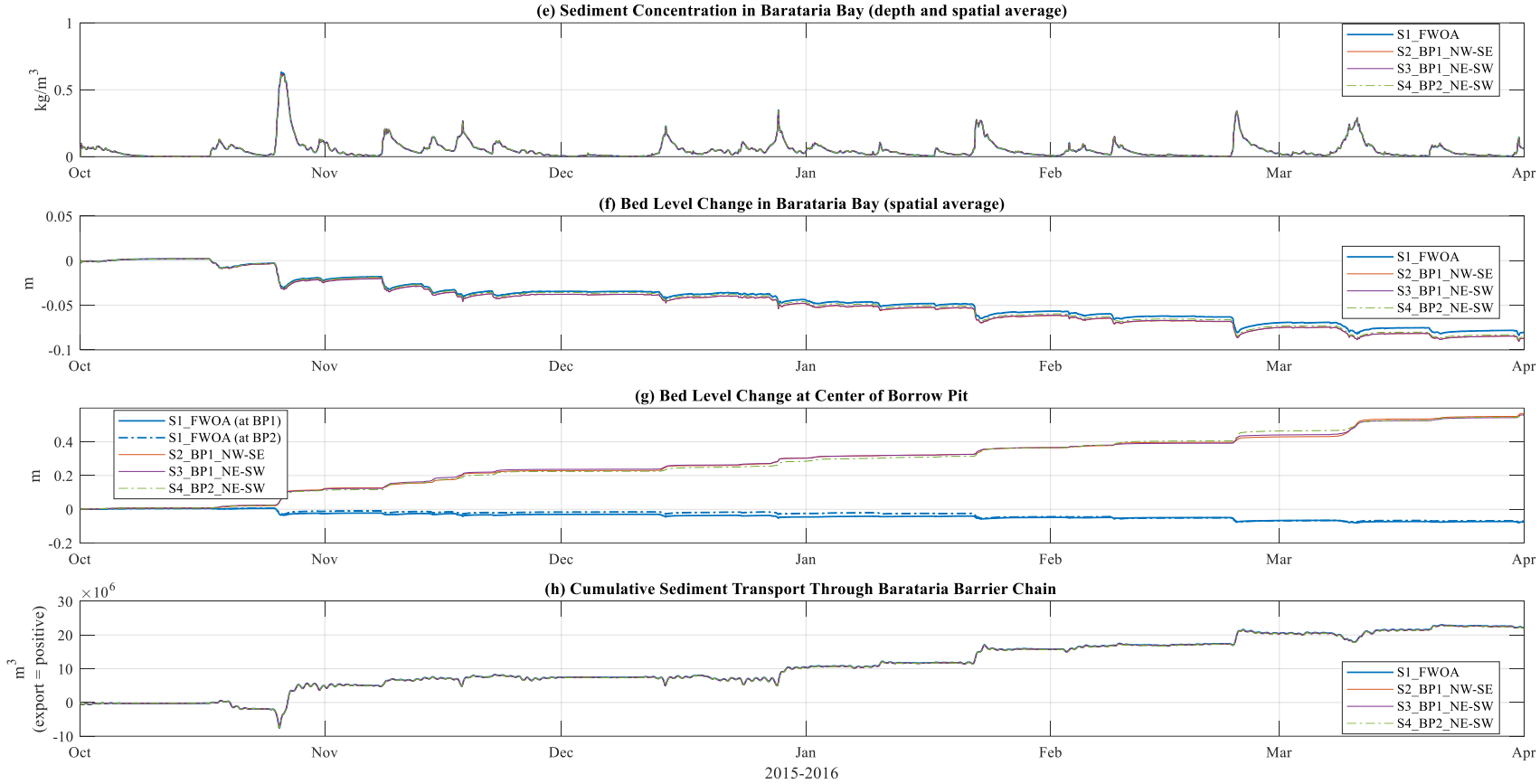

Figure B-2. Cold front conditions (Oct 2015 – Apr 2016, simulation results from the first decade): simulated (a) water level (in vicinity of both borrow pits), (b) significant wave height (at center of borrow pit), (c) flow velocity magnitude (at center of borrow pit), (d) combined wave-current bed shear stress (at center of borrow pit), (e) sediment concentration (spatially and depth-averaged across Barataria Bay), (f) upscaled bed level change (spatially averaged across Barataria Bay), (g) upscaled bed level change at the center of the borrow pit, and (h) cumulative sediment transport (export = positive) through the Barataria Barrier Chain, i.e., Caminada Pass, Barataria Pass, Pass Abel, Quatre Bayou Pass, and Pass Ronquille. The S1_FWOA (Scenario 1 Future Without Action) results in subfigures (b), (c), (d), and (g) are taken from the location where Borrow Pit 1 would be situated in Scenario 2 and 3 (solid line), and where Borrow Pit 2 is situated in Scenario 4 (dashed line).

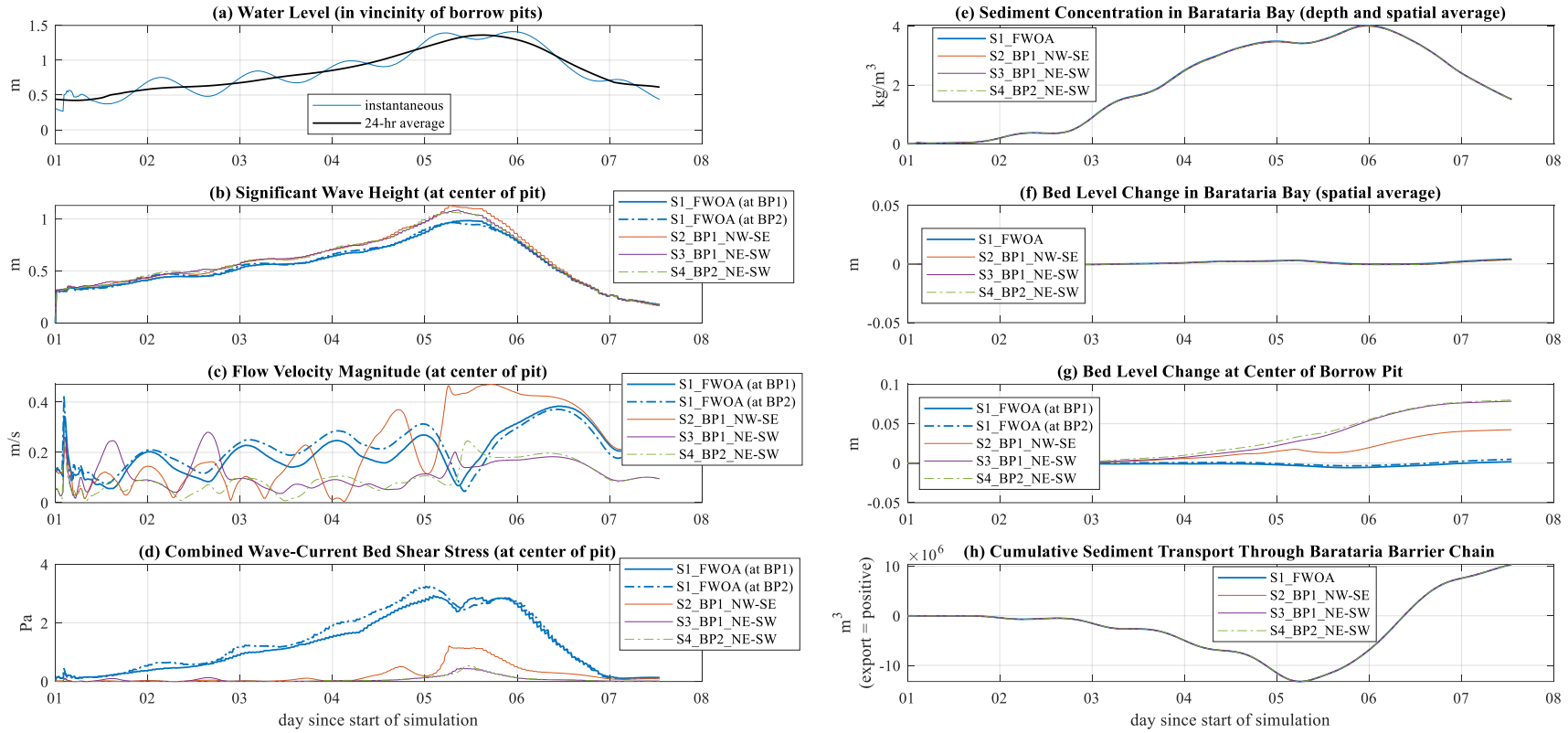

Figure B-3. Tropical cyclone ID357 (simulated during the first decade): simulated (a) water level (in vicinity of both borrow pits), (b) significant wave height (at center of borrow pit), (c) flow velocity magnitude (at center of borrow pit), (d) combined wave-current bed shear stress (at center of borrow pit), (e) sediment concentration (spatially and depth-averaged across Barataria Bay), (f) bed level change (spatially averaged across Barataria Bay), (g) bed level change at the center of the borrow pit, and (h) cumulative sediment transport (export = positive) through the Barataria Barrier Chain, i.e., Caminada Pass, Barataria Pass, Pass Abel, Quatre Bayou Pass, and Pass Ronquille. The S1_FWOA (Scenario 1 Future Without Action) results in subfigures (b), (c), (d), and (g) are taken from the location where Borrow Pit 1 would be situated in Scenario 2 and 3 (solid line), and where Borrow Pit 2 is situated in Scenario 4 (dashed line).

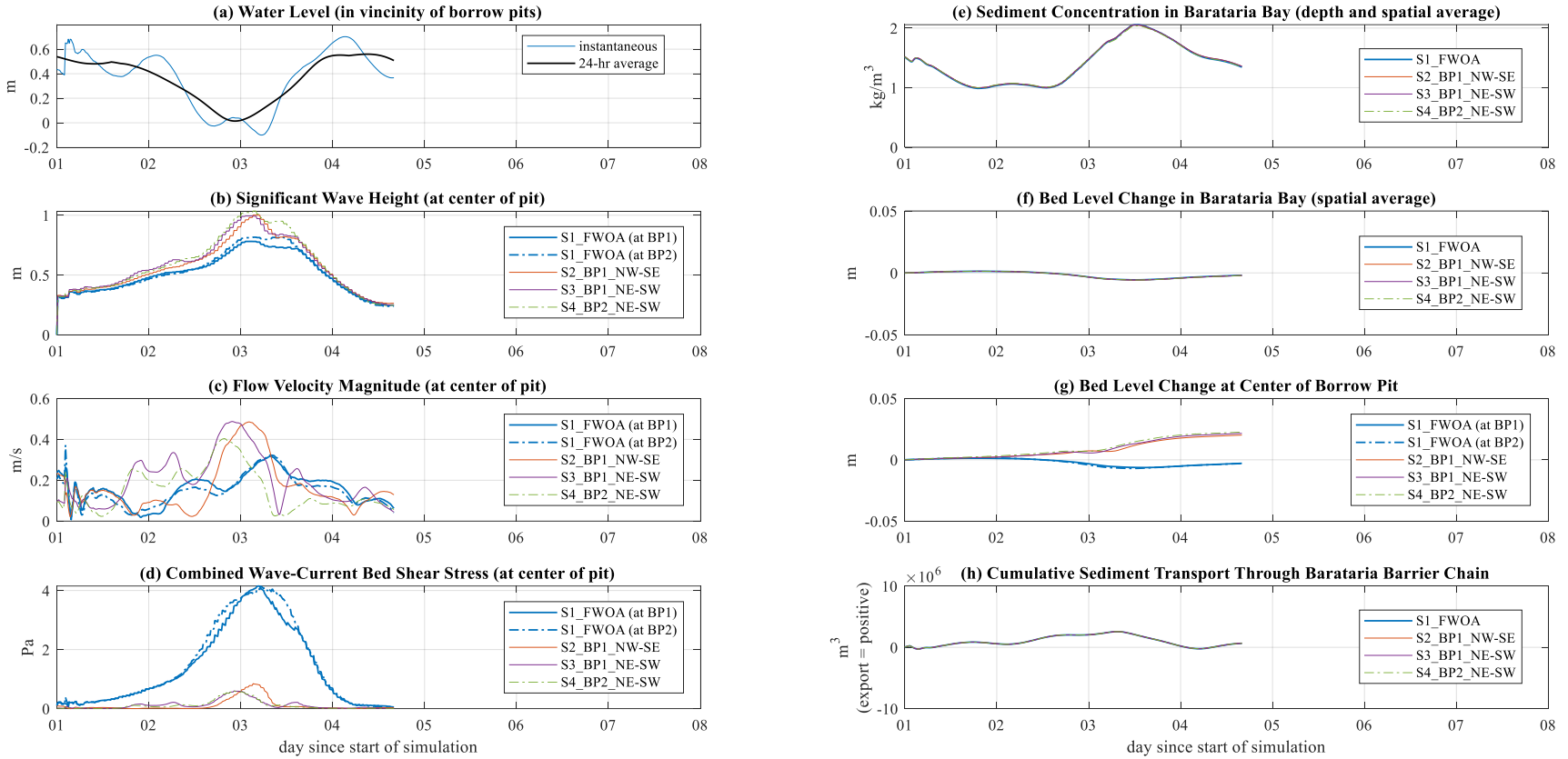

Figure B-4. Tropical cyclone ID102 (simulated during the first decade): simulated (a) water level (in vicinity of both borrow pits), (b) significant wave height (at center of borrow pit), (c) flow velocity magnitude (at center of borrow pit), (d) combined wave-current bed shear stress (at center of borrow pit), (e) sediment concentration (spatially and depth-averaged across Barataria Bay), (f) bed level change (spatially averaged across Barataria Bay), (g) bed level change at the center of the borrow pit, and (h) cumulative sediment transport (export = positive) through the Barataria Barrier Chain, i.e., Caminada Pass, Barataria Pass, Pass Abel, Quatre Bayou Pass, and Pass Ronquille. The S1_FWOA (Scenario 1 Future Without Action) results in subfigures (b), (c), (d), and (g) are taken from the location where Borrow Pit 1 would be situated in Scenario 2 and 3 (solid line), and where Borrow Pit 2 is situated in Scenario 4 (dashed line).

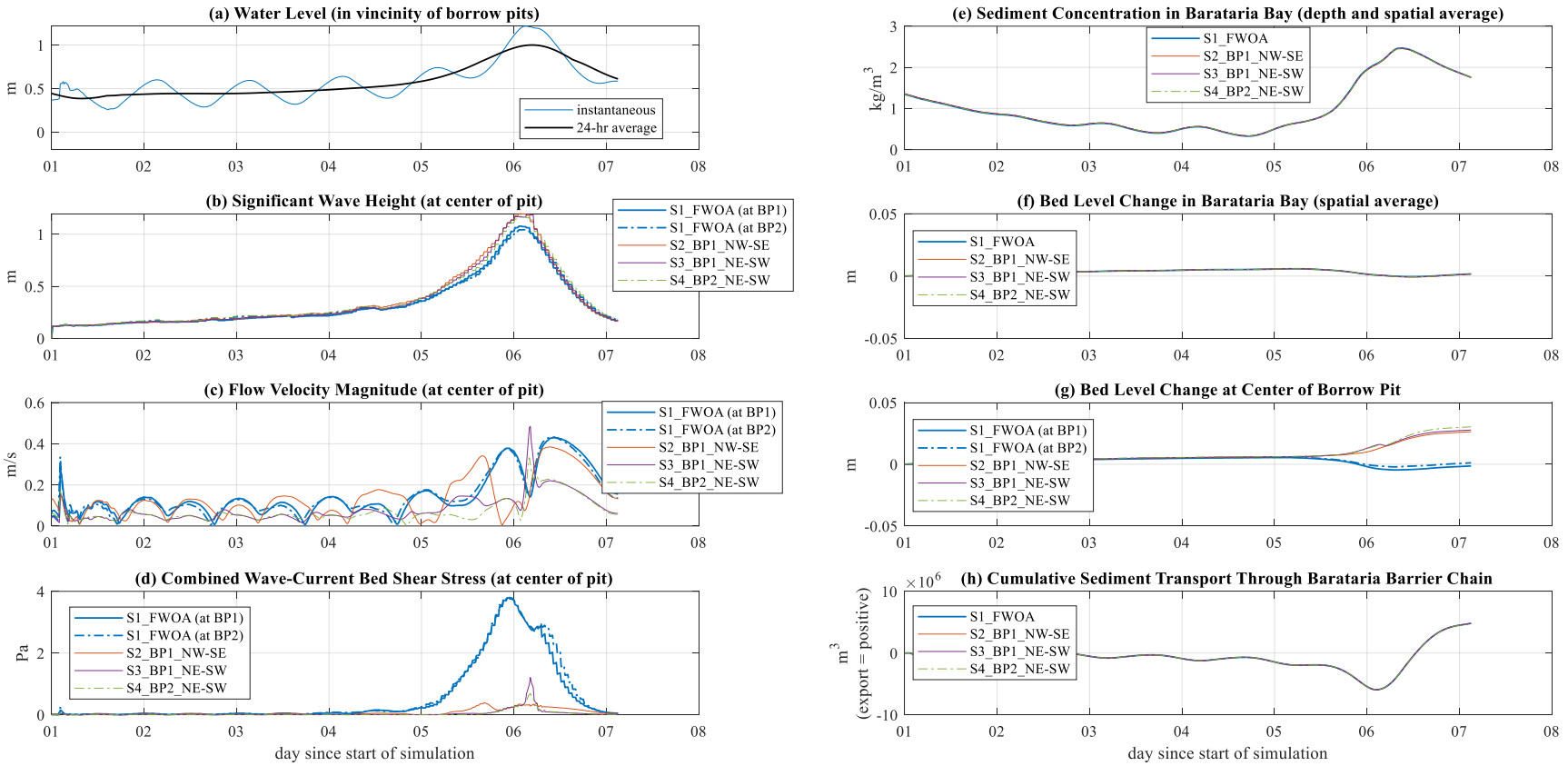

Figure B-5. Tropical cyclone ID584 (simulated during the first decade): simulated (a) water level (in vicinity of both borrow pits), (b) significant wave height (at center of borrow pit), (c) flow velocity magnitude (at center of borrow pit), (d) combined wave-current bed shear stress (at center of borrow pit), (e) sediment concentration (spatially and depth-averaged across Barataria Bay), (f) bed level change (spatially averaged across Barataria Bay), (g) bed level change at the center of the borrow pit, and (h) cumulative sediment transport (export = positive) through the Barataria Barrier Chain, i.e., Caminada Pass, Barataria Pass, Pass Abel, Quatre Bayou Pass, and Pass Ronquille. The S1_FWOA (Scenario 1 Future Without Action) results in subfigures (b), (c), (d), and (g) are taken from the location where Borrow Pit 1 would be situated in Scenario 2 and 3 (solid line), and where Borrow Pit 2 is situated in Scenario 4 (dashed line).

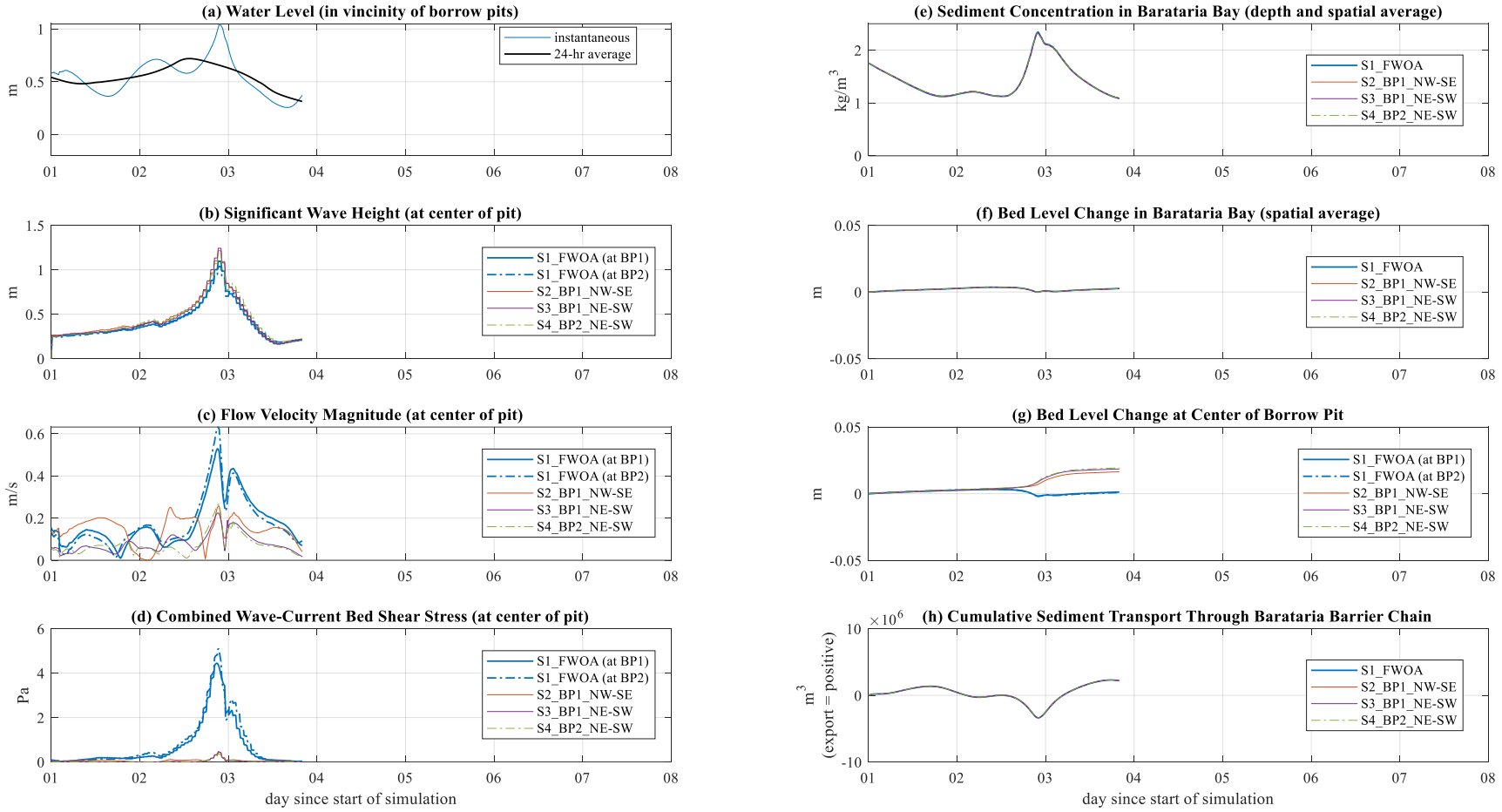

Figure B-6. Tropical cyclone ID600 (simulated during the first decade): simulated (a) water level (in vicinity of both borrow pits), (b) significant wave height (at center of borrow pit), (c) flow velocity magnitude (at center of borrow pit), (d) combined wave-current bed shear stress (at center of borrow pit), (e) sediment concentration (spatially and depth-averaged across Barataria Bay), (f) bed level change (spatially averaged across Barataria Bay), (g) bed level change at the center of the borrow pit, and (h) cumulative sediment transport (export = positive) through the Barataria Barrier Chain, i.e., Caminada Pass, Barataria Pass, Pass Abel, Quatre Bayou Pass, and Pass Ronquille. The S1_FWOA (Scenario 1 Future Without Action) results in subfigures (b), (c), (d), and (g) are taken from the location where Borrow Pit 1 would be situated in Scenario 2 and 3 (solid line), and where Borrow Pit 2 is situated in Scenario 4 (dashed line).

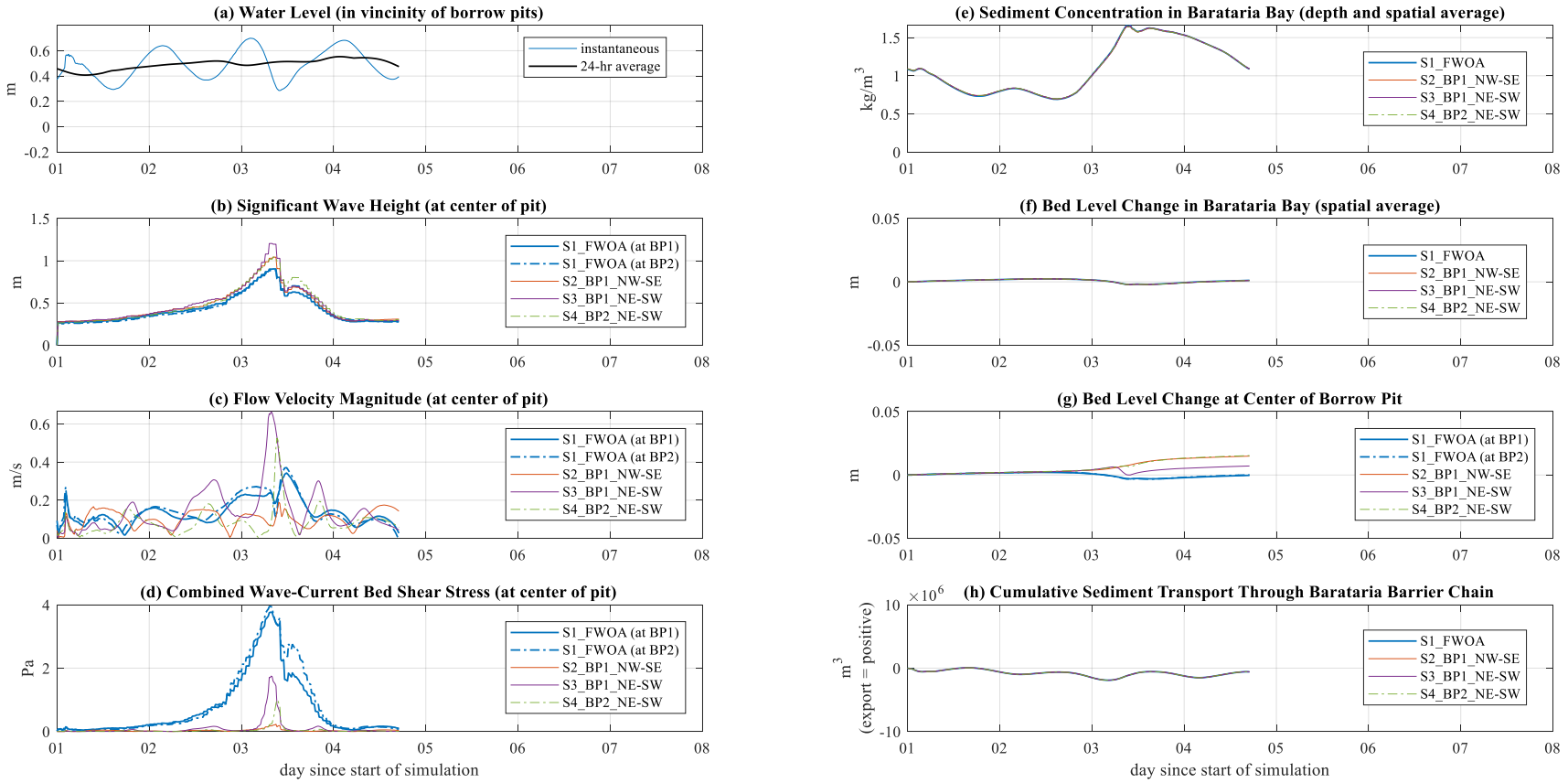

Figure B-7. Tropical cyclone ID298 (simulated during the first decade): simulated (a) water level (in vicinity of both borrow pits), (b) significant wave height (at center of borrow pit), (c) flow velocity magnitude (at center of borrow pit), (d) combined wave-current bed shear stress (at center of borrow pit), (e) sediment concentration (spatially and depth-averaged across Barataria Bay), (f) bed level change (spatially averaged across Barataria Bay), (g) bed level change at the center of the borrow pit, and (h) cumulative sediment transport (export = positive) through the Barataria Barrier Chain, i.e., Caminada Pass, Barataria Pass, Pass Abel, Quatre Bayou Pass, and Pass Ronquille. The S1_FWOA (Scenario 1 Future Without Action) results in subfigures (b), (c), (d), and (g) are taken from the location where Borrow Pit 1 would be situated in Scenario 2 and 3 (solid line), and where Borrow Pit 2 is situated in Scenario 4 (dashed line).

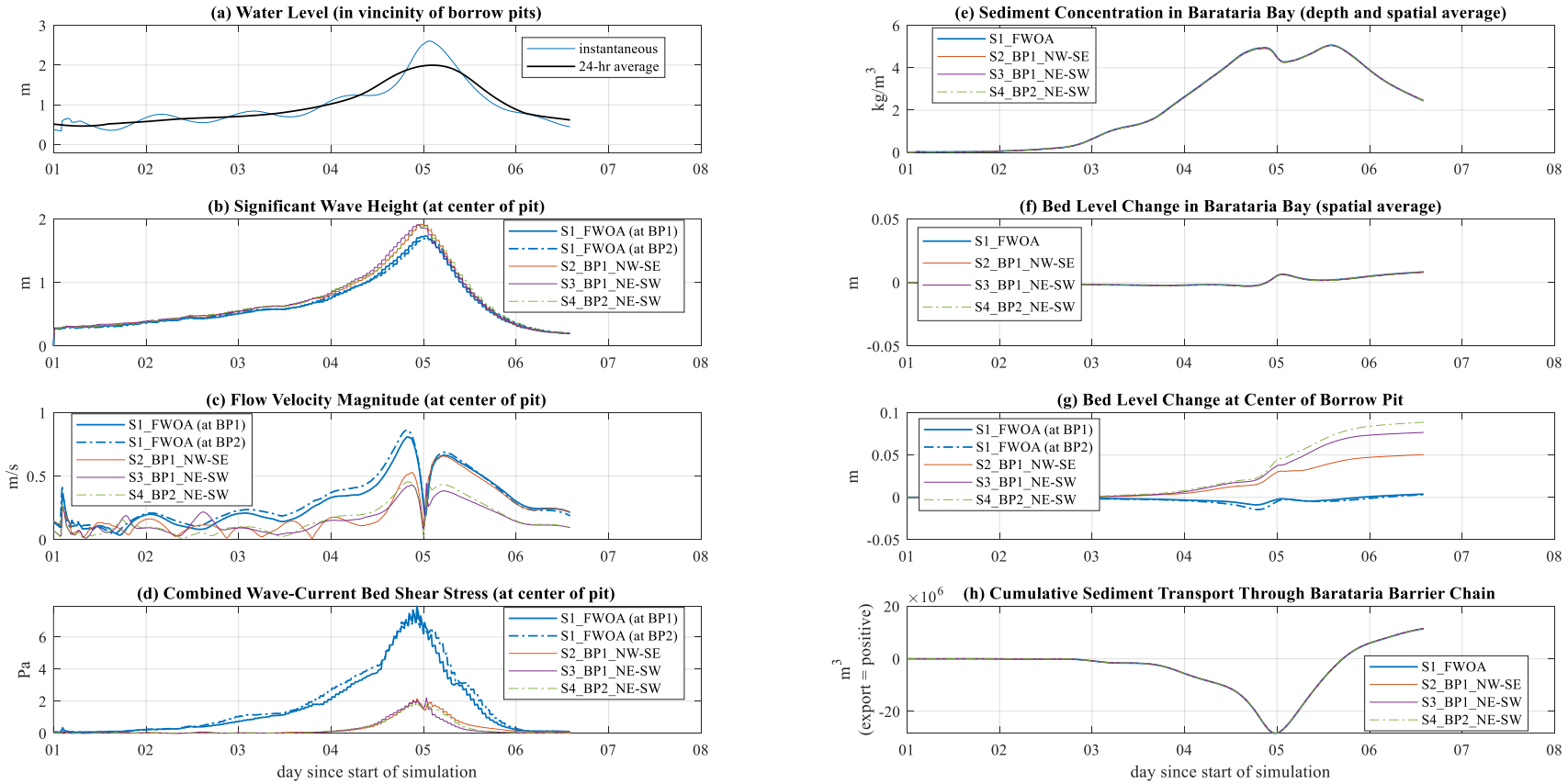

Figure B-8. Tropical cyclone ID508 (simulated during the second decade): simulated (a) water level (in vicinity of both borrow pits), (b) significant wave height (at center of borrow pit), (c) flow velocity magnitude (at center of borrow pit), (d) combined wave-current bed shear stress (at center of borrow pit), (e) sediment concentration (spatially and depth-averaged across Barataria Bay), (f) bed level change (spatially averaged across Barataria Bay), (g) bed level change at the center of the borrow pit, and (h) cumulative sediment transport (export = positive) through the Barataria Barrier Chain, i.e., Caminada Pass, Barataria Pass, Pass Abel, Quatre Bayou Pass, and Pass Ronquille. The S1_FWOA (Scenario 1 Future Without Action) results in subfigures (b), (c), (d), and (g) are taken from the location where Borrow Pit 1 would be situated in Scenario 2 and 3 (solid line), and where Borrow Pit 2 is situated in Scenario 4 (dashed line).

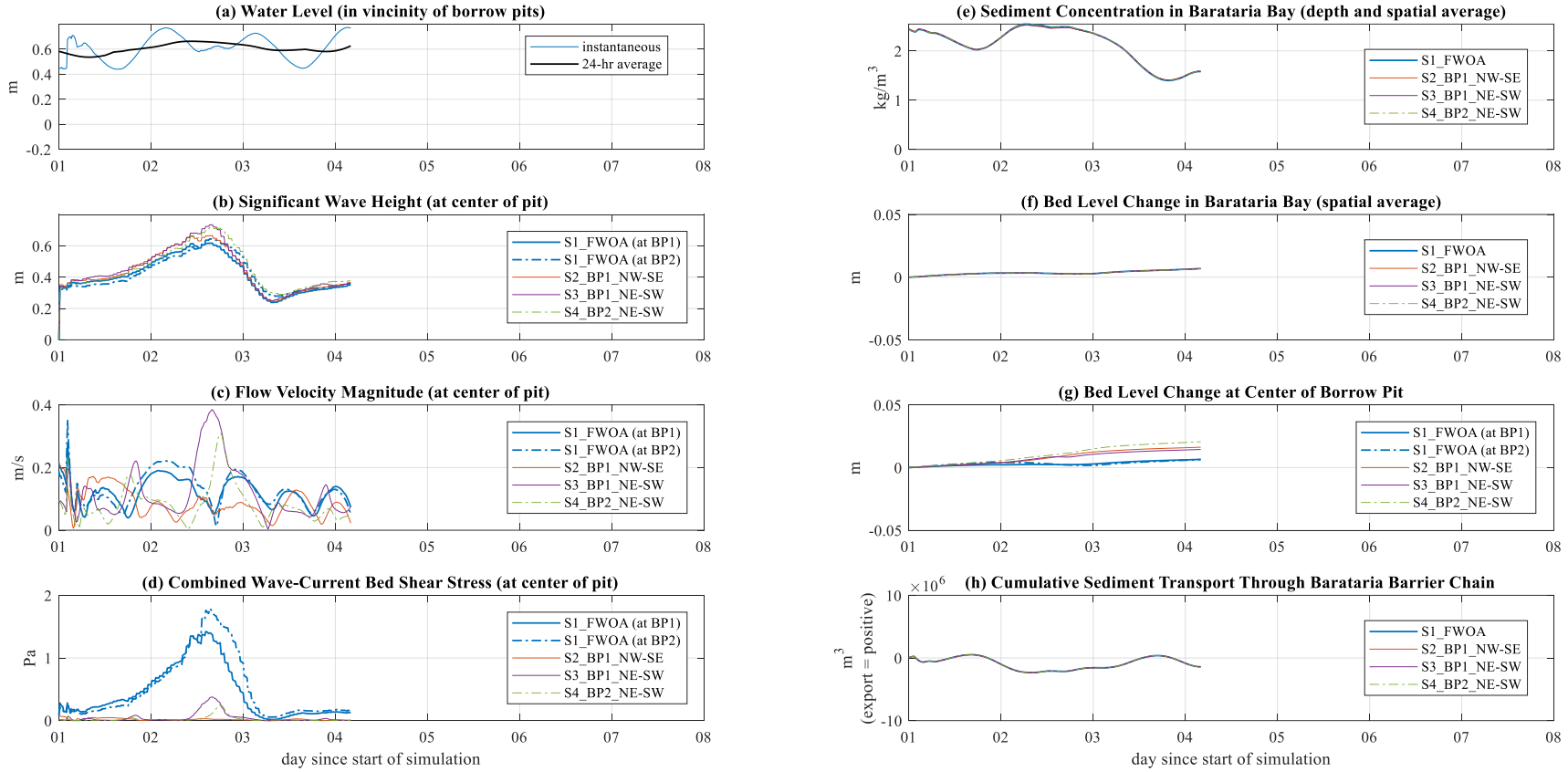

Figure B-9. Tropical cyclone ID544 (simulated during the second decade): simulated (a) water level (in vicinity of both borrow pits), (b) significant wave height (at center of borrow pit), (c) flow velocity magnitude (at center of borrow pit), (d) combined wave-current bed shear stress (at center of borrow pit), (e) sediment concentration (spatially and depth-averaged across Barataria Bay), (f) bed level change (spatially averaged across Barataria Bay), (g) bed level change at the center of the borrow pit, and (h) cumulative sediment transport (export = positive) through the Barataria Barrier Chain, i.e., Caminada Pass, Barataria Pass, Pass Abel, Quatre Bayou Pass, and Pass Ronquille. The S1_FWOA (Scenario 1 Future Without Action) results in subfigures (b), (c), (d), and (g) are taken from the location where Borrow Pit 1 would be situated in Scenario 2 and 3 (solid line), and where Borrow Pit 2 is situated in Scenario 4 (dashed line).

B.2 MAPS: HYDRODYNAMICS DURING COLD FRONT

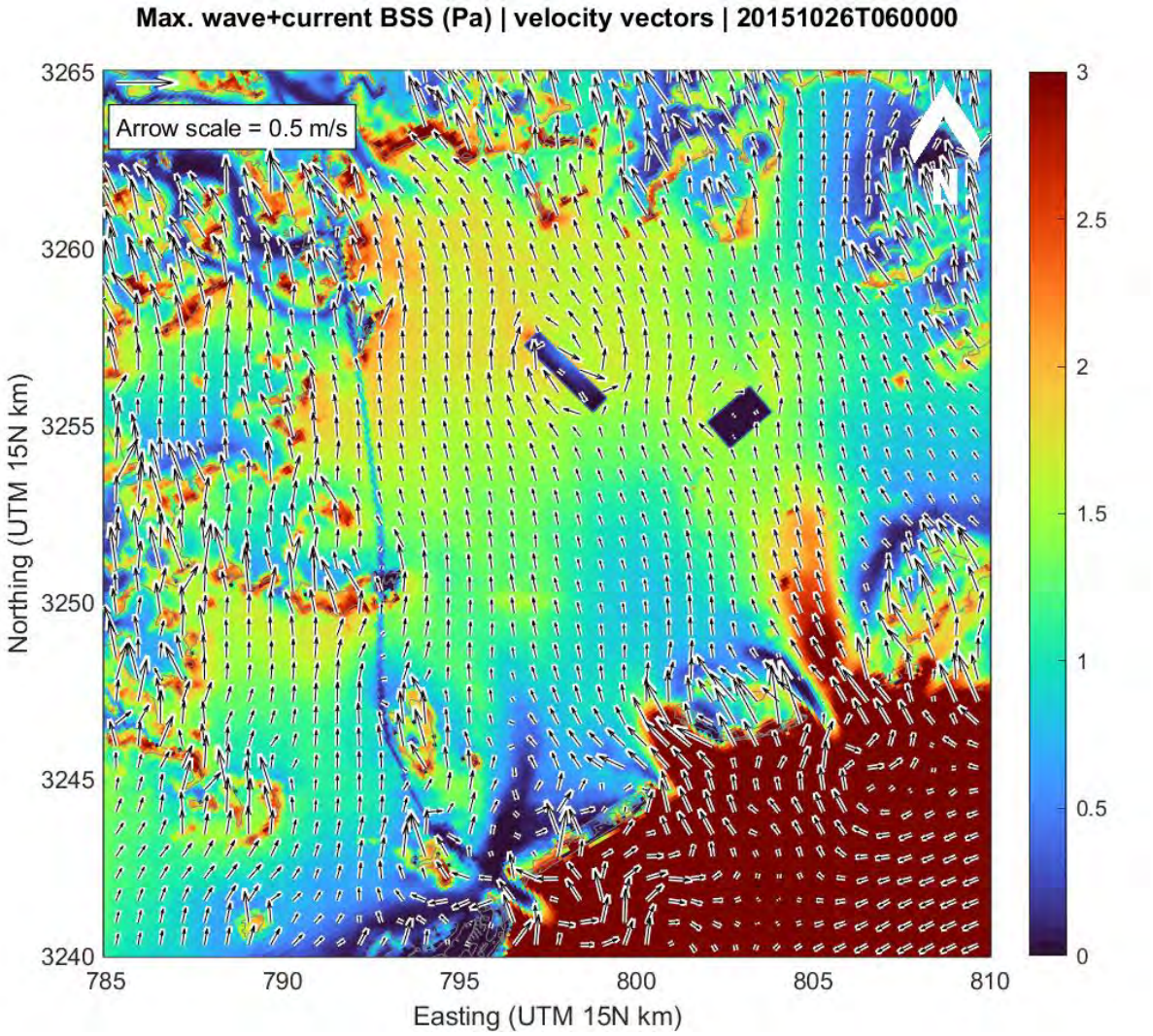

Figure B-10. Instantaneous bed shear stress (combined wave+current) for Scenario 5 (Borrow Pit 1 in NW-SE orientation and Borrow Pit 2) along with flow velocity vectors at 6 a.m. on October 26th, 2015, during relatively strong pre-frontal southerly winds several hours before the passing of a cold front. Notably, strong northwesterly currents are observed in Barataria Bay, however, relatively strong currents in the opposite (southeastern) direction as found within Borrow Pit 1 (i.e., the western borrow pit). Figure B-11 shows the water level and wind vectors for the same area at the same point in time.

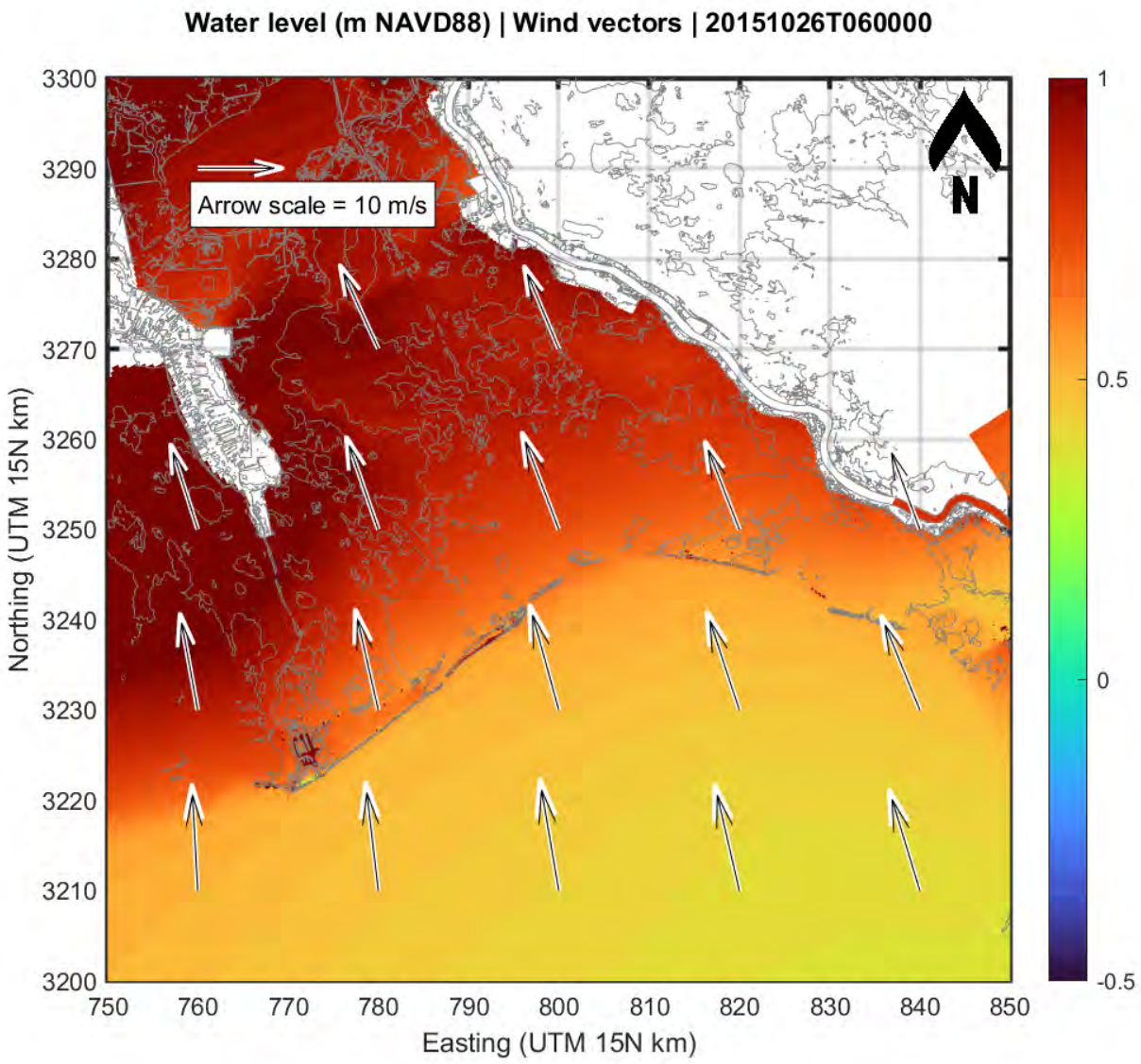

Figure B-11. Instantaneous water level for Scenario 5 (Borrow Pit 1 in NW-SE orientation and Borrow Pit 2) along with wind vectors at 6 a.m. on October 26th, 2015 (same moment in time as Figure B-10), during relatively strong pre-frontal southerly winds several hours before the passing of a cold front. Wind-driven water level setup leads to water levels that locally exceed 1 m NAVD88 in northern Barataria.

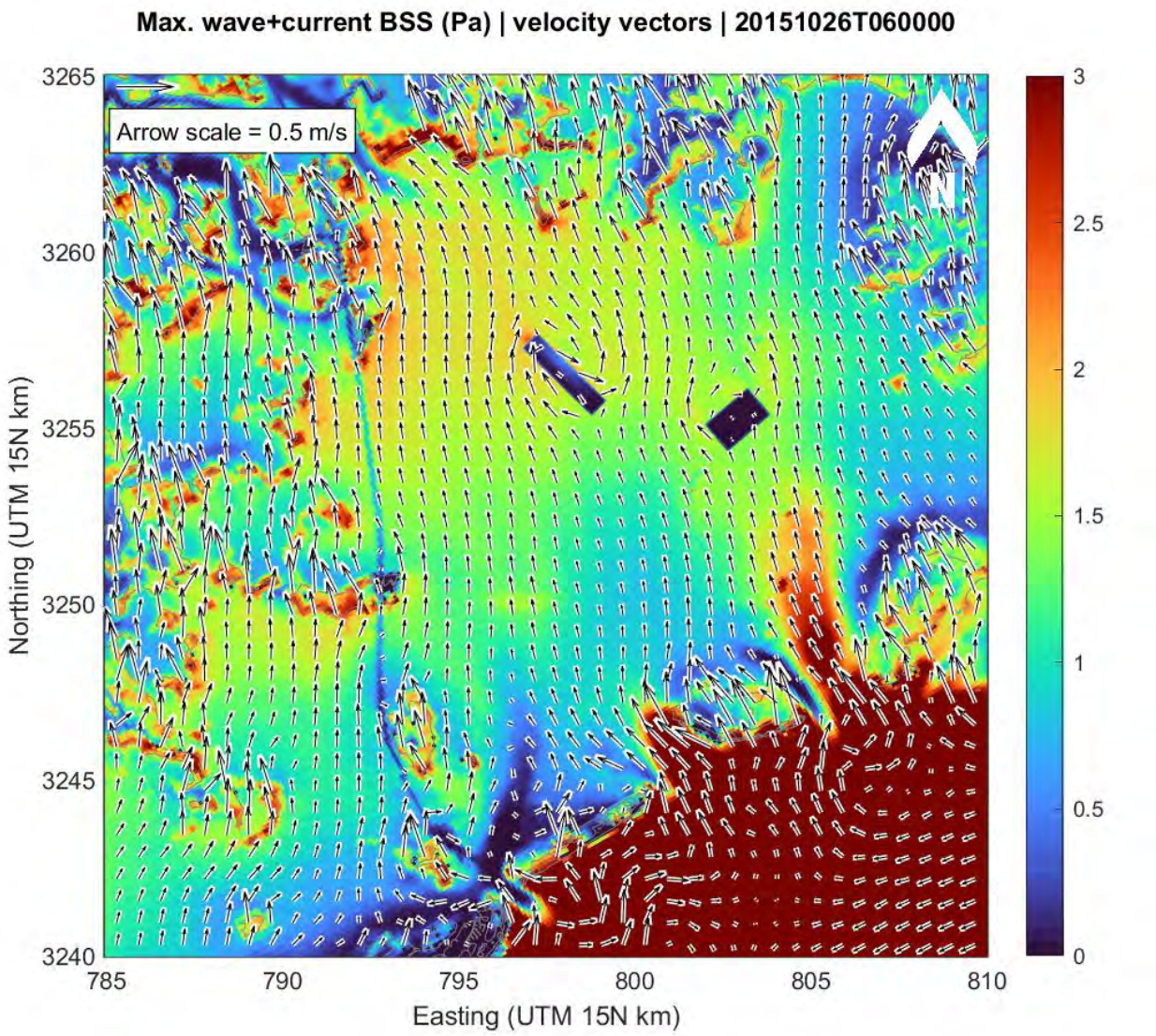

Figure B-12. Instantaneous bed shear stress (combined wave+current) for Scenario 5 (Borrow Pit 1 in NW-SE orientation and Borrow Pit 2) along with flow velocity vectors at 6 p.m. on October 26th, 2015, during the passing of a cold front. The currents within Borrow Pit 1 (i.e., the western borrow pit) are noticeably larger than the currents in the surrounding area of the pit. Figure B-13 shows the water level and wind vectors for the same area at the same point in time.

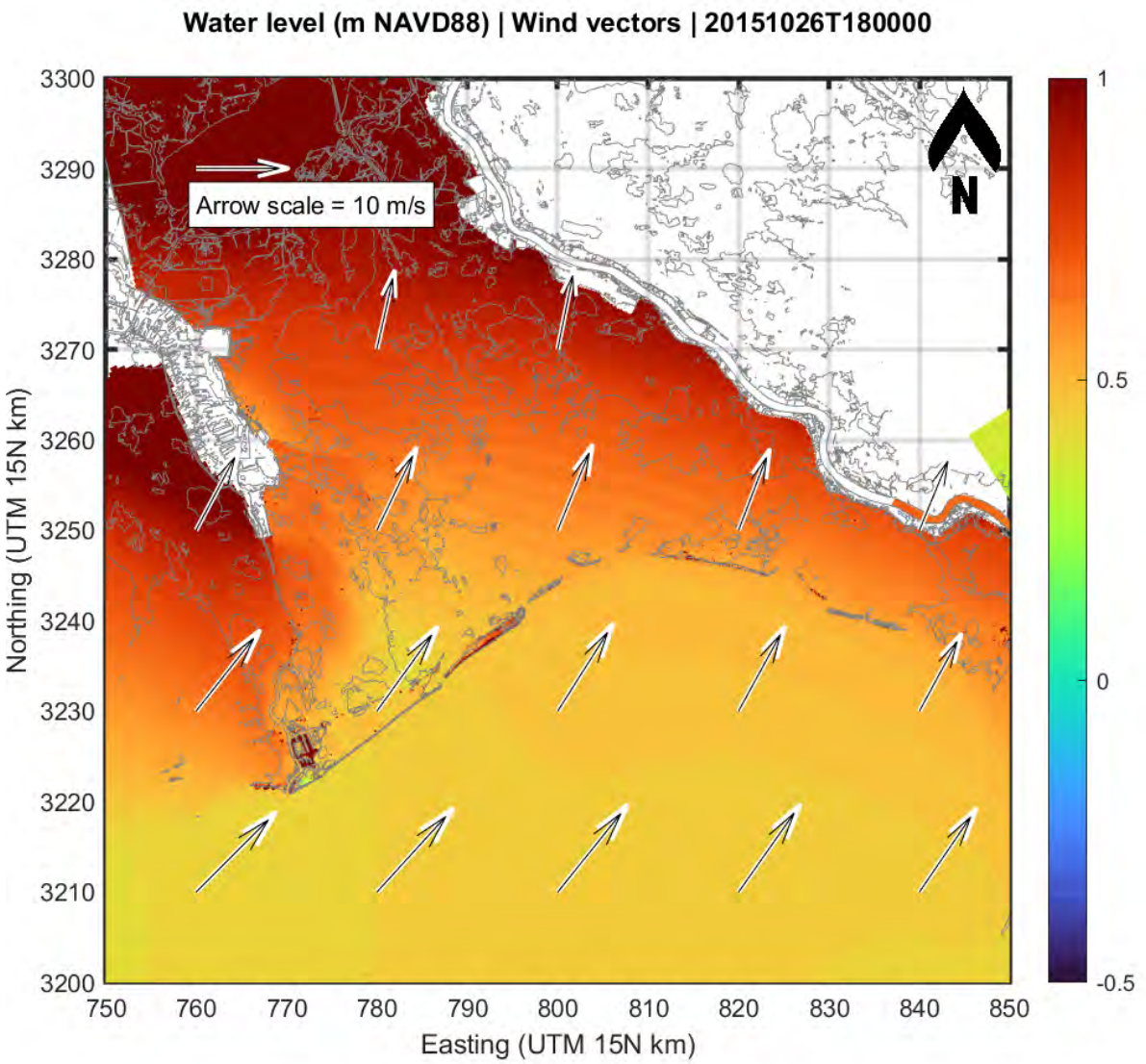

Figure B-13. Instantaneous water level for Scenario 5 (Borrow Pit 1 in NW-SE orientation and Borrow Pit 2) along with wind vectors at 6 p.m. on October 26th, 2015 (same moment in time as Figure B-12), during the passing of a cold front. The wind-driven water level set-up in the Barataria basin started to decrease compared to Figure B-11.

B.3 MAPS: HYDRODYNAMICS DURING TROPICAL STORM

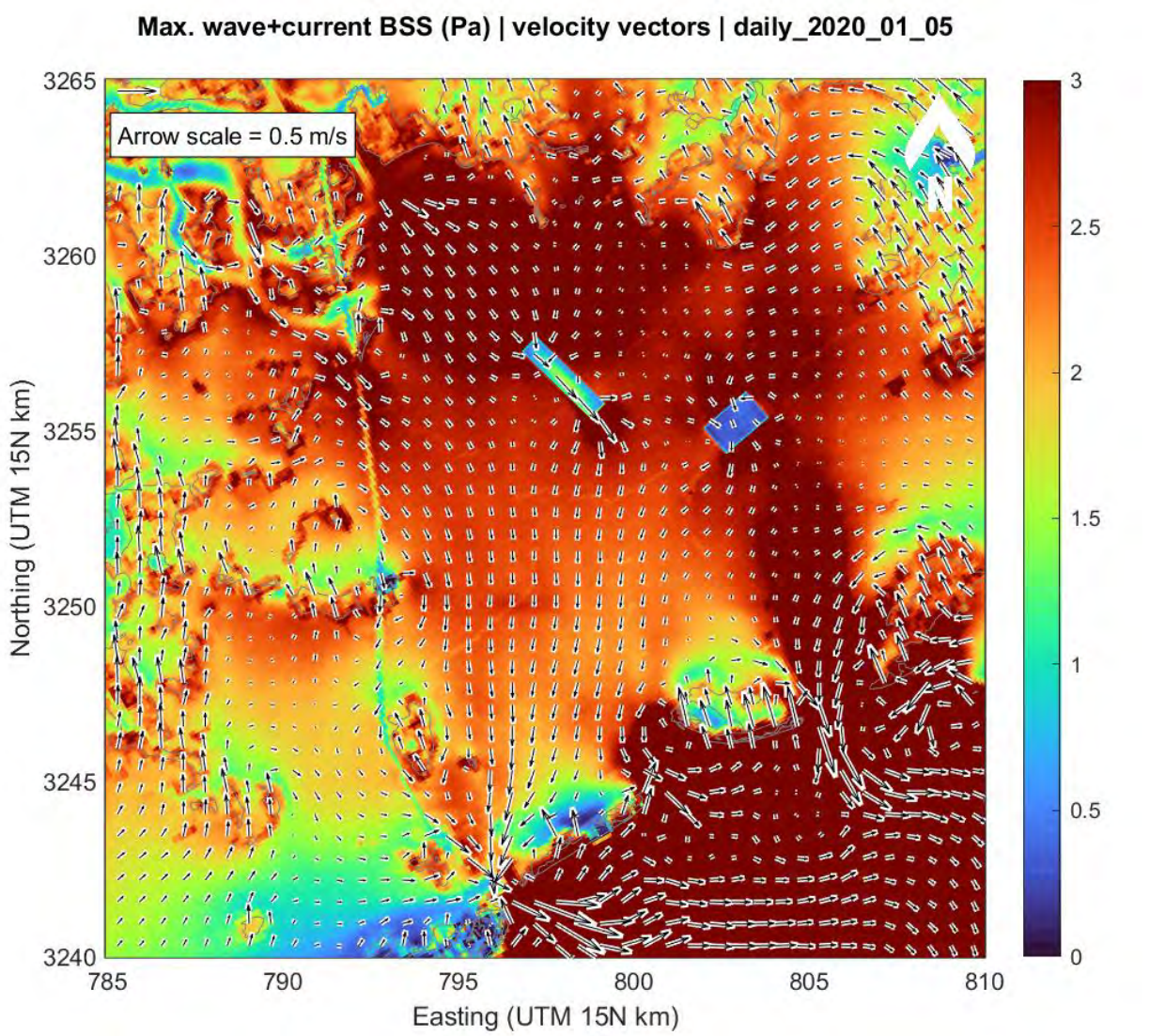

Figure B-14. Daily average bed shear stress (combined wave+current) for Scenario 5 (Borrow Pit 1 in NW-SE orientation and Borrow Pit 2) at the peak impact of a synthetic tropical storm approaching western Louisiana, along with flow velocity vectors. The velocity vectors represent residual currents resulting from averaging over a 24-hour time window. Notably, strong southeasterly currents are observed within Borrow Pit 1 (i.e., the western borrow pit). Figure B-15 shows the water level and wind vectors for the same area at the same point in time.

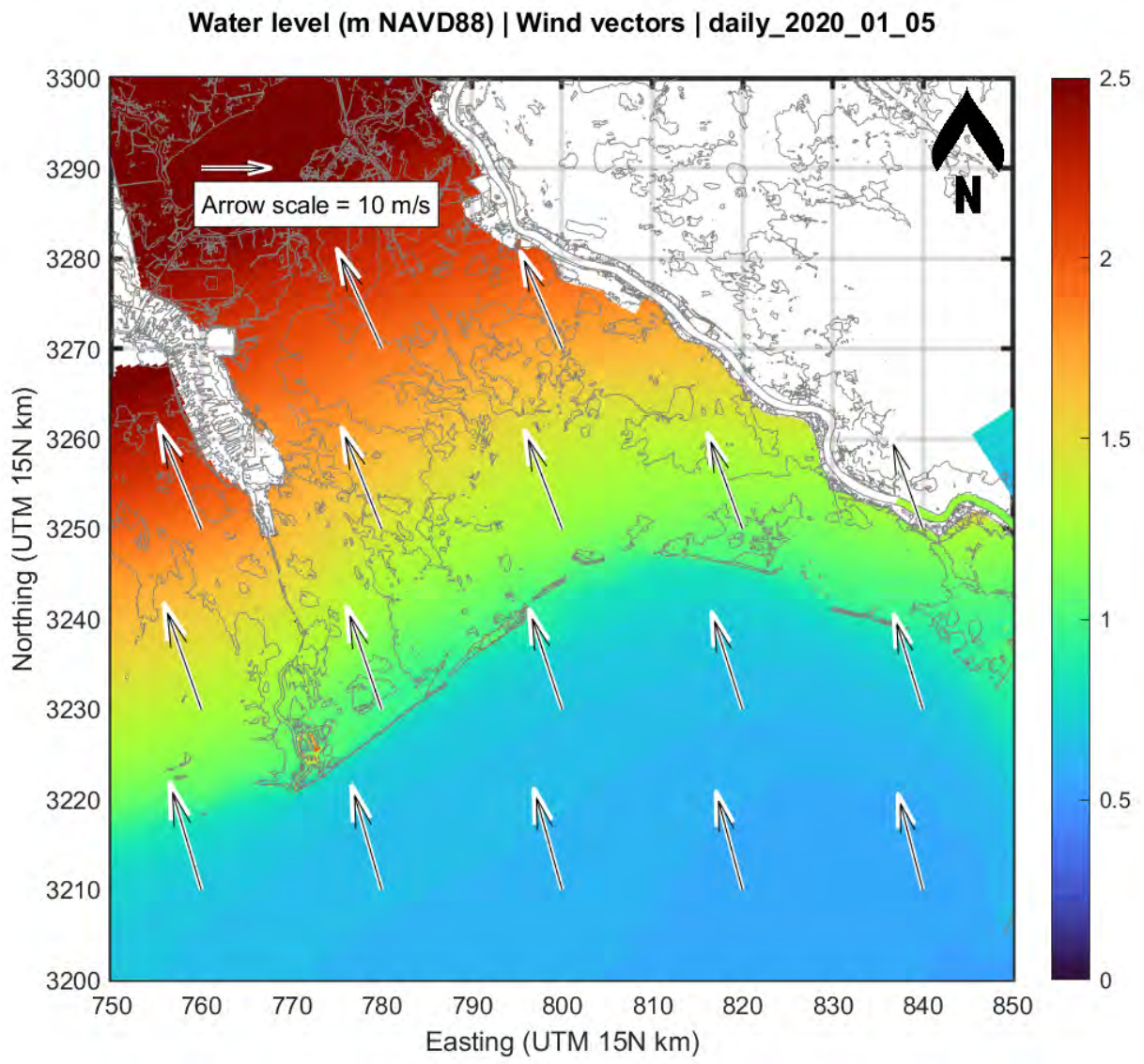

Figure B-15. Daily average water level for Scenario 5 (Borrow Pit 1 in NW-SE orientation and Borrow Pit 2) at the peak impact of a synthetic tropical storm approaching western Louisiana, along with wind vectors (at the same moment in time as Figure B-14) . Wind-driven water level setup leads to water levels that locally exceed 2.5 m NAVD88 in northern Barataria.

B.4 MAPS: BED LEVEL CHANGE IN BAY OVER TIME

Model results for all scenarios (Figure B-16 through Figure B-20) suggest that the Barataria Bay floor will degrade and subside over a 20-year period by approximately 20–30 cm of which ~13 cm can be attributed to subsidence alone. Additionally, the model shows decimeter-to-meter scale erosion and deposition in the vicinity of tidal inlets and flood and ebb-tidal deltas.

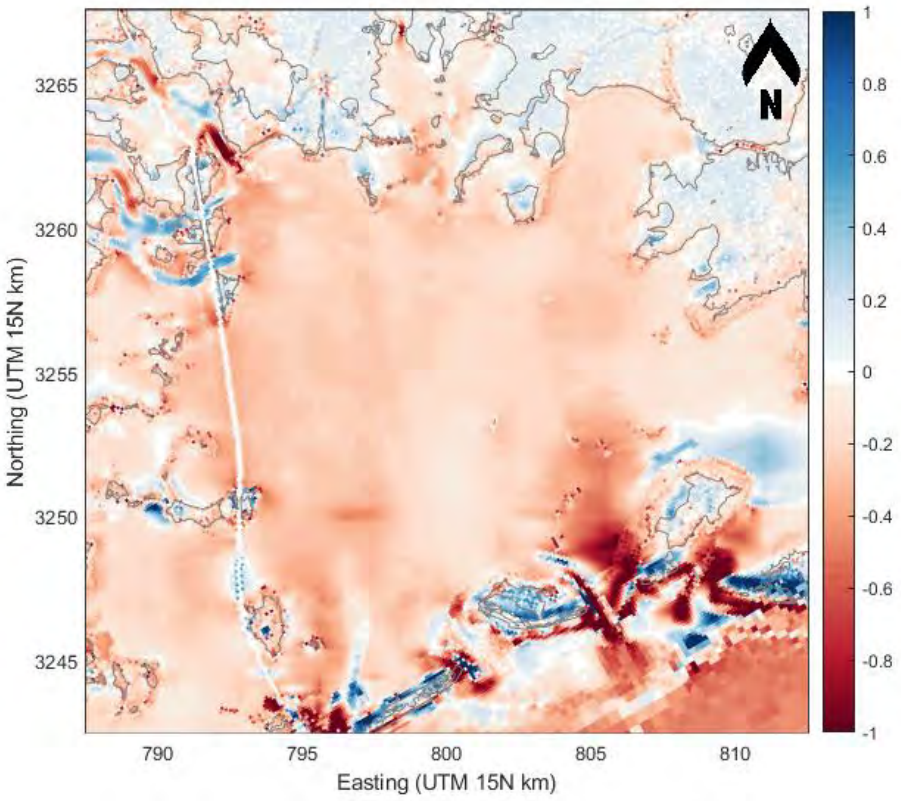

Figure B-16. Modeled bed level change (m) at Barataria Bay for S1 (FWOA) after 20 years.

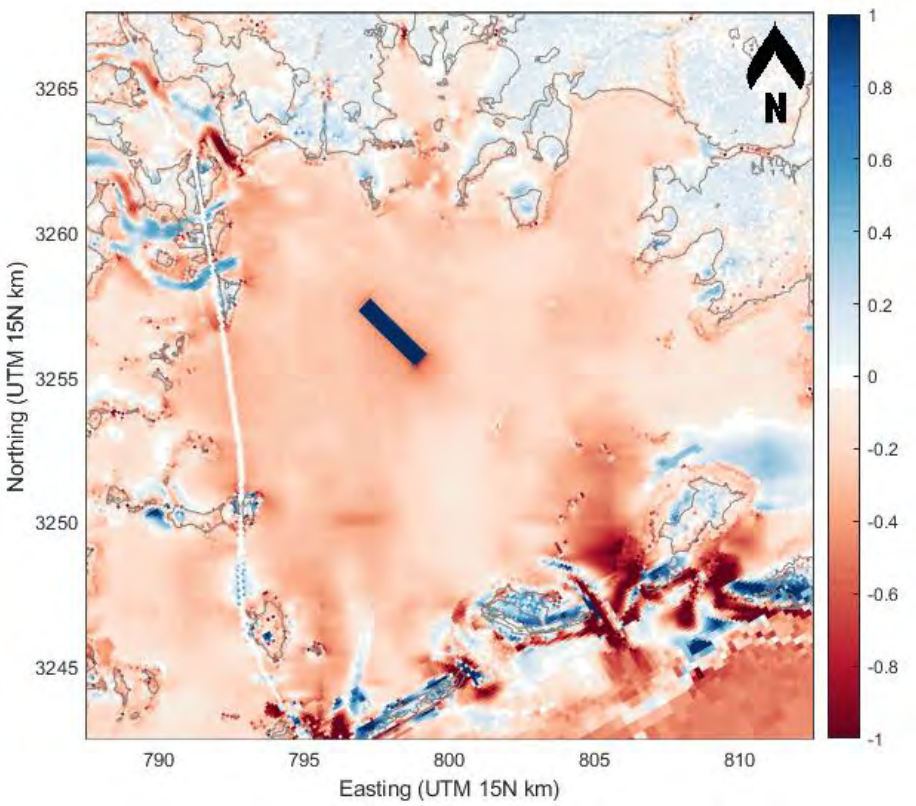

Figure B-17. Modeled bed level change (m) at Barataria Bay for S2 (BP1 in NW-SE orientation) after 20 years.

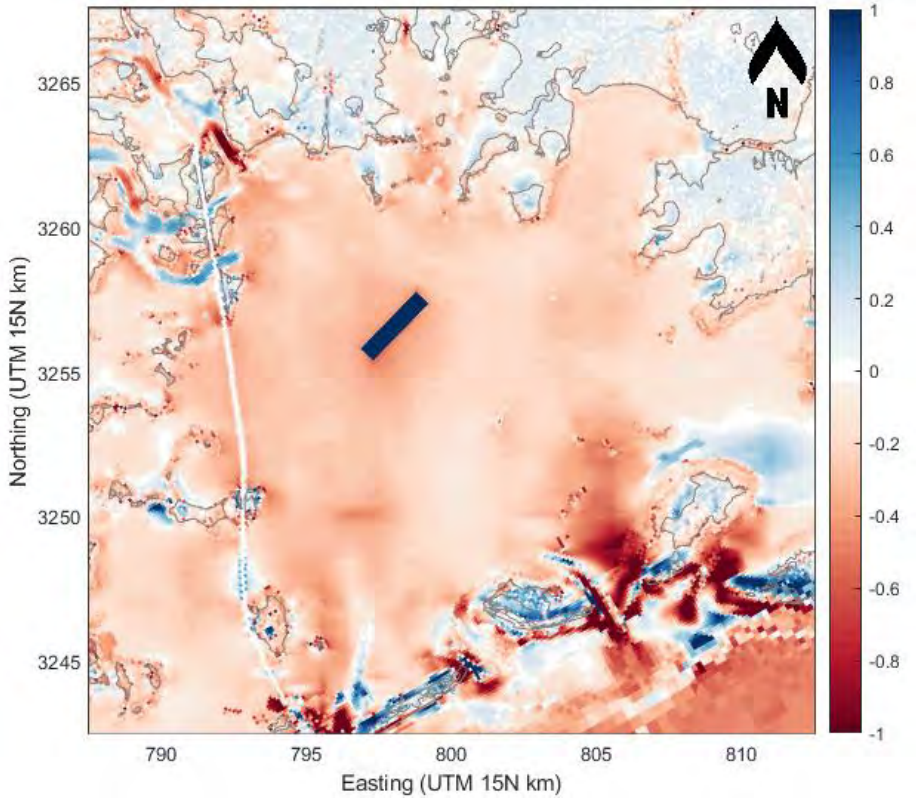

Figure B-18. Modeled bed level change (m) at Barataria Bay for S3 (BP1 in NE-SW orientation) after 20 years.

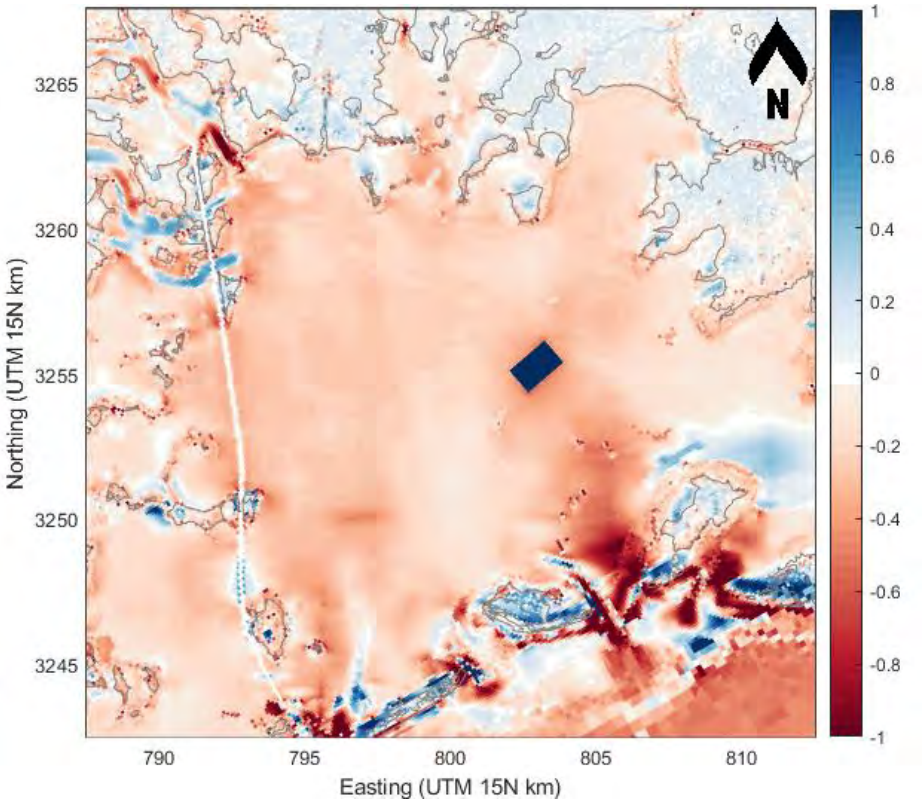

Figure B-19. Modeled bed level change (m) at Barataria Bay for S4 (BP2) after 20 years.

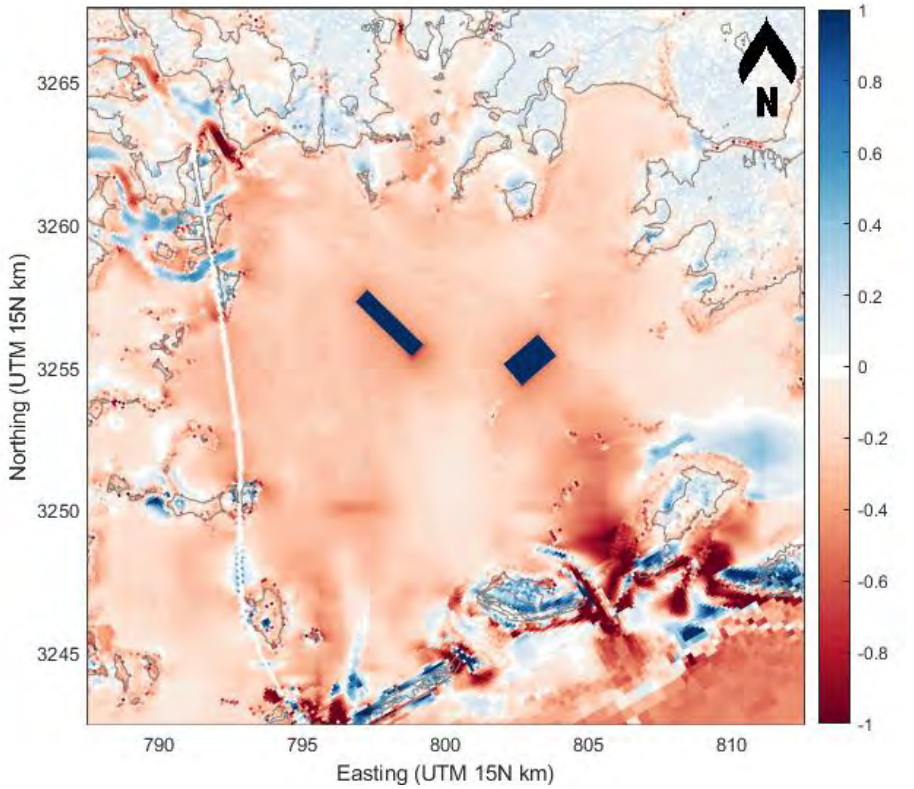

Figure B-20. Modeled bed level change (m) at Barataria Bay for S5 (BP1 in NW-SE orient. and BP2 in NE-SW orientation) after 10 years.

B.5 MAPS: BORROW PIT IMPACTS TO BAY MORPHOLOGY

To isolate the influence of borrow pits alone, a baseline simulation (S1) was conducted using the same environmental forcing but did not include the borrow pits. Borrow pit impacts, isolated from other morphological change driven by environmental conditions, were then obtained by subtracting bed level change between scenarios with and without pit (Figure B-21 through Figure B-24).

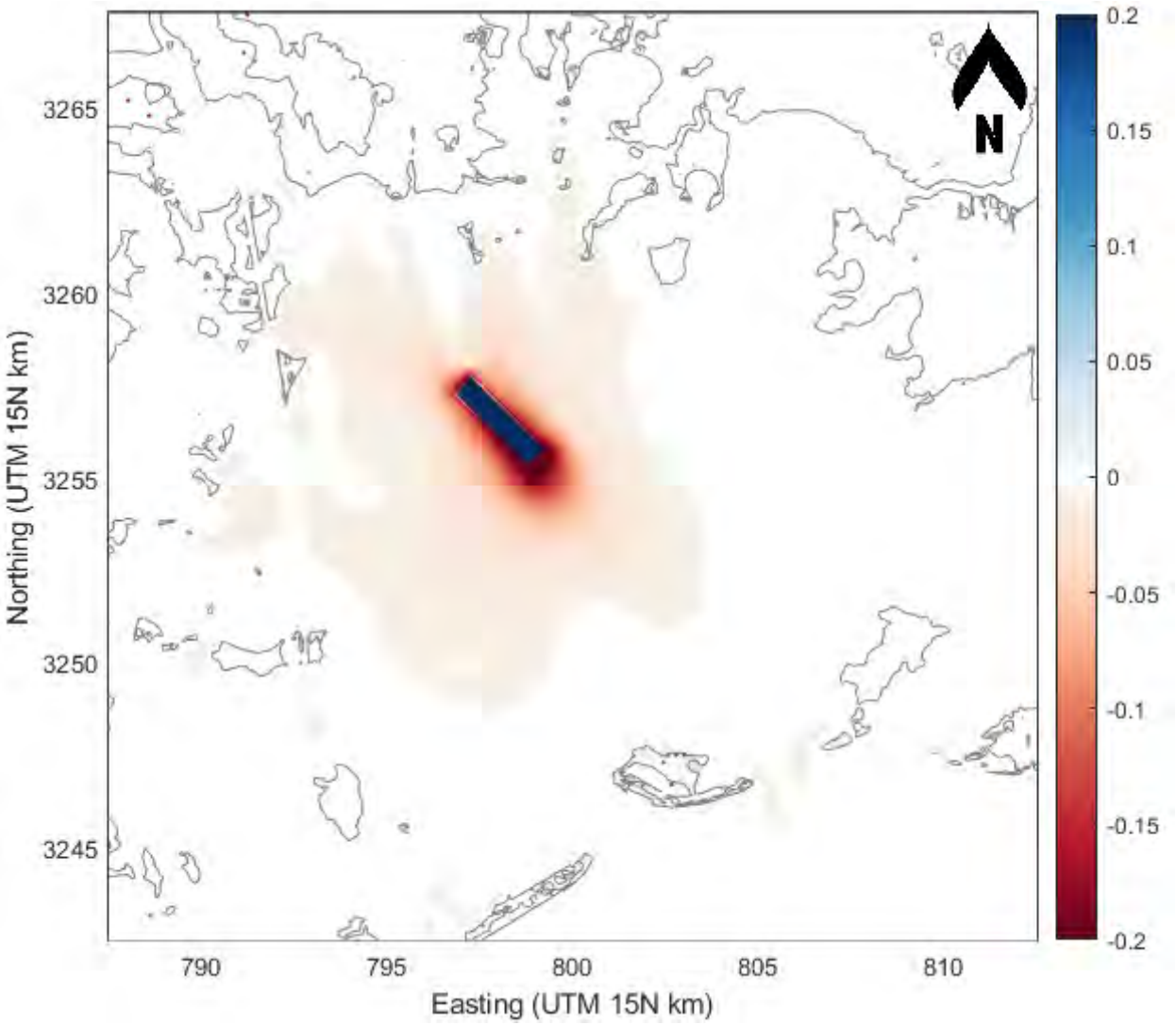

Figure B-21. Modeled bed level change (m) at Barataria Bay differenced to FWOA for S2 (BP1 in NW-SE orientation) after 20 years.

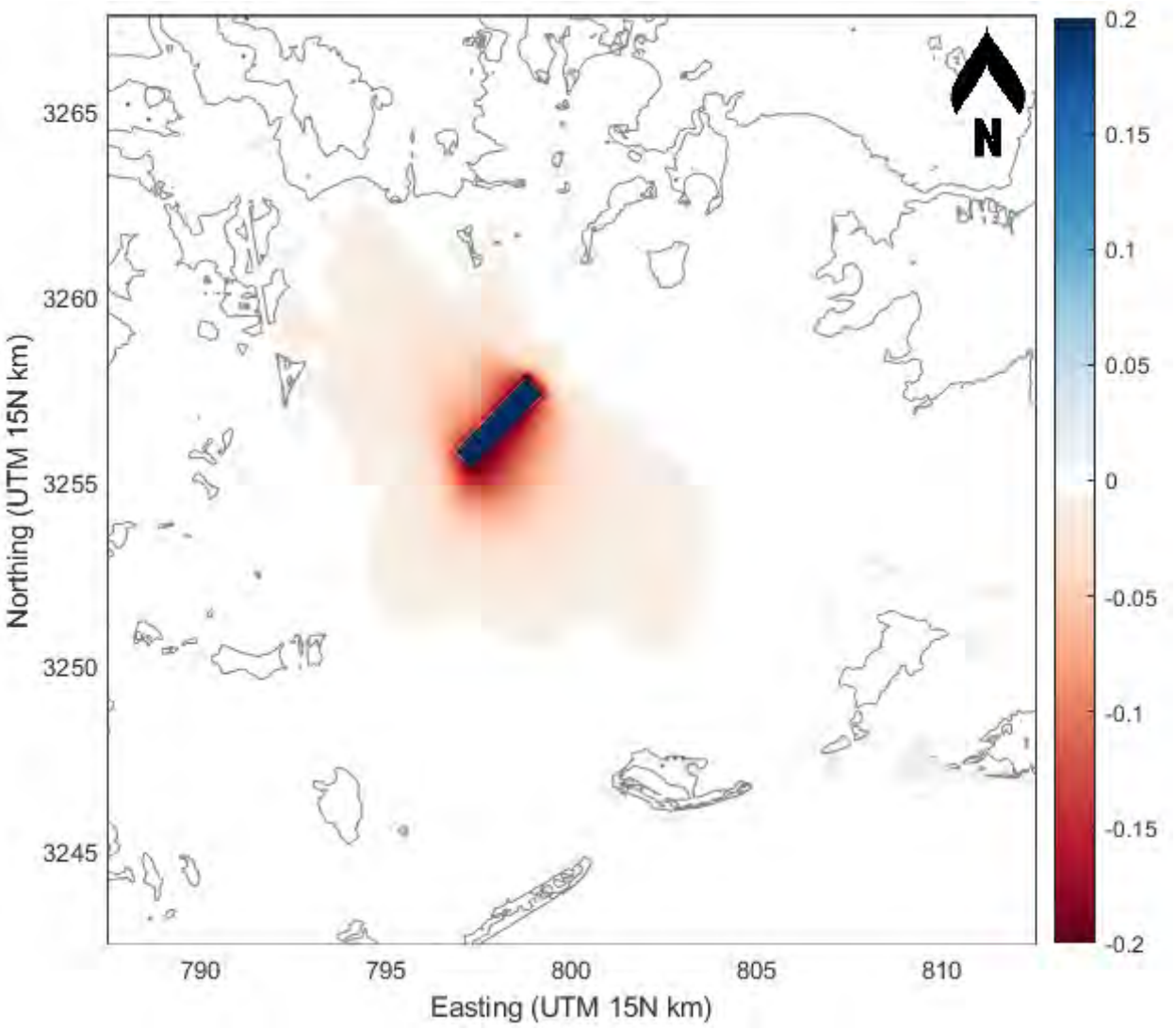

Figure B-22. Modeled bed level change (m) at Barataria Bay differenced to FWOA for S3 (BP1 in NE-SW orientation) after 20 years.

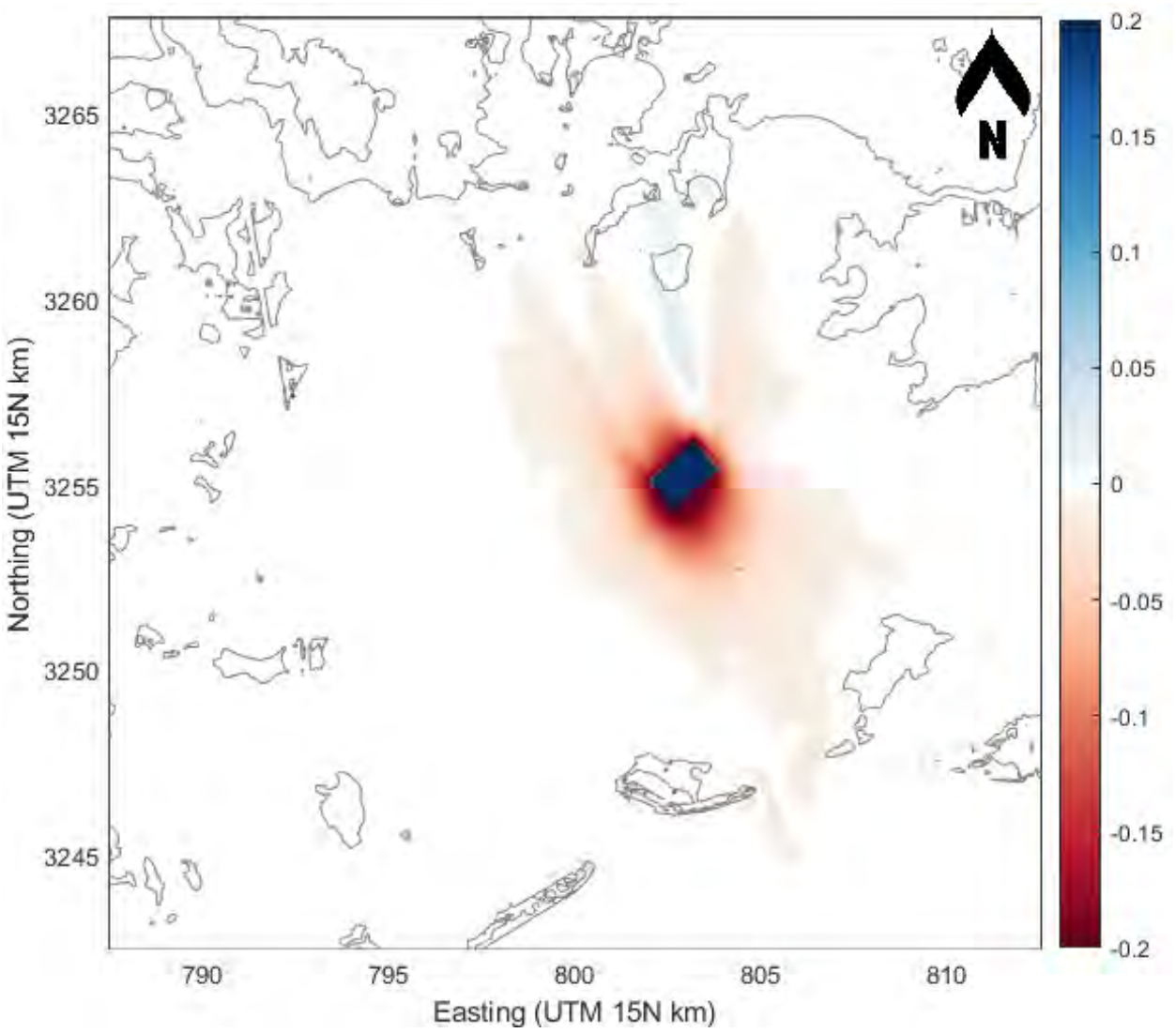

Figure B-23. Modeled bed level change (m) at Barataria Bay differenced to FWOA for S4 (BP2) after 20 years.

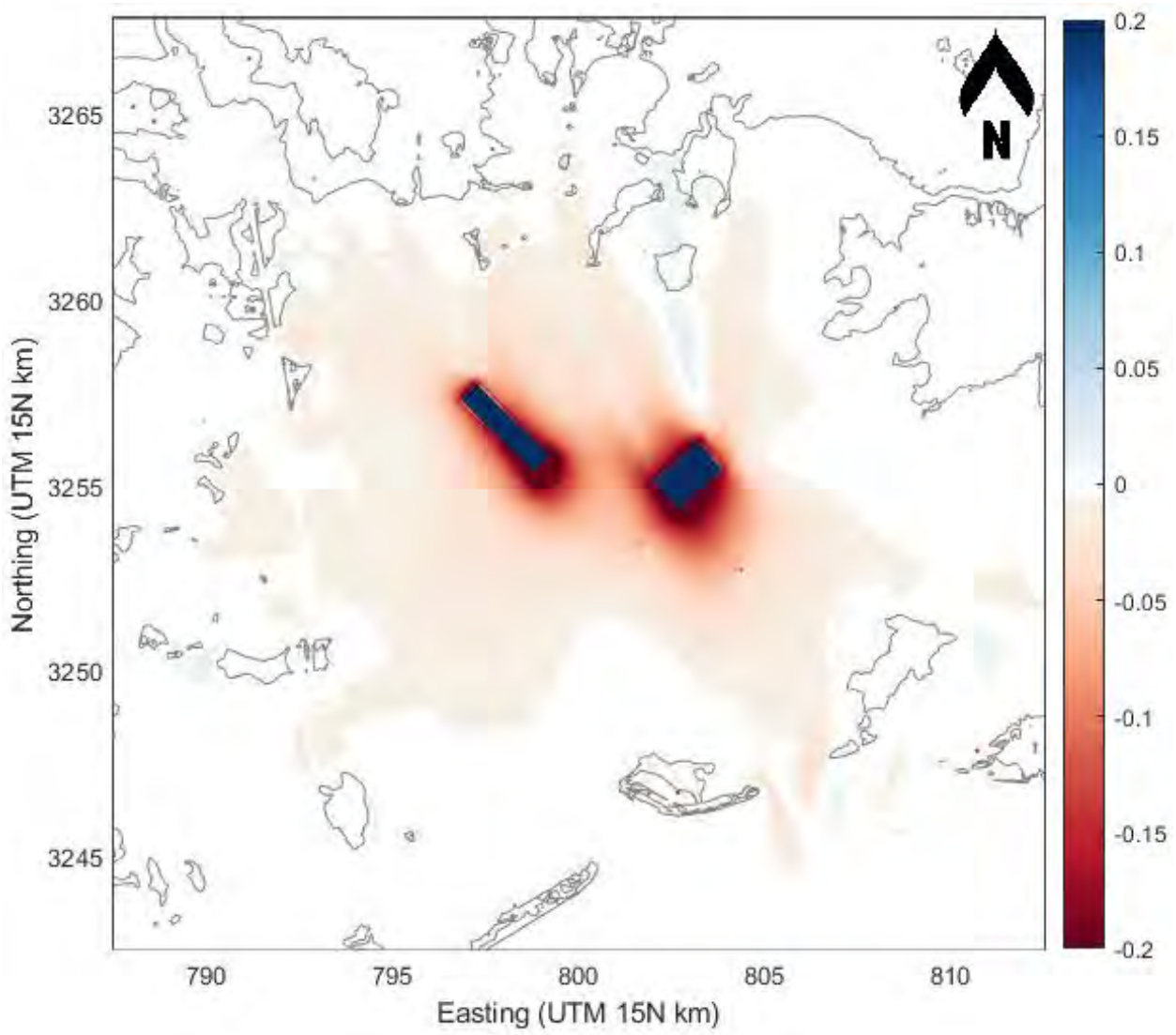

Figure B-24. Modeled bed level change (m) at Barataria Bay differenced to FWOA for S5 (BP1 in NW-SE orientation and BP2 in NE-SW orientation) after 20 years.

B.6 TABLES: BORROW PIT INFILLING CATEGORIZED BY METEOROLOGICAL CONDITIONS

Table B-1 presents infilling volumes (in 1,000s m³) categorized by the individual simulations that represent various meteorological conditions, consisting of quiescent conditions, cold fronts, and specific tropical cyclones identified by their respective ID numbers. Similar infilling volumes are observed across scenarios. Table B-2, which highlights the influence of the three meteorological conditions on borrow pit infilling, reveals that the majority (>80%) of infilling occurs during cold fronts, while a significantly smaller portion (<20%) takes place during tropical storms. Minimal infilling (~2%) occurs during quiescent conditions.

Table B-1. Borrow pit infilling volumes (1,000 m³) for all individual simulations that are part of the modeling framework, across all borrow pit scenarios (S1 through S5).

		S2	S3	S4	S5	
		Borrow Pit 1 (NW-SE)	**Borrow Pit 1 (NE-SW)**	**Borrow Pit 2 (NE-SW)**	**Borrow Pit 1 (NW-SE)**	**Borrow Pit 2 (NE-SW)**
First decade (2020-2029)	Quiescent conditions	10	13	15	10	15
	Cold fronts	999	951	928	997	927
	Tropical cyclone (ID0357)	99	130	132	100	129
	Tropical cyclone (ID0102)	42	42	47	41	46
	Tropical cyclone (ID0584)	46	49	51	47	50
	Tropical cyclone (ID0600)	28	31	32	28	31
	Tropical cyclone (ID0298)	26	23	29	26	28
Second decade (2030-2039)	Quiescent conditions	33	36	41	32	41
	Cold fronts	916	936	1020	909	1001
	Tropical cyclone (ID0508)	89	123	139	83	137
	Tropical cyclone (ID0544)	28	27	36	28	35

Table B-2. Contribution of the three different meteorological conditions (quiescent, cold fronts, and tropical cyclones) to borrow pit infilling over the full 20-year simulation period, for all individual borrow pit scenarios (S1 through S5) and averaged for all scenarios.

	S2	S3	S4	S5		AVERAGE
	Borrow Pit 1 (NW-SE)	Borrow Pit 1 (NE-SW)	Borrow Pit 2 (NE-SW)	Borrow Pit 1 (NW-SE)	Borrow Pit 2 (NE-SW)	
Quiescent conditions	2%	2%	2%	2%	2%	**2%**
Cold fronts	83%	80%	79%	83%	79%	**81%**
Tropical cyclones	15%	18%	19%	15%	19%	**17%**

APPENDIX C. OBSERVED INFILLING FROM PREVIOUS STUDIES

This appendix contains results from a previous study conducted under the BAMM Program by CB&I (2015), in which bathymetric and geophysical data was collected to evaluate borrow areas for hypoxia and infilling rates. Bathymetric surveys were conducted for various in-bay and offshore borrow areas, and are shown in

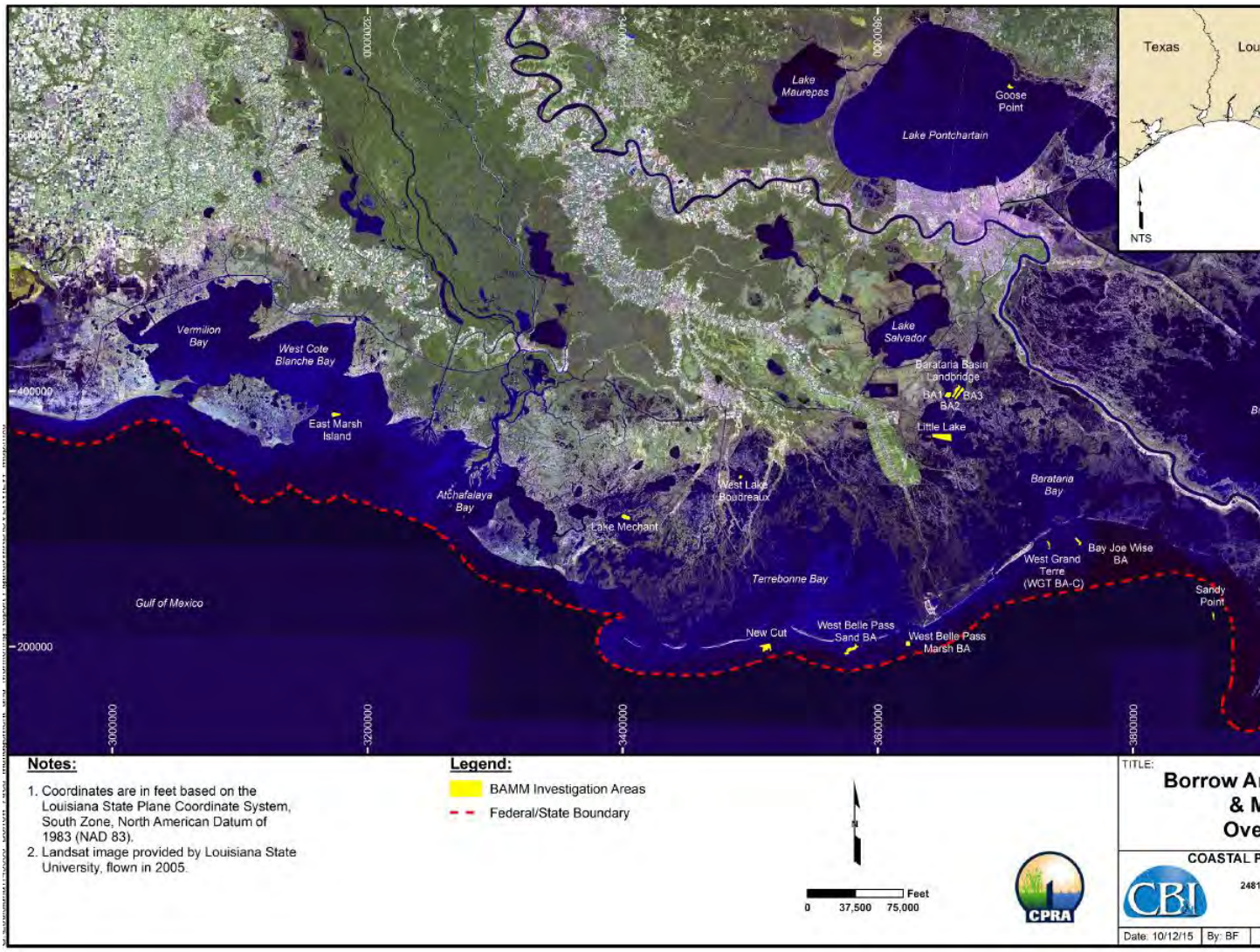

Figure C-1 and listed in Table C-1. The model results were compared with infilling rates listed in a previous study from CB&I (2015), specifically focusing on borrow areas that are similar to those investigated in the present study (i.e., Litte Lake, Barataria Basin Landbridge, and Goose Point). These borrow areas located inland and lack a major source of fluvial sediment. Infilling rates are generally higher for borrow pits that are located offshore (e.g., West Belle Pass, Bay Joe Wise, Sandy Point) or if they are exposed to a major fluvial source of sediment (e.g., East Marsh Island).

Table C-1. Measured borrow area infilling estimated from post-dredge and difference surfaces. Note: Reprinted from the Louisiana Borrow Area Management and Monitoring (BAMM) Program *report by CB&I (2015).*

Borrow Area	As built Survey Date	CB&I Survey Date	Time Period (years)	Infilled Volume (cy)	Infilling Rate (cy/yr)	Ave. Depth Infilling (ft)	Max Infilling Depth (ft)	Infilling Rate (ft/yr)
Lake Mechant	8/1/2009	5/26/2013	3.8	1,222,000	320,000	1.3	7.4	0.3
West Lake Boudreaux	10/1/2009	5/20/2013	3.6	774,000	212,900	8	15.7	2.2
East Marsh Island	12/29/2011	5/25/2013	1.4	2,986,000	2,124,500	7	12.7	5.0
Little Lake	10/1/2006	5/18/2013	6.6	2,554,000	385,100	1.2	11.4	0.2
Goose Point	8/1/2009	5/12/2013	3.8	401,000	106,100	1.6	5.3	0.4
Barataria Basin Landbridge (BA1, BA2, BA3)	5/1/2010	5/16/2013	3.0	3,248,000	1,067,100	2	13.7	0.7
New Cut	2/1/2006	5/16/2013	7.3	1,007,000	138,100	1.2	23.5	0.2
West Belle Pass Marsh	12/1/2012	6/13/2013	0.5	104,000	208,600	1.4	12.6	2.8
West Grand Terre	7/1/2010	5/19/2013	2.9	1,136,000	393,800	2.5	6	0.9
Sandy Point	11/1/2012	6/11/2013	0.6	201,000	346,100	1.4	12.5	2.4
Bay Joe Wise	05/24/2009	6/11/2013	4.0	6,326,000	1,581,510	20	34.2	5.0

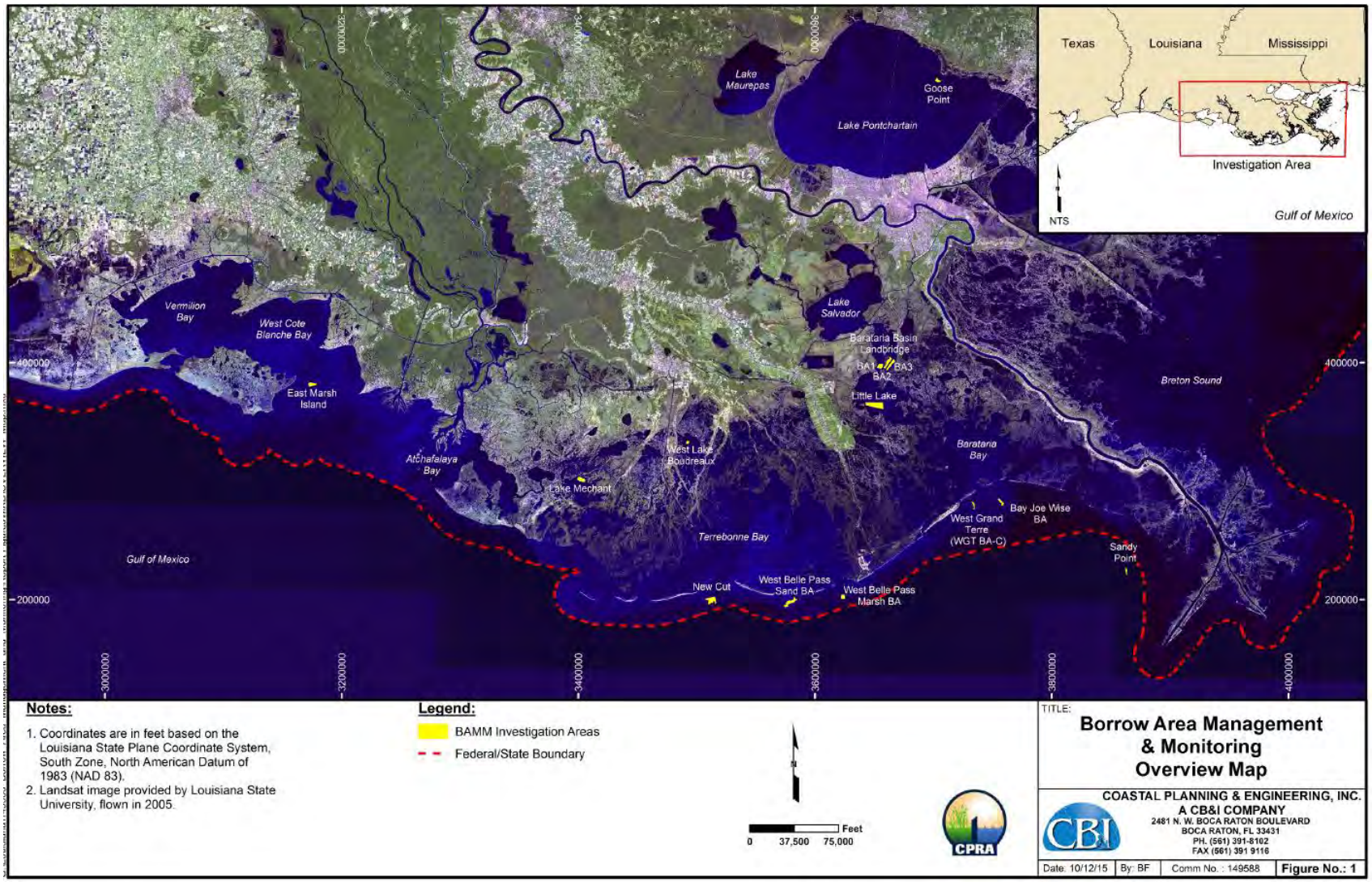

Figure C-1. Overview map of borrow areas in southeast Louisiana that were investigated by CB&I as part of the BAMM program. Note: Reprinted from the Louisiana Borrow Area Management and Monitoring (BAMM) Program *report by CB&I (2015).*

1110 RIVER ROAD S., SUITE 200
BATON ROUGE, LA 70802

(225) 448-2813
WWW.THEWATERINSTITUTE.ORG